Linear Time Invariant Models for Integrated Flight and Rotor Control

A Dissertation

Presented to

The Academic Faculty

by

Fahri Ersel Olcer

In Partial Fulfillment

of the Requirements for the Degree

Doctor of Philosophy in the

School of Aerospace Engineering

Georgia Institute of Technology

August 2011

Linear Time Invariant Models for Integrated Flight and Rotor Control

Approved by:

Dr. J.V.R. Prasad, Advisor
School of Aerospace Engineering
Georgia Institute of Technology

Dr. Lakshmi N. Sankar
School of Aerospace Engineering
Georgia Institute of Technology

Dr. Daniel P. Schrage
School of Aerospace Engineering
Georgia Institute of Technology

Dr. Mark F. Costello
School of Aerospace Engineering
Georgia Institute of Technology

Dr. Chengjian He
Advanced Rotorcraft Technology, Inc.

Date Approved: July 8, 2011

ACKNOWLEDGEMENTS

I would like to thank to my thesis advisor Dr. Prasad and my thesis committee members Dr. Schrage, Dr. Sankar, and Dr. He for letting me have the opportunity to work with them in various portions of this thesis and finally considering my efforts for the PhD degree. This study is partially funded under the NASA Cooperative Agreement #NNX07AP33A at the Georgia Institute of Technology with Dr. Wayne Johnson as the technical monitor. I'd like to thank to the people at NASA Ames Mark Tischler and Colin Theodore for their contributions, and Jinggen Zhao from ART.

I would like to thank to my colleagues and friends in the School of Aerospace Engineering at Georgia Tech, Michael Abraham, Michael Osmon for their contribution in my work and collaboration in joint projects. I would also like to thank my friends and colleagues for their extraordinary friendship and support through my years toward this degree, Keeryun Kang, Jongki Moon, Ivan Grill, Michael Acheson, Giyun Chung, M. Emre Gunduz , Manuj Dhingra, E. Orcun Kozaka, Burak Korkut, Oguz Karvan, Faruk and Can Cavusoglu bros, G. Basak Bayraktar, Vasu Manivanan, Alexander Robledo, James Rigsby, Jeremy Bain. I would like to express my sincere appreciation for my mom for what I am today and what I might be in the future. I would like to share my deepest joy on this success with my beloved wife Goksen for being the amazing person of my life.

TABLE OF CONTENTS

LIST OF TABLES

LIST OF FIGURES

LIST OF SYMBOLS AND ABBREVIATIONS

α	Angle of attack
β	Flapping angle
β_{1c}	Tip path plane longitudinal tilt angle
β_{1s}	Tip path plane lateral tilt angle
γ	Lock number
γ_{xy}	Coherence
δ	Flap angle
δ_c	cyclic component of flap angle
μ	Advance ratio
ν	Non-rotating flapping frequency
Φ_δ	Phase angle between flap and angle of attack
θ_{IBC}	Individual Blade Control input
Ψ	Azimuth angle
ω	Airfoil frequency
ω_δ	Trailing edge flap frequency
1D	1 Dimensional
2D	2 Dimensional
ADS-33	Aeronautical Design Standard 33
AoA	Angle of Attack
B	Blade Tip Loss Factor
BVI	Blade Vortex Interaction
Bo	Tip path plane collective flap (coning)

Bd	Tip path plane differential
Bc	Tip path plane longitudinal
Bs	Tip path plane lateral
b	half chord length
b_δ	half chord length of flap
CC	Constant Coefficient
CFD	Computational Fluid Dynamics
c_d	Airfoil Drag Coefficient
c_l	Airfoil Lift Coefficient
c_m	Airfoil Moment Coefficient
dBo	Time rate of tip path plane coning
dBd	Time rate of tip path plane differential
dBc	Time rate of tip path plane longitudinal
dBs	Time rate of tip path plane lateral
dZo	Time rate of tip path plane collective lag
dZd	Time rate of tip path plane differential lag
dZc	Time rate of tip path plane cosine cyclic lag
dZs	Time rate of tip path plane sine cyclic lag
D(ψ)	LTP damping matrix
E_i	Error index for Eigenvalues
EMP	Exponentially Modulated Periodic
FLOP	Floating Point Operations
FTM	Floquet Transition Matrix
FTMo	FTM after body periodicity suppressed

$G(\psi)$	LTP state matrix associated with inputs
GHM	Generic Helicopter Model
HHC	Higher Harmonic Control
I	Identity Matrix
IBC	Individual Blade Control
$J^{(1)}$	Error index, Time Domain
$J^{(2)}$	Error index, Frequency Domain
k_α	Reduced frequency of airfoil section
k_δ	Reduced frequency of flap section
$K(\psi)$	LTP stiffness matrix
LTI	Linear Time Invariant with harmonics of rotor states
LTIo	Linear Time Invariant after body periodicity suppressed
LTI*	Linear Time Invariant with harmonics of all states
LTP	Linear Time Periodic
LTPo	Linear Time Periodic after body periodicity suppressed
Lo	Inflow average state
Lc	Inflow cosine harmonic state
Ls	Inflow sine harmonic state
M	Mach Number
MBC	Multi Blade Coordinates
NNET	Neural Network
N_b	Number of blades
N_s	Total number of states in the LTI
ns_o	Number of non-rotor original states

ns_r	Number of original rotor states
n_o	Number of outputs
n_t	Number of discrete time steps
n_ω	Number of frequencies sampled
n_h	Number of harmonics
OBC	On Blade Control
P	Body roll rate
P(ψ)	LTP output matrix associated with states
phi	Body roll attitude
q	Body pitch rate
Q	Equation imbalance
Q(ψ)	LTP output matrix associated with first derivative of states
R	Radius of blade
R(ψ)	LTP output matrix associated with inputs
r	Body yaw rate
ROM	Reduced Order Model
T, T_c	Transfer Function
TEF	Trailing Edge Flap
t	Time
the	Body pitch attitude
U, u	Input vector
V	Velocity
Vx	Body x velocity component
Vy	Body y velocity component

Vz	Body z velocity component
W	Weighting for Time Domain Metric
W_y	Weighting for Frequency Domain Metric
X, x	State vector
Y, y	Output vector
Zo	Tip path plane collective lag
Zc	Tip path plane cosine cyclic lag
Zs	Tip path plane sine cyclic lag
Zo	Tip path plane differential lag

Operands

$\Delta(\ )$	Increment or change
$(\dot{})$	First derivative with respect to time
$(\ddot{})$	Second derivative with respect to time
$()_o$	Average component of time periodic signal
$()_{\#c}$	Cosine component of time periodic signal
$()_{\#s}$	Sine component of time periodic signal
H	Harmonic analysis operator
/rev	Frequency normalized by rotor speed

SUMMARY

Recent developments on individual blade control (IBC) and physics based reduced order models of various on-blade control (OBC) actuation concepts are opening up opportunities to explore innovative rotor control strategies for improved rotor aerodynamic performance, reduced vibration and BVI noise, and improved rotor stability, etc. Further, recent developments in computationally efficient algorithms for the extraction of Linear Time Invariant (LTI) models are providing a convenient framework for exploring integrated flight and rotor control, while accounting for the important couplings that exist between body and low frequency rotor response and high frequency rotor response. Formulation of linear time invariant (LTI) models of a nonlinear system about a periodic equilibrium using the harmonic domain representation of LTI model states has been studied in the literature. This thesis presents an alternative method and a computationally efficient scheme for implementation of the developed method for extraction of linear time invariant (LTI) models from a helicopter nonlinear model in forward flight. The fidelity of the extracted LTI models is evaluated using response comparisons between the extracted LTI models and the nonlinear model in both time and frequency domains. Moreover, the fidelity of stability properties is studied through the eigenvalue and eigenvector comparisons between LTI and LTP models by making use of the Floquet Transition Matrix. For time domain evaluations, individual blade control (IBC) and On-Blade Control (OBC) inputs that have been tried in the literature for vibration and noise control studies are used. For frequency domain evaluations, frequency sweep inputs are used to obtain frequency responses of fixed system hub loads to a single blade IBC input. The evaluation results demonstrate the fidelity of the

extracted LTI models, and thus, establish the validity of the LTI model extraction process for use in integrated flight and rotor control studies.

CHAPTER 1 INTRODUCTION

1.1 Overview

Active control of rotor blade sections or entire blades expands the control space of the rotorcraft applications as opposed to swashplate control. Individual Blade Control (IBC) and On-Blade Control (OBC) concepts have enabled researchers to show possibilities of extensive improvements for power consumption [1, 2, 3, 4, 5], vibration [1, 2, 3, 5, 6], noise [2, 3, 7, 6], gust response alleviation [8] and many other areas such as wind turbines [9]. These studies focused only on rotor control, disregarding their effects on the handling qualities and stability of the entire vehicle. The control space of such applications has been explored either through parametric studies, in terms of magnitude and phasing, or by integrating input-output controllers in simulations and tests [10], missing all the essential benefits of having linear systems. While higher flight control bandwidth can be achieved through innovative integrated flight and rotor control designs with the aid of IBC and OBC concepts, the implications of such higher bandwidth control on handling qualities and vehicle-pilot-biodynamic coupling, etc. need to be carefully assessed before they can be fully realized.

Due to the periodic nature of helicopter rotors, the linearized models extracted from nonlinear models of a rotorcraft will have periodic coefficients unless rotor states are omitted or the vehicle is in hover condition without any cyclic input. Though stability analysis of the extracted linear time periodic (LTP) models can be performed using the Floquet stability theory, this does not provide a convenient framework for controller synthesis and design as the available control design tools for LTP systems are few in

number [11]. Further, the handling qualities specifications for small amplitude maneuvers as prescribed in the Aeronautical Design Standard (ADS-33) are based on a linear time invariant (LTI) model, and thus cannot be directly accounted for in the controller design process using LTP models. If linearized models in time invariant form are made available, it will open up the choice of available design and analysis tools to a rotorcraft control designer [11]. The aim of this study is to fill this gap in the literature with a computationally more efficient method and provide thorough fidelity for the response and stability characteristics of the proposed LTI method.

1.2 Literature Review

Reformulation of Linear Time Periodic systems in order to arrive at Linear Time Invariant exists in the literature and has attracted attention in several areas of physics and engineering. The Floquet-Lyapunov transformation [12], which dates back to 1883, is the most known, and it has been used particularly for system stability estimations in the rotorcraft community. A series of works cited by Peters and Hohenemser in their 1970 work [13] showed the emerging use of this method in the rotorcraft community in the 1960's by researchers such as Loewy [14], Sissingh [15], Lowis [16], and Wilde [17]. Authors also supported their work with citations of the works of Crimi [18] and Pirulli et. al [19], showing the relation between the Floquet Method [12] and the Hill's Method [20] which is also from the same era and stems from another branch of reformulation, presented in the next paragraph.

The Floquet-Lyapunov transformation takes the time varying periodic state matrices and creates a monodromy matrix by integration at the end of one period. Ultimately, this transition matrix determines the stability of the system such that if all the

eigenvalues of the monodromy matrix lie within the unit circle, the system is said to be stable. This property is due to the integration of a time periodic state matrix at one revolution. Mathematically it is an unfortunate mapping of the eigenvalues from imaginary domain by a tangent function whose inverse is actually a multivalued function and creates confusion during the reverse mapping. This confusion had been the focus of many researchers that sought a single integer part. Recently, Peters presented in his work [21] that indeed all integer multiples arising from the inverse tangent function are true, consistent with the fact that a Linear Time Periodic system does not have a single frequency for each mode; instead, there exist a infinite number of frequencies for every mode, and the multi-values of the inverse tangent function simply represent this.

Another branch of reformulation methods deals with the structure and dimension of the system. These methods were collectively presented in a survey [22] by authors from the electrics community and were later adopted, extended and verified with contributions from the rotorcraft community [23]. This historical perspective is an example of the interdisciplinary importance of the subject.

Of those adopted, the time lifting method is one of the earliest and still the most commonly used. It approaches the time varying problem by packing the discrete signals collected within a period into a vector. In this way, it creates a time invariant system of the sampled time periodic system with an increased size of input and output channels, as many as the number of sampled discrete time steps. Another approach, called cyclic reformulation, performs a similar job but this time not only the input and output vectors but also the state vector, thus the state matrix, are extended. These methods have been analytically proven to have consistent stability results with the system from which they are originated but none of the references used herein provided high fidelity work.

Frequency lifted and Fourier reformulations are analogous to the preceding methods, respectively, with the important caveat that they are directly represented in the frequency domain for all the harmonics. In frequency lifted reformulation, only inputs and outputs are processed for a harmonic representation similar to that of the time lifted reformulation. In the Fourier reformulation, this process is performed for inputs and outputs as well as for the states, under the assumption that the periodic system is in an Exponentially Modulated Periodic (EMP) regime. Both of these frequency domain reformulations coincide when their harmonic transfer function for the system is presented.

These methods have certain characteristics which change either the structure or the dimension of the linear system, and reformulations always lead to a particular class of time invariant models. Likewise every time-periodic system can be reformulated as a time invariant form, but it is not necessarily true that every time invariant system has a corresponding time periodic representation.

These mentioned methods available in the literature for transformation of LTP models to time-invariant form have certain disadvantages for control system design purposes. For instance, in the Lyapunov-Floquet transformation method [23, 24], the system matrix of the LTP model is transformed into a time-invariant form using the time varying Lyapunov-Floquet transformation matrix. However, the control matrix of the transformed model will still be time-periodic. In order to overcome this difficulty, an auxiliary system is constructed with pseudo control variables which bear no resemblance to the control vector of the LTP model. Controller design is carried out on the auxiliary system, and control laws for the time periodic system are constructed from feedback signals of the auxiliary system. However, this method suffers from the disadvantage of needing to compute the state transition matrices of the LTP model over one rotor period

in order to construct the Lyapunov-Floquet transformation matrix. Analytical approximations of the coefficient matrices using the shifted Chebyshev polynomials of the first kind provide an efficient means in the state transition matrix computations. While the computational effort is significantly improved by the use of such closed form approximations, the accuracy of the results is significantly influenced by the number of terms used in the analytical approximations, and such an approach becomes numerically very sensitive. The transformation using discrete-time methods, such as time lifting and frequency lifting methods [22], also suffer from the same disadvantage of a need for state transition matrices.

Hill's Method [20], which is a Fourier based frequency domain reformulation, is widely seen for stability assessment studies by authors from various areas of science including electrics [25], shaft and bearing design [26], wind energy [9] and rotorcraft. Although these studies showed remarkable success at assessing the stability properties of the system correctly, none of them mentioned a control system design. This is seen as a particular gap in the literature, and it may, in part, be the result of the fact that states represented in terms of Fourier coefficients do not resemble a physical meaning for the control system design, yet the transformation of such pseudo-states to a physically meaningful form adds similar disadvantages as those mentioned earlier for the other methods.

The use of harmonic analyzers as part of the linearization step to extract a time invariant linear model for the specific application of flight control and higher harmonic control is explored by Cheng et. al in [11, 27]. The extracted LTI model consists of the body states, time averaged rotor states, harmonic analyzer states, pilot controls and higher harmonic controls. Using such a model, Cheng et al. [11, 27] showed that it becomes feasible to consider the important coupling between the body states and the

higher frequency rotor response in a combined flight and vibration controller design. By using numerical perturbations to individual harmonic components of periodic states of a nonlinear system, Cheng et al formulated LTI models with average and harmonic components of rotor response as pseudo states[27]. Although these publications presented a framework for control oriented LTI systems composed of physically meaningful pseudo-states, those studies were computationally inefficient due to entirely numerical perturbation schemes both for average and harmonics states and stability assessment based on their proposed methodology was missing.

The evolution of the IBC and OBC concepts starts with Higher Harmonic Control (HHC). Although the term may literally imply for any type of input (swashplate, IBC or OBC etc.), it is particularly used for higher harmonic excitation of the swashplate controls in the rotorcraft community [1]. Earlier attempts go back to the 1950's [28], when the effect of 2/rev inputs was analytically investigated and tested. Those researches showed beneficial results of 2/rev inputs on the power consumption, and it was assessed that the source of the improvement was due to the delay of the stall on the retreating side of the rotor. Analytical studies also show that for an N-bladed rotor vibrations occur at N/rev frequency in the non-rotating frame are caused by the vibrations at N-1/rev, N/rev, and N+1/rev frequencies taking place in the rotating frame [29]. It was suggested that use of those three distinct frequencies could attenuate the vibrations, which was also tested in the HHC applications [1]. Although it was tested on actual size rotors [1], one major drawback of HHC through swashplate inputs was that the swashplate might have only three input channels, which was sufficient only for two or three bladed rotors. Advances in technology provided the ability to introduce Individual Blade Control [2, 3, 30] and On-Blade Control [7, 8, 4] concepts on actual size rotors and helicopters that eventually

increased number of input channels. A comprehensive review of the methods for vibration reduction can be found in [31].

1.3 Present Work

Linear system matrices of rotorcraft applications are dominated by periodic coefficients. Available tools for transformation of LTP models to time-invariant suffer from certain disadvantages and may not be suitable for larger size (number of states, and harmonics) applications as discussed in the literature review sections of this chapter. The present work intends to fill that gap in this area by making use of harmonic components of LTP model while constructing the LTI matrices of the same system, which makes the present method, a computationally efficient tool for studies concerning interactions between high and low frequency controllers. Moreover, a thorough validity check of the proposed LTI model, in terms of response and stability characteristics, is also studied. The present work reformulates the LTI system matrices in terms of harmonic coefficients of the LTP matrices of the same system as opposed to earlier attempts by Cheng et al. [11] whereas perturbations are applied to the nonlinear model and harmonic decomposition of the response is extracted. The method is tested to prove its fidelity by observing both time and frequency domain responses using high fidelity rotorcraft models that contain IBC/OBC type input channels. Apart from the response validations, the stability characteristics of the LTI models are also observed using both simplified analytical and numerical models so that interpreting the relation between them becomes esier. The present work then concludes by carrying out parametric studies in order to determine the required number of harmonics to match the stability characteristics of high fidelity rotorcraft models under the proposed fidelity criteria.

The objective of this thesis is to develop, validate and assess certain requirements of the LTI models that can be used for controller synthesis and design. This thesis describes the development and validation of such an LTI model along with the model development milestones in order to make use of state-of-the-art innovative capabilities present in the literature.

1.4 Organization of Dissertation

Chapter 1 first gives an overview of the current problem that forms the basis of this thesis in context with the literature review and assessing the gap in the literature. Then, subsections review particular areas surrounding this problem in the literature. Chapter 1 concludes by giving the ultimate goal of this thesis and explains the roadmap to achieve that goal.

Chapter 2 deals with the models that were used in this thesis, explaining model properties and giving additional details if specific model selections or changes needed to be done, such as model development or simplification. Once the base FLIGHTLAB model is introduced, the chapter gives the formulation of LTP and LTI models.

Chapter 3 studies the stability aspects of the LTI models as obtained from analytical and FLIGHTLAB models. The objective is to understand the stability properties of the LTI models in contrast with the reference LTP model from which they are originated and to define viable fidelity criteria in terms of eigenvalue comparisons between LTP and LTI systems so that a concrete basis can be constructed for the fidelity of stability characteristics.

Chapter 4 provides the evaluation results of the developed method for the extraction of LTI models from a nonlinear model of a generic helicopter when an IBC

input channel is used for excitation. First, the chapter introduces the metrics used in the LTI model fidelity evaluations. Next, it provides the fidelity evaluation results of response characteristics for the case of individual blade control applications. It then presents an evaluation of the response characteristics in two sections, time and frequency domain responses.

Chapter 5 first explains the reduced order aerodynamic modeling of a flap actuator. It then explains how, in order to model the sensitivity of the aerodynamics of blade sections due to actuation of trailing edge flap elements, adaptive neural networks are trained using an extensive CFD data. These models are then tested before they are integrated into the FLIGHTLAB model. The chapter continues by discussing how various scenarios are tested in the FLIGHTLAB environment to extract time and frequency response data. For validation purposes, Chapter 5 then extracts an LTI model of the FLIGHTLAB model by incorporating a reduced order aerodynamic model, and concludes by evaluating time and frequency responses.

CHAPTER 2 LTI MODEL FORMULATION

The purpose of this chapter is to provide the details of the proposed augmented linear time invariant model formulation along with the required prior steps for formulation and application. These steps include the modeling properties of the FLIGHTLAB model and the extraction of the Linear Time Periodic model of the FLIGHTLAB model at a desired trim condition. The first section of this chapter covers the baseline modeling details used in this thesis. It first describes the generic helicopter model (GHM) available in FLGIHTLAB, and then gives in detail the enhancements of the GHM, such as inflow model, elastic blades. A brief introduction to the modeling of the input channels concludes this section.

The following model enhancements are based on practical application purposes in that all of them are tied to the HHC of the rotor blades for vibration reduction and other active rotor control applications. In a hierarchical order, HHC, IBC, and OBC have been used for such purposes, and following the timeline both the application and modeling of these concepts evolved from simple to complex. HHC is an application particularly related with higher harmonics used on a swashplate, whereas IBC resembles the additional pitch input to the individual blades either on top of swashplate input or on its own. Therefore, modeling of such inputs is fairly simple in comprehensive rotor codes in contrast to the OBC. An OBC is a generic name for the active controller located on the blade that alters the aerodynamic properties of the sections on which they are mounted. The integrated trailing edge flap is the type of OBC concept used in this study in a dedicated chapter where its details are given prior to the applications.

Friedman and Millott [[31] suggested that HHC had reached its maturity, however the lack of its practical use was also mentioned relating to its cost and technical limitations. In order to represent analytical and experimental studies of the HHC era following articles are selected. Molusis [32] had analytical studies for optimal controls, Hammond [33] had extensive wind tunnel tests on the HHC concepts and Taylor [34] ran simulations with HHC concepts integrated models.

Following the same survey article by Friedman it is know that Kretz [35] had pioneered the IBC approach in the literature. IBC concept could overcome some disadvantages of the HHC which were experienced during the practical application phase while taking advantage of all the analytical and experimental findings HHC concepts achieved. Eventually one of the targets was reduction in vibration levels seen on the helicopter fuselage along with the other benefits such as gust alleviation, attitude stabilization, and augmentation for lag damping as they were seen in works by Ham [36, 37].

As it was stated here, HHC and IBC concepts are identical in the analytical sense as they excite the entire blade. On-Blade Control (OBC) concepts in general encompass trailing edge flaps [7], deployable gurney flaps [38], blowing-and-suction concepts [39], Miniature Trailing-Edge Effectors [40] and many more. As it was stated by Friedman [[31] that the importance of these concepts is that required excitations which may rise up to 100s of rotational speed can be provided by these concepts without having the need for exciting the entire blade, thus saving significant power requirement. Although these methods emerging more recently than the former two it was noticed in the survey paper [[31] that indeed in 1972, Lemnios and Smith [41] presented the servo-flap concept. Friedman and Millott also caught an important aspect on the OBC concepts in their 1994 survey paper, referring it to the former studies such as presented by Robinson in [42, 43]

that when modeling of OBC concepts are concerned unsteady aerodynamic effects becomes essential for the entire system, through particularly affecting torsional response.

Elastic blade and higher fidelity inflow models have a significant impact on the higher harmonics of the rotor; therefore, they are considered a baseline for the response studies. During the research for this work it is noticed and also reported in the literature [44, 45] that having not only one of these modeling options but both at the same time has a much more significant impact on the correlations between the predicted and wind tunnel test vibration levels. Similar results were also obtained in another recent work [46], where an unsteady lifting line model and and a prescribed wake model are used together.

The second section of this chapter presents the formulation of the LTP model from a nonlinear model.

The final section of this chapter presents the formulation of LTI in terms of harmonic coefficients of the LTP model. In order to demonstrate the use of analytical equations presented here, the appendix presents an LTI model of a generic LTP model with limited number of harmonics.

2.1 Baseline Helicopter Model in FLIGHTLAB

The Generic Helicopter Model (GHM) available in FLIGHTLAB is a roughly 15,000 pounds gross weight, 4 bladed helicopter model with rigid blades attached to the hub through flap and lag hinges. It has a canted tail rotor providing both anti-torque and lift, a stabilator designed to anticipate pitch attitude and rate, and a vertical fin to reduce the work load of the tail rotor in forward flight. GHM has very similar characteristics to the

UH-60 Blackhawk helicopter which is studied in the literature extensively. GHM of FLIGHTLAB is also studied in the literature, used as a reference model in Padfield's book [48], also appeared on the articles by Voskuijl et. al in [49, 50] and can be found in similar studies.

The controller of the stabilator is turned off in this study; likewise, all the other stability augmentation systems (analog and digital SAS and pitch bias actuator) are turned off. This enables the use of pilot inputs during linearization since there is no interference between the swashplate and pilot inputs. A 3-state inflow model is incorporated in the model to account for the induced velocities through the rotor disk, and no interference effects are turned on. This model is used as the baseline throughout this thesis except where any model enhancements or simplifications are needed for the particular study. The main rotor angular speed is 27 radian per second or 4.3 hertz approximately.

2.1.1 Inflow Model Enhancements

FLIGHTLAB provides both variants of Peters-He inflow model which is a dynamic wake inflow model and vortex-wake models. Vortex-wake models includes source terms in their governing equations [51] which makes them not suitable for linearization purposes whereas dynamic inflow models are linear in nature. Therefore, considering the linearization purposes of this study Peters-He inflow [52] model with 3 different levels of modeling (3-state, 15-state and 33-state) are selected.

The GHM uses a 3-state inflow model which is a reduced version of the Peters-He Dynamic Inflow model that accounts for the average and first harmonic azimuth variation and a linear radial variation of the induced velocities. The equivalent model to this can be found in the early literature and it is known as Pitt-Peters model [53]. This

inflow model is used in the stability investigations of the LTI models during this study for its simplicity.

The 3-state inflow model is a 1st order approximation and comes short when the input bandwidth is increased to at least 4/rev. Therefore, during the response characteristics investigations of this study higher fidelity alternatives, both 15-state and 33-state models are used. The former has an up to 4 harmonic azimuth variation and a 4th order polynomial representation of the radial distribution, whereas the latter one has an increased polynomial variation to the 8th order.

2.1.2 Elastic Blade Modeling

As already stated, the GHM has 4 blades, each modeled as a rigid body attached to the hub through flap and lag hinges. Although this model is sufficient for performance and some vibration applications, the elastic blade option is required for modeling much higher vibrations and to improve fidelity at 4/rev vibrations. In FLIGHTLAB, elastic blade modeling can be achieved by two methods, the finite element blade model, which is 1D beam modeling, and modal reduction. Modal representation makes use of the modal analysis results such as modal frequencies, damping, and mode shapes associated with each mode. In case of full rotorcraft model application for the purpose of LTI model generation, modal representation is sufficient; hence, it is selected with available generic modal data that has 2 elastic modes, 1 for flapping and 1 coupled flap and lag mode. Each elastic mode is an additional cost of 8 states in the linearized model therefore 2 elastic modes doubles the size of the rotor states to 32 in total.

2.1.3 Modeling of the Input Channels

This section gives brief details on the modeling of the used input channels. Individual Blade Control was used as the baseline input channel in order to obtain the response

characteristics of FLIGHTLAB and LTI models. On-blade control concept by means of Trailing-Edge Flaps was selected as the secondary input channel that LTI studies are carried out in this study. Since modeling of the OBC required much more comprehensive study, its details are given in a dedicated chapter later where Reduced Order Modeling TEFs is explained and verified.

Individual Blade Control modeling in FLIGHTLAB is done by existing individual blade pitch components, which are normally controlled by the swashplate inputs only. In order to retain the trim algorithms of FLIGHTLAB, swashplate controls were preserved but additional input channels were created that directly excited the individual blade pitch angles. Thus, this modeling technique did not alter the modeling fidelity in any form.

In contrast to Individual Blade Modeling, On-Blade Control is a more advanced concept that requires additional modeling information in order to incorporate the configuration properties of OBC elements and to account for the aerodynamic effects depending on the selected OBC concept. This study used quarter chord trailing edge flap type OBC elements for application purposes. Each blade was enhanced with such elements between 50% to 95% radial position where OBC inputs were considered.

2.2 Linear Time Periodic Model Formulation

Consider a nonlinear system of the form

$$f(X, \dot{X}, \ddot{X}, U) = 0 \tag{1}$$

where X, $\dot{X}$ and $\ddot{X}$ are respectively the position, velocity, and acceleration vectors, and U is the control vector. Let $((\overline{X}(\psi),\overline{U}(\psi)))$ represent a periodic equilibrium of the system of Eq. (1) such that

(2)

$$\overline{X}(\psi + 2\pi) = \overline{X}(\psi), \quad \overline{U}(\psi + 2\pi) = U(\psi)$$

A linearization of Eq. (1) can be obtained by considering changes from equilibrium as

$$x(\psi) = X(\psi) - \overline{X}(\psi), \quad u(\psi) = U(\psi) - \overline{U}(\psi) \tag{3}$$

and expanding Eq. (1) about the periodic equilibrium in its Taylor series to first order as

$$f(\overline{X}, \dot{\overline{X}}, \ddot{\overline{X}}, \overline{U}) + \left[\frac{\partial f}{\partial \ddot{X}}\right]\ddot{x} + \left[\frac{\partial f}{\partial \dot{X}}\right]\dot{x} + \left[\frac{\partial f}{\partial X}\right]x + \left[\frac{\partial f}{\partial U}\right]u = 0 \tag{4}$$

The partial derivatives in Eq. (4) are obtained at the selected periodic equilibrium. Since the periodic equilibrium also must satisfy Eq. (1), the above equation reduces to

$$\left[\frac{\partial f}{\partial \ddot{X}}\right]\ddot{x} + \left[\frac{\partial f}{\partial \dot{X}}\right]\dot{x} + \left[\frac{\partial f}{\partial X}\right]x + \left[\frac{\partial f}{\partial U}\right]u = 0 \tag{5}$$

which can be rearranged into the form

$$\ddot{x} = -K(\psi)x - D(\psi)\dot{x} + G(\psi)u \tag{6}$$

where

$$K(\psi) = \left[\frac{\partial f}{\partial \ddot{X}}\right]^{-1}\left[\frac{\partial f}{\partial X}\right] \tag{7.a}$$

$$D(\psi) = \left[\frac{\partial f}{\partial \ddot{X}}\right]^{-1}\left[\frac{\partial f}{\partial \dot{X}}\right] \tag{7.b}$$

$$G(\psi) = -\left[\frac{\partial f}{\partial \ddot{X}}\right]^{-1}\left[\frac{\partial f}{\partial U}\right] \tag{7.c}$$

Likewise, the output equation of the nonlinear system of Eq. (1) is defined as

$$Y = g(X, \dot{X}, \ddot{X}, U) \tag{8}$$

where Y is the vector of outputs. At a periodic equilibrium, the value of the output is given in Eq. (9).

$$\overline{Y} = g(\overline{X}, \dot{\overline{X}}, \ddot{\overline{X}}, \overline{U}) \tag{9}$$

A linearized form of the output equation is obtained by expanding Eq. (8) about the periodic equilibrium in its Taylor series to first order as

$$Y = g(\overline{X}, \dot{\overline{X}}, \ddot{\overline{X}}, \overline{U}) + \left[\frac{\partial g}{\partial \ddot{X}}\right]\ddot{x} + \left[\frac{\partial g}{\partial \dot{X}}\right]\dot{x} + \left[\frac{\partial g}{\partial X}\right]x + \left[\frac{\partial g}{\partial U}\right]u \tag{10}$$

Substituting Eqs. (6) and (9) into Eq. (10) results in

$$y = P(\psi)x + Q(\psi)\dot{x} + R(\psi)u \tag{11}$$

where *y* represents a change in the output *Y* from its equilibrium value $\overline{Y}$, and *P, Q* and *R* matrices can be obtained using

$$P(\psi) = \left[\frac{\partial g}{\partial X}\right] - \left[\frac{\partial g}{\partial \ddot{X}}\right]K(\psi) \tag{12.a}$$

$$Q(\psi) = \left[\frac{\partial g}{\partial \dot{X}}\right] - \left[\frac{\partial g}{\partial \ddot{X}}\right]D(\psi) \tag{12.b}$$

$$R(\psi) = \left[\frac{\partial g}{\partial U}\right] + \left[\frac{\partial g}{\partial \ddot{X}}\right]G(\psi) \tag{12.c}$$

2.3 Linear Time Invariant Model Formulation

The linear time periodic (LTP) model of Eqs. (6) and (11) is converted into a linear time invariant (LTI) form using the following approximation of *x*;

$$x = x_o + \sum_{n=1}^{N} x_{nc}\cos n\psi + x_{ns}\sin n\psi \tag{13}$$

where x_o is the average component and x_{nc} and x_{ns} are respectively the n/rev cosine and sine harmonic components of *x*. Likewise, control (*u*) and output (y) of Eq. (11) are expanded in terms of harmonic components as

$$u = u_o + \sum_{m=1}^{M} u_{mc} \cos m\psi + u_{ms} \sin m\psi \tag{14}$$

$$y = y_o + \sum_{l=1}^{L} y_{lc} \cos l\psi + y_{ls} \sin l\psi \tag{15}$$

Now defining an augmented state, control and output vectors in terms of their respective average and harmonic components as

$$x_{aug} = \left[x_o{}^T .. x_{ic}{}^T \quad x_{is}{}^T .. x_{jc}{}^T \quad x_{js}{}^T .. \dot{x}_o{}^T .. \dot{x}_{ic}{}^T \quad \dot{x}_{is}{}^T .. \dot{x}_{jc}{}^T \quad \dot{x}_{js}{}^T .. \right]^T \tag{16}$$

$$u_{aug} = \left[u_o{}^T .. \quad u_{mc}{}^T \quad u_{ms}{}^T .... \right]^T \tag{17}$$

$$y_{aug} = \left[y_o{}^T .. \quad y_{lc}{}^T \quad y_{ls}{}^T ... \right]^T \tag{18}$$

where x_o is the average component, x_{ic}, x_{is} are respectively the i^{th} harmonic cosine and sine components of x, u_o is the average component and u_{mc}, u_{ms} are respectively the m^{th} harmonic cosine and sine components of u, and y_o is the average component and y_{lc}, y_{ls} are respectively the l^{th} harmonic cosine and sine components of y. Using the augmented state, control and output vectors as described above, the LTP model of Eqs. (6) and (11) can be approximated into an LTI form as

$$\dot{x}_{aug} = \begin{bmatrix} A_{11} & A_{12} \\ A_{21} & A_{22} \end{bmatrix} x_{aug} + \begin{bmatrix} B_1 \\ B_2 \end{bmatrix} u_{aug} \tag{19}$$

$$y_{aug} = \begin{bmatrix} C_1 & C_2 \end{bmatrix} x_{aug} + \begin{bmatrix} E \end{bmatrix} u_{aug} \tag{20}$$

For consideration of Eq. 6, Eq. 13 is differentiated with respect to time twice,

$$\dot{x} = \dot{x}_o + \sum_{n=1}^{N} \left(x'_{nc} \cos(n\psi) + x'_{ns} \sin(n\psi) \right) \tag{21}$$

$$\ddot{x} = \ddot{x}_o + \sum_{n=1}^{N} \left(x''_{n.c} \cos(n\psi) + x''_{n.s} \sin(n\psi) \right) \tag{22}$$

where

$$x'_{nc} = \dot{x}_{nc} + n \cdot \Omega \cdot x_{ns}$$
$$x'_{ns} = \dot{x}_{ns} - n \cdot \Omega \cdot x_{nc}$$
$$x''_{nc} = \ddot{x}_{nc} + 2n \cdot \Omega \cdot \dot{x}_{ns} - (n\Omega)^2 \cdot \ddot{x}_{nc}$$
$$x''_{ns} = \ddot{x}_{ns} - 2n \cdot \Omega \cdot \dot{x}_{nc} - (n\Omega)^2 \cdot \ddot{x}_{ns}$$
$$n = 1,2,....., N$$

Substituting Eqs.(21) and (22) into Eq. (6) results as in Eq. (23)

$$\begin{aligned} \ddot{x}_o + \sum_{n=1}^{N} (x''_{nc} \cos(n\psi) + x''_{ns} \sin(n\psi)) = & -D(\psi)\left(\dot{x}_o + \sum_{n=1}^{N} \left(x'_{nc} \cos(n\psi) + x'_{ns} \sin(n\psi) \right) \right) \\ & -K(\psi)\left(x_o + \sum_{n=1}^{N} \left(x_{nc} \cos(n\psi) + x_{ns} \sin(n\psi) \right) \right) \\ & +G(\psi)\left(u_o + \sum_{m=1}^{M} \left(u_{mc} \cos(m\psi) + u_{ms} \sin(m\psi) \right) \right) \end{aligned} \tag{23}$$

The average and individual harmonic components of Eq. (23) can be obtained by employing the harmonic analysis on the both sides of the equation. Average component (x_o) is obtained by averaging the integration of Eq. (23) over one period.

$$\begin{aligned} \ddot{x}_o = \quad & \frac{1}{2\pi} \int_0^{2\pi} -D(\psi)\left(\dot{x}_o + \sum_{n=1}^{N} \left(x'_{nc} \cos(n\psi) + x'_{ns} \sin(n\psi) \right) \right) d\psi \\ & + \frac{1}{2\pi} \int_0^{2\pi} -K(\psi)\left(x_o + \sum_{n=1}^{N} \left(x_{nc} \cos(n\psi) + x_{ns} \sin(n\psi) \right) \right) d\psi \\ & + \frac{1}{2\pi} \int_0^{2\pi} G(\psi)\left(u_o + \sum_{m=1}^{M} \left(u_{mc} \cos(m\psi) + u_{ms} \sin(m\psi) \right) \right) d\psi \end{aligned} \tag{24}$$

Likewise, the equation for the i^{th} harmonic cosine (x_{ic}) and sine (x_{is}) components are obtained in Eqs. (25) and (26), respectively.

$$\begin{aligned} x''_{ic} = \frac{1}{\pi}\int_0^{2\pi} -D(\psi)\left(\dot{x}_o + \sum_{n=1}^{N}\left(x'_{nc}\cos(n\psi) + x'_{ns}\sin(n\psi)\right)\right)\cos(i\psi)d\psi \\ + \frac{1}{\pi}\int_0^{2\pi} -K(\psi)\left(x_o + \sum_{n=1}^{N}\left(x_{nc}\cos(n\psi) + x_{ns}\sin(n\psi)\right)\right)\cos(i\psi)d\psi \\ + \frac{1}{\pi}\int_0^{2\pi} G(\psi)\left(u_o + \sum_{m=1}^{M}\left(u_{mc}\cos(m\psi) + u_{ms}\sin(m\psi)\right)\right)\cos(i\psi)d\psi \end{aligned} \tag{25}$$

$$\begin{aligned} x''_{is} = \frac{1}{\pi}\int_0^{2\pi} -D(\psi)\left(\dot{x}_o + \sum_{n=1}^{N}\left(x'_{nc}\cos(n\psi) + x'_{ns}\sin(n\psi)\right)\right)\sin(i\psi)d\psi \\ + \frac{1}{\pi}\int_0^{2\pi} -K(\psi)\left(x_o + \sum_{n=1}^{N}\left(x_{nc}\cos(n\psi) + x_{ns}\sin(n\psi)\right)\right)\sin(i\psi)d\psi \\ + \frac{1}{\pi}\int_0^{2\pi} G(\psi)\left(u_o + \sum_{m=1}^{M}\left(u_{mc}\cos(m\psi) + u_{ms}\sin(m\psi)\right)\right)\sin(i\psi)d\psi \end{aligned} \tag{26}$$

Using the notation given in Eq. (27),

$$\begin{aligned} D^{nc}(\psi) &= D(\psi)\cos(n\psi) \\ D^{ns}(\psi) &= D(\psi)\sin(n\psi) \\ K^{nc}(\psi) &= K(\psi)\cos(n\psi) \\ K^{ns}(\psi) &= K(\psi)\sin(n\psi) \\ G^{mc}(\psi) &= G(\psi)\cos(m\psi) \\ G^{ms}(\psi) &= G(\psi)\sin(m\psi) \end{aligned} \tag{27}$$

Eqs. (24), (25) and (26) can be rewritten in the following form: Eqs. (28), (29) and (30).

$$\ddot{x}_o = \frac{1}{2\pi}\int_0^{2\pi}\left(-D(\psi)\dot{x}_o - \sum_{n=1}^{N}\left(D^{nc}(\psi)\dot{x}_{nc} + D^{ns}(\psi)\dot{x}_{ns}\right) - \sum_{n=1}^{N}\left(n\Omega D^{nc}(\psi)x_{ns} - n\Omega D^{ns}(\psi)x_{nc}\right)\right)d\psi \quad (28)$$
$$+\frac{1}{2\pi}\int_0^{2\pi}\left(-K(\psi)x_o - \sum_{n=1}^{N}\left(K^{nc}(\psi)x_{nc} + K^{ns}(\psi)x_{ns}\right) + G(\psi)u_o + \sum_{m=1}^{M}\left(G^{mc}(\psi)u_{mc} + G^{ms}(\psi)u_{ms}\right)\right)d\psi$$

$$\ddot{x}_{ic} = (i\Omega)^2 x_{ic} - 2i\Omega\dot{x}_{is}$$
$$+\frac{1}{\pi}\int_0^{2\pi}\left(-D(\psi)\dot{x}_o - \sum_{n=1}^{N}\left(D^{nc}(\psi)\dot{x}_{nc} + D^{ns}(\psi)\dot{x}_{ns}\right) - \sum_{n=1}^{N}\left(n\Omega D^{nc}(\psi)x_{ns} - n\Omega D^{ns}(\psi)x_{nc}\right)\right)\cos(i\psi)d\psi \quad (29)$$
$$+\frac{1}{\pi}\int_0^{2\pi}\left(-K(\psi)x_o - \sum_{n=1}^{N}\left(K^{nc}(\psi)x_{nc} + K^{ns}(\psi)x_{ns}\right) + G(\psi)u_o + \sum_{m=1}^{M}\left(G^{mc}(\psi)u_{mc} + G^{ms}(\psi)u_{ms}\right)\right)\cos(i\psi)d\psi$$
$$i = 1, 2, 3, ...N$$

$$\ddot{x}_{is} = (i\Omega)^2 x_{is} + 2i\Omega\dot{x}_{ic}$$
$$+\frac{1}{\pi}\int_0^{2\pi}\left(-D(\psi)\dot{x}_o - \sum_{n=1}^{N}\left(D^{nc}(\psi)\dot{x}_{nc} + D^{ns}(\psi)\dot{x}_{ns}\right) - \sum_{n=1}^{N}\left(n\Omega D^{nc}(\psi)x_{ns} - n\Omega D^{ns}(\psi)x_{nc}\right)\right)\sin(i\psi)d\psi \quad (30)$$
$$+\frac{1}{\pi}\int_0^{2\pi}\left(-K(\psi)x_o - \sum_{n=1}^{N}\left(K^{nc}(\psi)x_{nc} + K^{ns}(\psi)x_{ns}\right) + G(\psi)u_o + \sum_{m=1}^{M}\left(G^{mc}(\psi)u_{mc} + G^{ms}(\psi)u_{ms}\right)\right)\sin(i\psi)d\psi$$
$$i = 1, 2, 3, ...N$$

After defining the operators given in Eq. (31), equations for the state vectors of LTI take their final form in Eqs. (32), (33) and (34).

$$H_{oM} = \frac{1}{2\pi}\int_0^{2\pi} M(\psi)d\psi$$
$$H_{icM} = \frac{1}{\pi}\int_0^{2\pi} M(\psi)\cos i\psi\, d\psi \quad (31)$$
$$H_{isM} = \frac{1}{\pi}\int_0^{2\pi} M(\psi)\sin i\psi\, d\psi$$
$$i = 1, 2, 3, ...N$$

$$\ddot{x}_o = -H_{oD}\dot{x}_o - \sum_{n=1}^{N}\left(H_{oD^{nc}}\dot{x}_{nc} + H_{oD^{ns}}\dot{x}_{ns}\right) - \sum_{n=1}^{N}\left(n\Omega H_{oD^{nc}}x_{ns} - n\Omega H_{oD^{ns}}x_{nc}\right)$$
$$- H_{oK}x_o - \sum_{n=1}^{N}\left(H_{oK^{nc}}x_{nc} + H_{oK^{ns}}x_{ns}\right) + H_{oG}u_o + \sum_{m=1}^{M}\left(H_{oG^{mc}}u_{mc} + H_{oG^{ms}}u_{ms}\right) \tag{32}$$

$$\ddot{x}_{ic} = (i\Omega)^2 x_{ic} - 2i\Omega\dot{x}_{is} - H_{icD}\dot{x}_o - \sum_{n=1}^{N}\left(H_{icD^{nc}}\dot{x}_{nc} + H_{icD^{ns}}\dot{x}_{ns}\right) - \sum_{n=1}^{N}\left(n\Omega H_{icD^{nc}}x_{ns} - n\Omega H_{icD^{ns}}x_{nc}\right)$$
$$- H_{icK}x_o - \sum_{n=1}^{N}\left(H_{icK^{nc}}x_{nc} + H_{icK^{ns}}x_{ns}\right) + H_{icG}u_o + \sum_{m=1}^{M}\left(H_{icG^{mc}}u_{mc} + H_{icG^{ms}}u_{ms}\right) \tag{33}$$
$$i = 1, 2, 3, ...N$$

$$\ddot{x}_{is} = (i\Omega)^2 x_{is} + 2i\Omega\dot{x}_{ic} - H_{isD}\dot{x}_o - \sum_{n=1}^{N}\left(H_{isD^{nc}}\dot{x}_{nc} + H_{isD^{ns}}\dot{x}_{ns}\right) - \sum_{n=1}^{N}\left(n\Omega H_{isD^{nc}}x_{ns} - n\Omega H_{isD^{ns}}x_{nc}\right)$$
$$- H_{isK}x_o - \sum_{n=1}^{N}\left(H_{isK^{nc}}x_{nc} + H_{isK^{ns}}x_{ns}\right) + H_{isG}u_o + \sum_{m=1}^{M}\left(H_{isG^{mc}}u_{mc} + H_{isG^{ms}}u_{ms}\right) \tag{34}$$
$$i = 1, 2, 3, ...N$$

Likewise, approximation to the output vector y given in Eq. (15) can be substituted into the output equation of LTP model, Eq. (11).

$$y_o + \sum_{l=1}^{L}\left(y_{l.c}\cos(l\psi) + y_{l.s}\sin(l\psi)\right) = Q(\psi)\left(\dot{x}_o + \sum_{n=1}^{N}\left(x'_{nc}\cos(n\psi) + x'_{ns}\sin(n\psi)\right)\right)$$
$$+ P(\psi)\left(x_o + \sum_{n=1}^{N}\left(x_{nc}\cos(n\psi) + x_{ns}\sin(n\psi)\right)\right) \tag{35}$$
$$+ R(\psi)\left(u_o + \sum_{m=1}^{M}\left(u_{mc}\cos(m\psi) + u_{ms}\sin(m\psi)\right)\right)$$

Extraction of the average and harmonic components of Eq. (35) yields the individual expressions for y_o, y_{lc} and y_{ls} as given in Eqs. (36), (37) and (38), respectively.

$$
\begin{aligned}
y_o = & \frac{1}{2\pi}\int_0^{2\pi}\left(Q(\psi)\left(\dot{x}_o + \sum_{n=1}^{N}\left(\dot{x}_{nc}\cos(n\psi) + \dot{x}_{ns}\sin(n\psi)\right)\right)\right)d\psi \\
& + \frac{1}{2\pi}\int_0^{2\pi}\left(Q(\psi)\left(\sum_{n=1}^{N}\left(n\Omega x_{ns}\cos(n\psi) - n\Omega x_{nc}\sin(n\psi)\right)\right)\right)d\psi \\
& + \frac{1}{2\pi}\int_0^{2\pi}\left(P(\psi)\left(x_o + \sum_{n=1}^{N}\left(x_{nc}\cos(n\psi) + x_{ns}\sin(n\psi)\right)\right)\right)d\psi \\
& + \frac{1}{2\pi}\int_0^{2\pi}\left(R(\psi)\left(u_o + \sum_{m=1}^{M}\left(u_{mc}\cos(m\psi) + u_{ms}\sin(m\psi)\right)\right)\right)d\psi
\end{aligned}
\tag{36}
$$

$$
\begin{aligned}
y_{lc} = & \frac{1}{\pi}\int_0^{2\pi}\left(Q(\psi)\left(\dot{x}_o + \sum_{n=1}^{N}\left(\dot{x}_{nc}\cos(n\psi) + \dot{x}_{ns}\sin(n\psi)\right)\right)\right)\cos(l\psi)d\psi \\
& + \frac{1}{\pi}\int_0^{2\pi}\left(Q(\psi)\left(\sum_{n=1}^{N}\left(n\Omega x_{ns}\cos(n\psi) - n\Omega x_{nc}\sin(n\psi)\right)\right)\right)\cos(l\psi)d\psi \\
& + \frac{1}{\pi}\int_0^{2\pi}\left(P(\psi)\left(x_o + \sum_{n=1}^{N}\left(x_{nc}\cos(n\psi) + x_{ns}\sin(n\psi)\right)\right)\right)\cos(l\psi)d\psi \\
& + \frac{1}{\pi}\int_0^{2\pi}\left(R(\psi)\left(u_o + \sum_{m=1}^{M}\left(u_{mc}\cos(m\psi) + u_{ms}\sin(m\psi)\right)\right)\right)\cos(l\psi)d\psi
\end{aligned}
\tag{37}
$$

$$
\begin{aligned}
y_{ls} = & \frac{1}{\pi}\int_0^{2\pi}\left(Q(\psi)\left(\dot{x}_o + \sum_{n=1}^{N}\left(\dot{x}_{nc}\cos(n\psi) + \dot{x}_{ns}\sin(n\psi)\right)\right)\right)\sin(l\psi)d\psi \\
& + \frac{1}{\pi}\int_0^{2\pi}\left(Q(\psi)\left(\sum_{n=1}^{N}\left(n\Omega x_{ns}\cos(n\psi) - n\Omega x_{nc}\sin(n\psi)\right)\right)\right)\sin(l\psi)d\psi \\
& + \frac{1}{\pi}\int_0^{2\pi}\left(P(\psi)\left(x_o + \sum_{n=1}^{N}\left(x_{nc}\cos(n\psi) + x_{ns}\sin(n\psi)\right)\right)\right)\sin(l\psi)d\psi \\
& + \frac{1}{\pi}\int_0^{2\pi}\left(R(\psi)\left(u_o + \sum_{m=1}^{M}\left(u_{mc}\cos(m\psi) + u_{ms}\sin(m\psi)\right)\right)\right)\sin(l\psi)d\psi
\end{aligned}
\tag{38}
$$

$$
\begin{aligned}
Q^{nc}(\psi) &= Q(\psi)\cos(n\psi) \\
Q^{ns}(\psi) &= Q(\psi)\sin(n\psi) \\
P^{nc}(\psi) &= P(\psi)\cos(n\psi) \\
P^{ns}(\psi) &= P(\psi)\sin(n\psi) \\
R^{mc}(\psi) &= R(\psi)\cos(m\psi) \\
R^{ms}(\psi) &= R(\psi)\sin(m\psi)
\end{aligned}
\tag{39}
$$

Using the notation defined in Eq. (39) and also making use of the same operator defined in Eq. (31), harmonic components of the output vector are obtained in Eqs. (40), (41) and (42).

$$
\begin{aligned}
y_o = {} & H_{oQ}\dot{x}_o + \sum_{n=1}^{N}\left(H_{oQ^{nc}}\dot{x}_{nc} + H_{oQ^{ns}}\dot{x}_{ns}\right) + \sum_{n=1}^{N}\left(n\Omega H_{oQ^{nc}}x_{ns} - n\Omega H_{oQ^{ns}}x_{nc}\right) \\
& + H_{oP}x_o + \sum_{n=1}^{N}\left(H_{oP^{nc}}x_{nc} + H_{oP^{ns}}x_{ns}\right) + H_{oR}u_o + \sum_{m=1}^{M}\left(H_{oR^{mc}}u_{mc} + H_{oR^{ms}}u_{ms}\right)
\end{aligned}
\tag{40}
$$

$$
\begin{aligned}
y_{lc} = {} & H_{lcQ}\dot{x}_o + \sum_{n=1}^{N}\left(H_{lcQ^{nc}}\dot{x}_{nc} + H_{lcQ^{ns}}\dot{x}_{ns}\right) + \sum_{n=1}^{N}\left(n\Omega H_{lcQ^{nc}}x_{ns} - n\Omega H_{lcQ^{ns}}x_{nc}\right) \\
& + H_{lcP}x_o + \sum_{n=1}^{N}\left(H_{lcP^{nc}}x_{nc} + H_{lcP^{ns}}x_{ns}\right) + H_{lcR}u_o + \sum_{m=1}^{M}\left(H_{lcR^{mc}}u_{mc} + H_{lcR^{ms}}u_{ms}\right)
\end{aligned}
\tag{41}
$$

$$
\begin{aligned}
y_{ls} = {} & H_{lsQ}\dot{x}_o + \sum_{n=1}^{N}\left(H_{lsQ^{nc}}\dot{x}_{nc} + H_{lsQ^{ns}}\dot{x}_{ns}\right) + \sum_{n=1}^{N}\left(n\Omega H_{lsQ^{nc}}x_{ns} - n\Omega H_{lsQ^{ns}}x_{nc}\right) \\
& + H_{lsP}x_o + \sum_{n=1}^{N}\left(H_{lsP^{nc}}x_{nc} + H_{lsP^{ns}}x_{ns}\right) + H_{lsR}u_o + \sum_{m=1}^{M}\left(H_{lsR^{mc}}u_{mc} + H_{lsR^{ms}}u_{ms}\right)
\end{aligned}
\tag{42}
$$

The final expressions that form the elements of Eqs. (19) and (20), presented also in [54], are included in the following:

$$A_{11}=\begin{bmatrix} 0.....0 & 0.....0 & 0..... \\ \cdots\cdots & \cdots\cdots & \cdots\cdots \\ 0.....0 & 0.....0 & 0..... \\ 0.....0 & 0.....0 & 0..... \\ \cdots\cdots & \cdots\cdots & \cdots\cdots \\ 0.....0 & 0.....0 & 0..... \\ 0.....0 & 0.....0 & 0..... \\ \cdots\cdots & \cdots\cdots & \cdots\cdots \end{bmatrix} \tag{43}$$

$$A_{12}=\begin{bmatrix} I.....0 & 0.....0 & 0..... \\ \cdots\cdots & \cdots\cdots & \cdots\cdots \\ 0.....I & 0.....0 & 0..... \\ 0.....0 & I.....0 & 0..... \\ \cdots\cdots & \cdots\cdots & \cdots\cdots \\ 0.....0 & 0.....I & 0..... \\ 0.....0 & 0.....0 & I..... \\ \cdots\cdots & \cdots\cdots & \cdots\cdots \end{bmatrix} \tag{44}$$

$$A_{21}=\begin{bmatrix} -H_{oK}\ldots(-H_{oK^{ic}}+i\Omega H_{oD^{is}}) & (-H_{oK^{is}}-i\Omega H_{oD^{ic}})\ldots(-H_{oK^{jc}}+j\Omega H_{oD^{js}}) & (-H_{oK^{js}}-j\Omega H_{oD^{jc}})\ldots\ldots \\ \cdots\cdots & \cdots\cdots & \cdots\cdots \\ -H_{icK}\ldots(i^2\Omega^2 I-H_{icK^{ic}}+i\Omega H_{icD^{is}}) & (-H_{icK^{is}}-i\Omega H_{icD^{ic}})\ldots(-H_{icK^{jc}}+j\Omega H_{icD^{js}}) & (-H_{icK^{js}}-j\Omega H_{icD^{jc}})\ldots\ldots \\ -H_{isK}\ldots(-H_{isK^{ic}}+i\Omega H_{isD^{is}}) & (i^2\Omega^2 I-H_{isK^{is}}-i\Omega H_{isD^{ic}})\ldots(-H_{isK^{jc}}+j\Omega H_{isD^{js}} & (-H_{isK^{js}}-j\Omega H_{isD^{jc}})\ldots\ldots \\ \cdots\cdots & \cdots\cdots & \cdots\cdots \\ -H_{jcK}\ldots(-H_{jcK^{ic}}+i\Omega H_{jcD^{is}}) & (-H_{jcK^{is}}-i\Omega H_{jcD^{ic}})\ldots(j^2\Omega^2 I-H_{jcK^{jc}}+j\Omega H_{jcD^{js}}) & (-H_{jcK^{js}}-j\Omega H_{jcD^{jc}})\ldots \\ -H_{jsK}\ldots(-H_{jsK^{ic}}+i\Omega H_{jsD^{is}}) & (-H_{jsK^{is}}-i\Omega H_{jsD^{ic}})\ldots(-H_{jsK^{jc}}+j\Omega H_{jsD^{js}}) & (j^2\Omega^2 I-H_{jsK^{js}}-j\Omega H_{jsD^{jc}})\ldots \\ \cdots\cdots & \cdots\cdots & \cdots\cdots \end{bmatrix} \tag{45}$$

$$A_{22}=\begin{bmatrix} -H_{oD}.....-H_{oD^{ic}} & -H_{oD^{is}}....-H_{oD^{jc}} & -H_{oD^{js}}..... \\ ..... & & \\ -H_{icD}...-H_{icD^{ic}} & (-2i\Omega I-H_{icD^{is}})..-H_{icD^{jc}} & -H_{icD^{js}}..... \\ -H_{isD}....(2i\Omega I-H_{isD_{ic}}) & -H_{isD_{is}}...-H_{isD_{jc}} & -H_{isD_{js}}..... \\ ..... & & \\ -H_{jcD}...-H_{jcD^{ic}} & -H_{jcD^{is}}..-H_{jcD^{jc}} & (-2j\Omega I-H_{jcD^{js}})..... \\ -H_{jsD}....-H_{jsD^{ic}} & -H_{jsD^{is}}...(2j\Omega I-H_{jsD^{jc}}) & -H_{jsD^{js}}..... \\ ..... & & \end{bmatrix} \tag{46}$$

$$B_1=\begin{bmatrix} 0 \\ . \\ 0 \\ 0 \\ . \\ 0 \\ 0 \\ . \end{bmatrix} \tag{47}$$

$$B_2=\begin{bmatrix} H_{oG}...H_{oG^{mc}} & H_{oG^{ms}}... \\ ..... & \\ H_{icG}...H_{icG^{mc}} & H_{icG^{ms}}... \\ H_{isG}...H_{isG^{mc}} & H_{isG^{ms}}... \\ ..... & \\ H_{jcG}...H_{jcG^{mc}} & H_{jcG^{ms}}... \\ H_{jsG}...H_{jsG^{mc}} & H_{jsG^{ms}}... \\ ..... & \end{bmatrix} \tag{48}$$

$$C_1=\begin{bmatrix} H_{oP}...(H_{oP^{ic}}-i\Omega H_{oQ^{is}}) & (H_{oP^{is}}+i\Omega H_{oQ^{ic}})...(H_{oP^{jc}}-j\Omega H_{oQ^{js}}) & (H_{oP^{js}}+j\Omega H_{oQ^{ic}}).....\\ ..... & & \\ H_{lcP}...(H_{lcP^{ic}}-i\Omega H_{lcQ^{is}}) & (H_{lcP^{is}}+i\Omega H_{lcQ^{ic}})...(H_{lcP^{jc}}-j\Omega H_{lcQ^{js}}) & (H_{lcP^{js}}+j\Omega H_{lcQ^{jc}}).....\\ H_{lsP}...(H_{lsP^{ic}}-i\Omega H_{lsQ^{is}}) & (H_{lsP^{is}}+i\Omega H_{lsQ^{ic}})....(H_{lsP^{jc}}-j\Omega H_{lsQ^{js}} & (H_{lsP^{js}}+j\Omega H_{lsQ^{jc}})..... \\ ..... & & \end{bmatrix} \tag{49}$$

$$C_2 = \begin{bmatrix} . H_{oQ} ..... H_{oQ^{ic}} & H_{oQ^{is}} .... H_{oQ^{jc}} & H_{oQ^{js}} ..... \\ ..... & ..... & ..... \\ .. H_{lcQ} ... H_{lcQ^{ic}} & H_{lcQ^{is}} .. H_{lcQ^{jc}} & H_{lcQ^{js}} ..... \\ H_{lsQ} .... H_{lsQ^{ic}} & H_{lsQ^{is}} ... H_{lsQ^{jc}} & H_{lsQ^{js}} ..... \\ ..... & ..... & ..... \end{bmatrix} \tag{50}$$

$$E = \begin{bmatrix} H_{oR} ... H_{oR^{mc}} & H_{oR^{ms}} ... \\ ..... & ..... \\ H_{lcR} ... H_{lcR^{mc}} & H_{lcR^{ms}} ... \\ H_{lsR} ... H_{lsR^{mc}} & H_{lsR^{ms}} ... \\ ..... & ..... \end{bmatrix} \tag{51}$$

Closed form expressions for the various elements of A_{12}, A_{22}, B_2, C_1, C_2 and E can be obtained in terms of the harmonic components of the LTP model matrices *D, K, G, P, Q* and *R*. For example, if the matrix $D(\psi)$ is expanded in terms of its harmonic components as

$$D(\psi) = D_o + \sum_{k=1}^{\infty} (D_{kc} \cos k\psi + D_{ks} \sin k\psi) \tag{52}$$

where D_o is the average component and D_{kc}, D_{ks} are respectively the k^{th} harmonic cosine and sine components of the matrix $D(\psi)$ such that

$$\begin{aligned} D_o &= \frac{1}{2\pi} \int_0^{2\pi} D(\psi) d\psi \\ D_{kc} &= \frac{1}{\pi} \int_0^{2\pi} D(\psi) \cos k\psi \, d\psi \\ D_{ks} &= \frac{1}{\pi} \int_0^{2\pi} D(\psi) \sin k\psi \, d\psi \\ & \qquad k = 1, 2, 3, ... \end{aligned} \tag{53}$$

then

$$H_{oD} = \frac{1}{2\pi}\int_0^{2\pi} D(\psi)d\psi = D_o$$

$$H_{oD^{ic}} = \frac{1}{2\pi}\int_0^{2\pi} D(\psi)\cos i\psi\, d\psi = \frac{D_{ic}}{2} \qquad (54)$$

$$H_{oD^{is}} = \frac{1}{2\pi}\int_0^{2\pi} D(\psi)\sin i\psi\, d\psi = \frac{D_{is}}{2}$$

$$i = 1, 2, 3, \ldots\ldots$$

$$H_{icD} = \frac{1}{\pi}\int_0^{2\pi} D(\psi)\cos i\psi\, d\psi = D_{ic} \qquad (55)$$

$$H_{isD} = \frac{1}{\pi}\int_0^{2\pi} D(\psi)\sin i\psi\, d\psi = D_{is}$$

$$i = 1, 2, 3, \ldots\ldots$$

$$H_{icD^{jc}} = \frac{1}{\pi}\int_0^{2\pi} D(\psi)\cos j\psi\cos i\psi\, d\psi$$

$$= D_o + \frac{D_{kc}}{2} \quad for\ \ i = j\ \ where\ k = i + j$$

$$= \frac{D_{kc} + D_{lc}}{2} \quad for\ \ i \neq j\ \ and\ i > j \qquad (56)$$

$$where\ k = i + j,\ \ l = i - j$$

$$= \frac{D_{kc} + D_{mc}}{2} \quad for\ \ i \neq j\ \ and\ \ j > i$$

$$where\ k = i + j,\ \ m = j - i$$

$$i = 1, 2, ..\ \ and\ \ j = 1, 2, ..$$

$$H_{icD^{js}} = \frac{1}{\pi}\int_0^{2\pi} D(\psi)\sin j\psi\cos i\psi\, d\psi$$

$$= \frac{D_{ks}}{2} \quad for\ \ i = j\ \ where\ k = i + j$$

$$= \frac{D_{ks} - D_{ls}}{2} \quad for\ \ i \neq j\ \ and\ i > j \qquad (57)$$

$$where\ k = i + j,\ \ l = i - j$$

$$= \frac{D_{ks} + D_{ms}}{2} \quad for\ \ i \neq j\ \ and\ \ j > i$$

$$where\ k = i + j,\ \ m = j - i$$

$$i = 1, 2, ..and\ \ \ j = 1, 2, ...$$

$$
\begin{aligned}
H_{isD^{jc}} &= \frac{1}{\pi}\int_0^{2\pi} D(\psi)\cos j\psi \sin i\psi \, d\psi \\
&= \frac{D_{ks}}{2} \quad for \;\; i = j \;\; where \; k = i + j \\
&= \frac{D_{ks} + D_{ls}}{2} \quad for \;\; i \neq j \;\; and \;\; i > j \\
&\qquad\qquad where \; k = i + j, \;\; l = i - j \\
&= \frac{D_{ks} - D_{ms}}{2} \quad for \;\; i \neq j \;\; and \;\; j > i \\
&\qquad\qquad where \; k = i + j, \;\; m = j - i \\
&\qquad\qquad i = 1, 2, \ldots \;\; and \;\; j = 1, 2, \ldots .
\end{aligned}
\tag{58}
$$

$$
\begin{aligned}
H_{isD^{js}} &= \frac{1}{\pi}\int_0^{2\pi} D(\psi)\sin j\psi \sin i\psi \, d\psi \\
&= D_o - \frac{D_{kc}}{2} \quad for \;\; i = j \;\; where \; k = i + j \\
&= \frac{D_{lc} - D_{kc}}{2} \quad for \;\; i \neq j \;\; and \; i > j \\
&\qquad\qquad where \; k = i + j, \;\; l = i - j \\
&= \frac{D_{mc} - D_{kc}}{2} \quad for \;\; i \neq j \;\; and \;\; j > i \\
&\qquad\qquad where \; k = i + j, \;\; m = j - i \\
&\qquad\qquad i = 1, 2, .. \; and \;\; j = 1, 2, ..
\end{aligned}
\tag{59}
$$

Likewise, expressions similar to the above can be obtained for the elements of the LTI model matrices involving “K”, “G”, “P”, “Q” and “R”. Following two examples and a generic example for even harmonic coefficients up to 8/rev in the Appendix titled as "LTI* Example" are given in order to support the understanding of LTI equation derived in this study.

Example 1.

For example, if one considers only the average component (x_o) and the 4th harmonic components (x_{4c}, x_{4s}) for an approximate LTI model, with

$$
X = \begin{bmatrix} x_o^T & x_{4c}^T & x_{4s}^T & \dot{x}_o^T & \dot{x}_{4c}^T & \dot{x}_{4s}^T \end{bmatrix}^T
$$

$$
\dot{X} = \begin{bmatrix} A_{11} & & A_{12} \\ A_{21} & & A_{22} \end{bmatrix} X + \begin{bmatrix} B \end{bmatrix}
$$

then where

$$A_{11} = \begin{bmatrix} 0 & 0 & 0 \\ 0 & 0 & 0 \\ 0 & 0 & 0 \end{bmatrix} \qquad A_{12} = \begin{bmatrix} I & 0 & 0 \\ 0 & I & 0 \\ 0 & 0 & I \end{bmatrix}$$

$$A_{21} = \begin{bmatrix} -H_{oK} & (-H_{oK_{4c}} + 4\Omega H_{oD_{4s}}) & (-H_{oK_{4s}} - 4\Omega H_{oD_{4c}}) \\ -H_{4cK} & (16\Omega^2 I - H_{4cK_{4c}} + 4\Omega H_{4cD_{4s}}) & (-H_{4cK_{4s}} - 4\Omega H_{4cD_{4c}}) \\ -H_{4sK} & (-H_{4sK_{4c}} + 4\Omega H_{4sD_{4s}}) & (16\Omega^2 I - H_{4sK_{4s}} - 4\Omega H_{4sD_{4c}}) \end{bmatrix}$$

$$A_{22} = \begin{bmatrix} -H_{oD} & -H_{oD_{4c}} & -H_{oD_{4s}} \\ -H_{4cD} & -H_{4cD_{4c}} & (-8\Omega I - H_{4cD_{4s}}) \\ -H_{4sD} & (8\Omega I - H_{4sD_{4c}}) & -H_{4sD_{4s}} \end{bmatrix}$$

$$B = \begin{bmatrix} 0 \\ 0 \\ 0 \\ H_{oG}u_o + \sum_{m=1}^{M} (H_{oG_{mc}}u_{mc} + H_{oG_{ms}}u_{ms}) \\ H_{4cG}u_o + \sum_{m=1}^{M} (H_{4cG_{mc}}u_{mc} + H_{4cG_{ms}}u_{ms}) \\ H_{4sG}u_o + \sum_{m=1}^{M} (H_{4sG_{mc}}u_{mc} + H_{4sG_{ms}}u_{ms}) \end{bmatrix}$$

Example 2.

If one considers only the average and the 1st harmonic components only, with

$$X = \begin{bmatrix} x_o^T & x_{1c}^T & x_{1s}^T & \dot{x}_o^T & \dot{x}_{1c}^T & \dot{x}_{1s}^T \end{bmatrix}^T$$

then

$$\dot{X} = \begin{bmatrix} A_{11} & A_{12} \\ A_{21} & A_{22} \end{bmatrix} X + \begin{bmatrix} B_1 \\ B_2 \end{bmatrix}$$

where

$$A_{11} = \begin{bmatrix} 0 & 0 & 0 \\ 0 & 0 & 0 \\ 0 & 0 & 0 \end{bmatrix} \qquad A_{12} = \begin{bmatrix} I & 0 & 0 \\ 0 & I & 0 \\ 0 & 0 & I \end{bmatrix}$$

$$A_{12} = \begin{bmatrix} -H_{oK} & (-H_{oK_{1c}} + \Omega H_{oD_{1s}}) & (-H_{oK_{4s}} - \Omega H_{oD_{1c}}) \\ -H_{1cK} & (\Omega^2 I - H_{1cK_{1c}} + \Omega H_{1cD_{1s}}) & (-H_{1cK_{1s}} - \Omega H_{1cD_{1c}}) \\ -H_{1sK} & (-H_{1sK_{1c}} + \Omega H_{1sD_{1s}}) & (\Omega^2 I - H_{1sK_{1s}} - \Omega H_{1sD_{1c}}) \end{bmatrix}$$

$$A_{22} = \begin{bmatrix} -H_{oD} & -H_{oD_{1c}} & -H_{oD_{1s}} \\ -H_{1cD} & -H_{1cD_{1c}} & (-2\Omega I - H_{1cD_{1s}}) \\ -H_{1sD} & (2\Omega I - H_{1sD_{4c}}) & -H_{1sD_{1s}} \end{bmatrix}$$

$$B_1 = \begin{bmatrix} 0 \\ 0 \\ 0 \end{bmatrix} \qquad B_2 = \begin{bmatrix} H_{oG}u_o + \sum_{m=1}^{M} (H_{oG_{mc}}u_{mc} + H_{oG_{ms}}u_{ms}) \\ H_{1cG}u_o + \sum_{m=1}^{M} (H_{1cG_{mc}}u_{mc} + H_{1cG_{ms}}u_{ms}) \\ H_{1sG}u_o + \sum_{m=1}^{M} (H_{1sG_{mc}}u_{mc} + H_{1sG_{ms}}u_{ms}) \end{bmatrix}$$

2.3.1 LTI Models from FLIGHTLAB

The LTI model extraction method described in the previous section is implemented within FLIGHTLAB [55] using the generalized force formulation written as

$$Q = f(U, X, \dot{X}, \ddot{X}) \tag{60}$$

where Q is the equation imbalance of Eq. (60). The control at each time step is iteratively solved to drive *Q* to zero for trim. The nonlinear model is first trimmed at a specified flight condition. Then a reference blade is set to the zero azimuth position and the periodic trim condition is recorded over one rotor revolution. With the reference blade at selected azimuthal steps, the values of *Q* due to perturbations in state/control are computed at each azimuthal step, and system matrices are obtained by computing the partial derivatives of *Q* with respect to individual state/control through central finite differencing. For example,

$$\frac{\partial f}{\partial X} \approx \frac{f(\overline{X}+\Delta X, \dot{\overline{X}}, \ddot{\overline{X}}, \overline{U}) - f(\overline{X}-\Delta X, \dot{\overline{X}}, \ddot{\overline{X}}, \overline{U})}{2\Delta X} \tag{61}$$

where ΔX is the selected value of the numerical perturbation. Likewise, partial derivatives of the output with respect to state/control perturbations are obtained. The numerically computed partial derivatives are used to assemble the LTP model matrices D(ψ), K(ψ), etc., using Eqs. (7) and (12) at the current azimuthal step. Also, additional components, such as D(ψ)·cos(kψ), D(ψ)·sin(kψ), K(ψ)·cos(kψ), K(ψ)·sin(kψ), etc., k=0, 1, 2,… required for harmonic decomposition (see Eq. 53) are also generated at each azimuthal step of the linearization. Therefore, once the linearization process is completed over one rotor revolution, it only takes a few algebraic operations (using Eqs. 43 through 51 and 53 through 59) to obtain an LTI model of selected order. The linearization can be configured to generate either a full, linearized model or a reduced order model as desired. For reduced order models, particularly the full rotorcraft models in this study, a quasi-static model reduction technique is applied by selecting the dynamically retained states while residualizing the neglected dynamics.

2.3.2 Computational Efficiency

Individual blade control (IBC) and On-Blade Control (OBC) inputs excite higher frequencies. A careful study is required to make an assessment of the number of harmonic states needed for good fidelity. As the required number of harmonic rotor states increases, the computational effort involved in the extraction of LTI model also increases. An assessment was made of the number of floating point operations (FLOP, see [69]) needed for an LTI model extraction. It was seen that with the current approach, the number of FLOP increases linearly with an increase in the number of harmonic states of the LTI model. This is in contrast to roughly a quadratic increase in number of FLOP with the number of harmonic states using the numerical scheme proposed in [11, 27] which involved individual harmonic component perturbations.

CHAPTER 3 LTI MODEL STABILITY PROPERTY EVALUATIONS

In this chapter, stability aspects of the LTI models as obtained from analytical and FLIGHTLAB models are studied. The objective is to understand the stability properties of the LTI models in contrast with the reference LTP model from which they are originated and to define viable fidelity criteria in terms of eigenvalue comparisons between LTP and LTI systems so that a concrete basis can be constructed for the fidelity of stability characteristics.

The chapter first introduces the models used for stability property evaluations. These are analytical models used to gain a fundamental understanding of and to test the validity of the methodology for stability characteristics of LTI models. The FLIGHTLAB models progressively improved to reach the generic helicopter model. Then the chapter continues by demonstrating the stability aspects of the LTI models, with results similar to the available results in the literature. The third section defines the self-claimed metric for the fidelity of the stability properties, including the rationale behind it. The accuracy of LTP results poses a challenge in this study, which was also noted in the literature review section, and the methodology for better accuracy of LTP models and achieved accuracy is explained in the forth section.

The fifth section explains in detail the proposed methodology, which covers the process of eigenvalue and eigenvector extraction from LTP and LTI models, and explains how the eigenvalues from each model are selected for comparison. Here, the self-claimed criteria is used. Sections 6 and 7 apply this methodology to analytical and FLIGHTLAB models, respectively. The analytical models and isolated rotor models of

FLIGHTLAB are intended to build an understanding of LTI stability characteristics and to help identify possible issues that may arise in a more complicated way in rotorcraft models.

3.1 Stability Aspects of Linear Time Invariant Models

Similar to the sine and cosine harmonic decomposition of rotor states as pseudo states considered in [11,27,47,56,54], a complementary approach known as Hill's Method [20, 57], which uses a complex representation of the harmonic decomposition of rotor states, has been developed in the literature. The stability properties of the resulting reduced order LTI models from Hill's Method have been investigated for non-rotorcraft applications, such as wind turbines [9], rotating bladed disks [58], and power electronics [59], etc., very few such results exist for rotorcraft applications in the literature in regard to the literature review made for this study. Further, stability results from such non-rotorcraft applications may not be directly transferrable to rotorcraft applications, as those non-rotorcraft applications are mostly void of the important and often complex rotor/body dynamic interactions present in a rotorcraft. Moreover, former [11, 27] and current LTI methods treat the body and inflow states with only average portion of the harmonic decomposition. The focus of this section is to fill this void in the literature through a systematic evaluation of the stability properties of reduced order LTI models extracted from a helicopter nonlinear model. The stability evaluations are carried out with different levels of LTI model approximations of the coupled rotor, inflow and body dynamics using a generic helicopter model available in FLIGHTLAB. The importance of this study is an understanding of the minimum number of harmonic rotor states needed

in the LTI model formulation in order to capture the stability properties, to a required level of fidelity, of selected modes of a nonlinear helicopter model.

In this study, the LTI model stability investigations were carried out using analytical and numerical FLIGHTLAB models. First, the stability properties of the nonlinear model about a selected equilibrium flight condition were obtained through a Floquet analysis of linear time periodic (LTP) models extracted from the nonlinear model in the vicinity of a periodic equilibrium. In order to arrive at the same level of accuracy with the analytical model, the study performed harmonic decomposition on the LTP model and used a sufficiently high number of harmonics to represent an equivalent LTP model that bore most of the fidelity of the original LTP in an analytical form. Next, LTI models of different orders (to include different harmonic components of rotor states) were formulated using the same harmonic coefficients of the LTP model, and a conventional eigenvalue analysis of the resulting LTI models was carried out using the function “EIG” available in FLIGHTLAB based on LAPACK routines[60]. A comparison was then made between the eigenvalues of the LTP model and those of the LTI model in order to assess the accuracy and modal properties of the constructed LTI models. Although Floquet theory has the drawback of ambiguity on the imaginary part of the system eigenvalues, error estimation on the eigenvalues of the LTI model is still possible through a comparison of the real parts of the eigenvalues from LTP and LTI models. The imaginary parts can be compared between LTP and LTI if a reference eigenvalues selection can be made.

The stability aspects of the LTI models were studied through the analysis of eigenvalues and eigenvectors. As was learned from Hill’s Method studies [57, 9], the eigenvalues of the LTI models with reformulation based on frequency domain had their number of states increased; thus, number of eigenvalues also increased. These studies

showed that when the number of Fourier coefficients approaches infinity, the eigenvalues are aligned at the same value on real axis for the same mode but their imaginary part increases in both positive and negative directions by integer products of fundamental frequency, essentially at integers when eigenvalues are normalized with respect to the fundamental frequency. It was also shown that all the eigenvectors associated with the same mode matched. These properties are adopted by the current LTI formulation as it is also a frequency domain reformulation except for the fact that it makes use of the harmonic components, whereas in Hill's Method, Fourier coefficients are used. As in Hill's Method studies, the Floquet Transition Matrix method was chosen as the tool to create reference eigenvalues of the system to be compared with those of the LTI. Unfortunately there is not an explicit solution for FTM, even for the analytically represented state matrices, since it is the solution of a set of time-periodic ordinary differential equations. The best option could be adopting a power series solution method, but it is unlikely to find a solution that resembles a power series of a known analytical function. Therefore, the only choice left for the user is numerical integration.

3.2 Models for Stability Analysis

Apart from the time and frequency domain oriented models, a more fundamental modeling breakdown is followed for stability assessment purposes. These models are grouped into two, first analytical isolated rotor models available in the literature [61] are constructed for basic understanding of stability assessment issues, and then full rotorcraft models are incorporated at several modeling and configuration levels in order to make parametric assessments on the stability properties that can be captured by the LTI.

3.2.1 Analytical Model for Stability Assessment Purposes

The analytical representation of 3 and 4 bladed isolated rotors was adopted from Biggers [61]. These equations are formed under the uniform blade properties consideration and they account only for limited aerodynamic effects through the Lock number, and most importantly through the advance ratio but they do not incorporate inflow dynamics.

The flapping equation, Eq. (62), of a single blade in the rotating frame is used for a 1-DOF model for the simplest analytical study that can exhibit time periodic characteristics, which is analogous to the “Mathieu Equation” [62] used in the studies on stability of the time periodic systems.

When this equation is transformed to the non-rotating frame using Multi Blade Coordinate Transformation for 3 and 4 bladed rotors, the following forms arise having the same number of equations with the number of blades. These equations in MBC form still exhibit the periodic characteristic, but the frequencies are multipled by the number of blades.

$$\ddot{\beta}_{1c} + \frac{\gamma}{8}\dot{\beta}_{1c} + \left(\nu^2 - 1 + \mu^2 \frac{\gamma}{16}\sin(4\psi)\right)\beta = 0 \tag{62}$$

$$\begin{pmatrix} \ddot{\beta}_o \\ \ddot{\beta}_{1c} \\ \ddot{\beta}_{1s} \end{pmatrix} + \begin{bmatrix} \frac{\gamma}{8}B^4 & 0 & \mu\frac{\gamma}{12}B^3 \\ 0 & \frac{\gamma}{8}B^4 + \mu\frac{\gamma}{12}B^3\sin(3\psi) & 2 - \mu\frac{\gamma}{12}B^3\cos(3\psi) \\ \mu\frac{\gamma}{6}B^3 & -2 - \mu\frac{\gamma}{12}B^3\cos(3\psi) & \frac{\gamma}{8}B^4 - \mu\frac{\gamma}{12}B^3\sin(3\psi) \end{bmatrix} \begin{pmatrix} \dot{\beta}_o \\ \dot{\beta}_{1c} \\ \dot{\beta}_{1s} \end{pmatrix}$$

$$+ \begin{bmatrix} \nu^2 & \mu^2\frac{\gamma}{16}B^2\sin(3\psi) & -\mu^2\frac{\gamma}{16}B^2\cos(3\psi) \\ \mu\frac{\gamma}{6}B^3 + \mu^2\frac{\gamma}{8}B^2\sin(3\psi) & \nu^2 - 1 + \mu\frac{\gamma}{6}B^3\cos(3\psi) & \frac{\gamma}{8}\left(B^4 + \frac{1}{2}\mu^2B^2\right) + \mu\frac{\gamma}{6}B^3\sin(3\psi) \\ -\mu^2\frac{\gamma}{8}B^2\cos(3\psi) & -\frac{\gamma}{8}\left(B^4 - \frac{1}{2}\mu^2B^2\right) + \mu\frac{\gamma}{6}B^3\sin(3\psi) & \nu^2 - 1 - \mu\frac{\gamma}{6}B^3\cos(3\psi) \end{bmatrix} \begin{pmatrix} \beta_o \\ \beta_{1c} \\ \beta_{1s} \end{pmatrix} = \begin{pmatrix} 0 \\ 0 \\ 0 \end{pmatrix} \tag{63.a}$$

$$\begin{pmatrix} \ddot{\beta}_o \\ \ddot{\beta}_{1c} \\ \ddot{\beta}_{1s} \\ \ddot{\beta}_2 \end{pmatrix} + \begin{bmatrix} \frac{\gamma}{8}B^4 & 0 & \mu\frac{\gamma}{12}B^3 & 0 \\ 0 & \frac{\gamma}{8}B^4 & 2 & \mu\frac{\gamma}{6}B^3\sin(2\psi) \\ \mu\frac{\gamma}{6}B^3 & -2 & \frac{\gamma}{8}B^4 & -\mu\frac{\gamma}{6}B^3\cos(2\psi) \\ 0 & \mu\frac{\gamma}{12}B^3\sin(2\psi) & -\mu\frac{\gamma}{12}B^2\cos(2\psi) & \frac{\gamma}{8}B^4 \end{bmatrix} \begin{pmatrix} \dot{\beta}_o \\ \dot{\beta}_{1c} \\ \dot{\beta}_{1s} \\ \dot{\beta}_2 \end{pmatrix}$$

$$+ \begin{bmatrix} \nu^2 & 0 & 0 & \mu^2\frac{\gamma}{8}B^2\sin(2\psi) \\ \mu\frac{\gamma}{6}B^3 & \nu^2 - 1 + \mu^2\frac{\gamma}{16}B^2\sin(4\psi) & \frac{\gamma}{8}\left(B^4 + \frac{1}{2}\mu^2B^2 - \frac{1}{2}\mu^2B^2\cos(4\psi)\right) & \mu\frac{\gamma}{6}B^3\cos(2\psi) \\ 0 & -\frac{\gamma}{8}\left(B^4 - \frac{1}{2}\mu^2B^2 + \frac{1}{2}\mu^2B^2\cos(4\psi)\right) & \nu^2 - 1 - \mu^2\frac{\gamma}{16}B^2\sin(4\psi) & \mu\frac{\gamma}{6}B^3\sin(2\psi) \\ \mu^2\frac{\gamma}{8}B^2\sin(2\psi) & \mu\frac{\gamma}{6}B^3\cos(2\psi) & \mu\frac{\gamma}{6}B^3\sin(2\psi) & \nu^2 \end{bmatrix} \begin{pmatrix} \beta_o \\ \beta_{1c} \\ \beta_{1s} \\ \beta_2 \end{pmatrix} = \begin{pmatrix} 0 \\ 0 \\ 0 \\ 0 \end{pmatrix} \tag{63.b}$$

3.2.2 FLIGHTLAB Models for Stability Assessment Purposes

Three different levels of modeling were used in order to address modeling related issues for stability assessment purposes (see Figure 1). The first two were isolated rotor models with and without inflow dynamics; therefore, an equivalent model of the earlier analytical model was constructed in the FLIGHTLAB environment and inflow dynamics were integrated to that. The objective of these 2 lesser fidelity models was to isolate model-related issues, understand the problem, and then step up the model fidelity. An equivalent model (4-bladed rotor with flap DOF) to the analytical isolated rotor was constructed first in order to verify the characteristics of the stability properties obtained with the earlier model. The fundamental difference between those two is that analytical model is limited, having only 2 harmonic components in its LTP model, whereas the numerical model has a much higher number of harmonics. Even though it is truncated (32 harmonics) for the purpose of accuracy of FTM construction, difference in the number of harmonics is still too large. In the next step, a 3-state inflow model was integrated to the isolated rotor model. Apart from creating a more realistic isolated rotor model, the inflow model provided non-rotor states in the system which were treated with average components only in the LTI model. This was an important step which revelaed how the stability properties are affected by average representation of non-rotor states since in the next step, the rotorcraft model; there were 8 more non-rotor states in addition to the inflow states. Finally, the GHM in FLIGHTLAB was used for stability assessment purposes for the LTI models. The rotor model was enhanced with lag DOF for a generic helicopter representation while preserving the other properties mentioned for the isolated rotor models (the flap DOF and the 3-state inflow) and rigid body properties added. Out of all the states related to rigid body only 8 conventional states

were included in the linearization, resulting in a full rotorcraft model with 27 states in its LTP model.

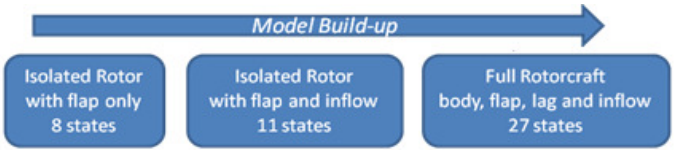

Figure 1. FLIGHLTAB Model Buildup for Stability Purposes

3.3 Metric for Stability Properties

The stability properties of the LTI model were assessed in terms of eigenvalues, and their fidelity was defined depending on how good the estimated eigenvalues were with respect to the eigenvalues of the reference LTP model. Fidelity is expected to improve when the number of harmonics increases as observed both in the current study and in the literature [9] as well. A self claimed metric is defined here to make an overall assessment of the fidelity of the LTI model.

It is observed that different modes can have distinct orders of magnitude, and consequently their absolute error can be different as well. Therefore a metric is needed that takes into account this variation among the different modes. Additionally, error criteria are needed that can aid in the observation of the improvement of the eigenvalues in terms of harmonic coefficients used in the LTI model.

With regard to these expectations, a decrease ratio is defined with respect to the error of the same mode compared to one when constant coefficient approximation is made. Good fidelity in the validation studies requires a decrease ratio of 0.001 or less.

3.4 Accuracy of LTP Eigenvalues

Eigenvalues of the LTP model were obtained through a process during which FTM was obtained first by integrating the LTP system matrix over one period. Then, the eigenvalues of this matrix were converted to the system domain. The computationally challenging part of this process arises if if the LTP system matrix is discrete, as it is observed for the FLIGHTLAB models. Since such a model would allow only constant time integration, its time resolution must be kept very fine; therefore, the computational cost of obtaining an LTP model out of a nonlinear model (i.e. FLIGHTLAB) becomes too expensive, whereas for an analytical model, built-in variable time integration schemes of commercial programs (i.e. MATLAB) can be utilized easily. Therefore analytical representation of LTP system matrices are used by putting the discrete LTP model through a harmonic analyzer and representing it by a very high number of harmonics, 32 in this study. This process provides the same level of accuracy in LTP eigenvalues between the analytical and numerical models while not much compromising the high fidelity of LTP model.

The accuracy of the FTM eigenvalues as obtained from an analytical form of system matrices are represented in Figure 2. An ODE solver available in MATLAB was used for time integration at the end of one period, and parametric studies were made for two available inputs of the function, absolute and relative tolerances. In Figure 2, each line represents a selection of different relative error varying between 10^{-1} and 10^{-12}, where the x axis is the absolute tolerance index. It was found that using 10^{-12} for the relative tolerance and 10^{-15} for the absolute tolerance will be the optimum choice and provide an accuracy of 10^{-15} overall for the eigenvalues of the FTM.

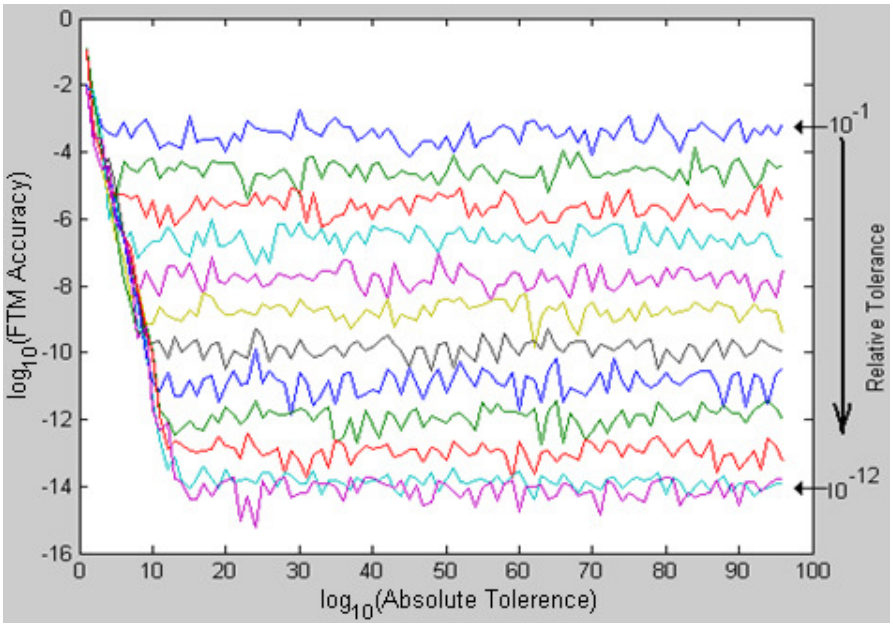

Figure 2. Error sensitivity with respect to Relative and Absolute Tolerances

3.5 Methodology

Prior to attacking the problem, one should first be aware of the known issues while making a comparison between eigenvalues of LTP and LTI. Eigenvalues of the LTP model can be obtained through the FTM by reverse mapping, which includes a multi-valued function, referred to as “inverse tangent”, on the other hand there are more eigenvalues after eigenanalysis of the LTI system matrix than the number of states that result from the use of the LTP model. However, consistent eigenvalues can be obtained from both methods for comparison if proper mathematical manipulation is performed. These manipulations, such as adding or subtracting a proper integer to or from the imaginary part of FTM result or picking the base eigenvalues of the LTI, do not alter fidelity since similar manipulations can be performed on both models and the absolute difference is always the same. As the number of eigenvalues increase, however, another problem emerges, that of which eigenvalue should be compared to which since

there are very close eigenvalues of different modes. This problem is also aggravated due to the fact that selection of base eigenvalues performs a remainder-like operation; thus, even if there is a significant difference between the imaginary parts of two distinct modes, they might be very close as they all end up between +/-1 range in non-dimensional form due to the FTM inverse mapping and the LTI base eigenvalue selection processes. In order to overcome that problem eigenvectors are used to relate the eigenvalues.

The methodology for assessing the fidelity of stability properties of reduced order LTI models followed in this study begins with stability analysis using the Floquet Method of a linear time periodic model extracted from a nonlinear model of a helicopter or rotor in the vicinity of equilibrium condition. FTM is obtained by making use of the variable time resolution ODE solver of MATLAB. This is directly possible for an analytical model and it is made possible for the discrete LTP models obtained from FLIGHTLAB after harmonic analysis as explained in the previous section. FTM eigenvalues are then transformed to the system-plane. While the real parts of a system eigenvalue can be uniquely determined in this step, the imaginary part becomes non-unique because of the multi-valued arctan relation involved in its determination. As noted in [9, 21], the non-uniqueness of the imaginary part is a consequence of the fundamental characteristic of a periodic system in which the oscillation contained in a modal solution derives from both the modal frequency as well as from the associated time dependent periodic mode shape without constraint on the distribution between the two. Various methods for addressing this ambiguity have been proposed in the literature (see [21]). The method put forward in [63] for the determination of modal frequency assumes that, when periodicity is mild, typical of cases with advance ratios in the range of 0.1 or less, the composition of eigenvector components, at least with respect to the dominant motions,

does not significantly deviate from the corresponding composition obtained from the constant coefficient approximation. A similar assumption is made in the present study in order to arrive at a basis for comparison between eigenvalues of LTI and LTP models. Base eigenvalues of LTP (λ_{LTP}) for comparison are arrived at by using the smallest in magnitude of the imaginary part (principal frequency) while transforming the FTM eigenvalues into the system-plane. LTI models of different orders (to include different harmonic components of rotor states) are formulated by using the algorithms developed in [47] and presented in this study. A conventional eigenvalue analysis of the resulting LTI models is carried out using the function "EIG," which is available in FLIGHTLAB [55] based on LAPACK routines [60]. For each of the selected LTI models, a set of base eigenvalues (λ_{LTI}) is obtained by matching the composition of the eigenvector elements associated with the 0^{th} harmonic components of states with the eigenvector elements of the FTM. The LTI model fidelity is assessed in this study by comparing the base eigenvalues of the LTI model (λ_{LTI}) with the base eigenvalues of the LTP (λ_{LTP}). Error in a base eigenvalue of an LTI model (λ_{iLTI}) is defined as its distance from the corresponding base eigenvalue of LTP (λ_{iLTP}) and is given by

$$Error = \left| \lambda_{iLTI} - \lambda_{iLTP} \right| \tag{64}$$

When comparing more than one eigenvalue, a composite error (E) is used for the isolated rotor model with flap DOF only since the order of magnitude for all eigenvalues of that model are the same.

$$E = log_{10}\left[\frac{1}{N_\lambda} \sum_{i=1}^{N_\lambda} \left| \lambda_{iLTI} - \lambda_{iLTP} \right| \right] \tag{65}$$

This averaging process can simplify the post-processing of the results, but if the eigenvalues and consequently their absolute errors are far apart, then this process might cause deficiencies in the judgment of their fidelity. Therefore, the usage of this averaging process is limited to the 8-state analytical model only where all eigenvalues and their absolute error is in the same order of magnitude and only in an analytical model for which a wide range of parametric studies are performed.

3.6 Stability Assessment Using Analytical Models

3.6.1 Limit to Constant Coefficient

Initially, an analytical model is studied as it approaches the 0 advance ratio, where periodicity disappears and the system becomes a constant coefficient. In other words where LTI representation with 0 harmonics is sufficient. This is shown in Figure 3 as the constant coefficient approximation produced results as good as those of any higher harmonic LTI representation after the advance ratio is reduced to 10^{-7}, whereas LTI with harmonics up to N_b/rev is good enough for an advance ratio of 0.01 and below, and LTI with harmonics up to $4N_b$/rev is always good for advance ratios starting at 1. This study verifies that the constant coefficient approximation is a subset of LTI methods with a limited number of harmonics, and it suggests that increasing the number of harmonics gradually will result in attaining sufficient stability.

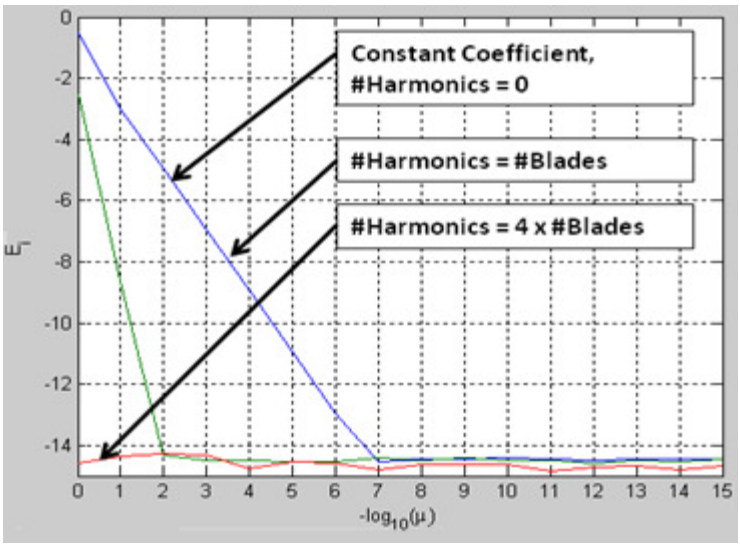

Figure 3. Error sensitivity analysis of LTI models

3.6.2 Effect of Higher Number of Harmonics on Eigenvalues

In Figure 4 and its close-up view, Figure 5, which focuses only on base values, a 4 bladed isolated rotor, as expressed in Eq. (63) in MBC form, is analyzed at 0.15 advance ratio. This study shows a typical result of an LTI stability analysis as compared to the FTM solution using a different numbers of harmonics. The eigenvalues, twice as many for each mode in LTI, are approximately aligned around the same real part with integer multiples of omega resulting in integer multiples in a non-dimensional form here, on the imaginary axis. A limited number of eigenvalues, associated with the highest frequency at each case, are slightly scattered along the real axis, but the rest of the eigenvalues can be visually identified at the same real part. This can be contributed to the effect of the higher harmonics of the original model on the highest harmonic modeled in the LTI, say when the LTI has harmonics up to 12/rev scattering of real part occurs only on the 12/rev ±2/rev where the effect of the higher harmonics (>12rev) of the original model is largest.

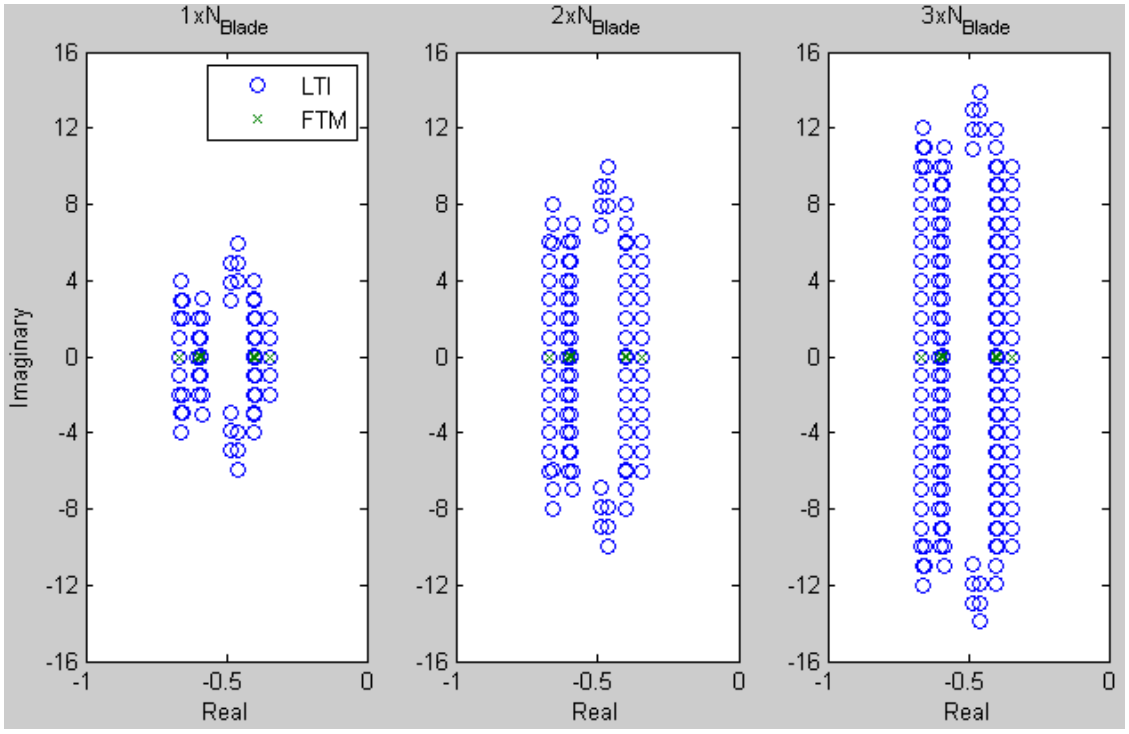

Figure 4. Eigenvalues of a generic LTI model with harmonics 1, 2, 3 times the number of blades

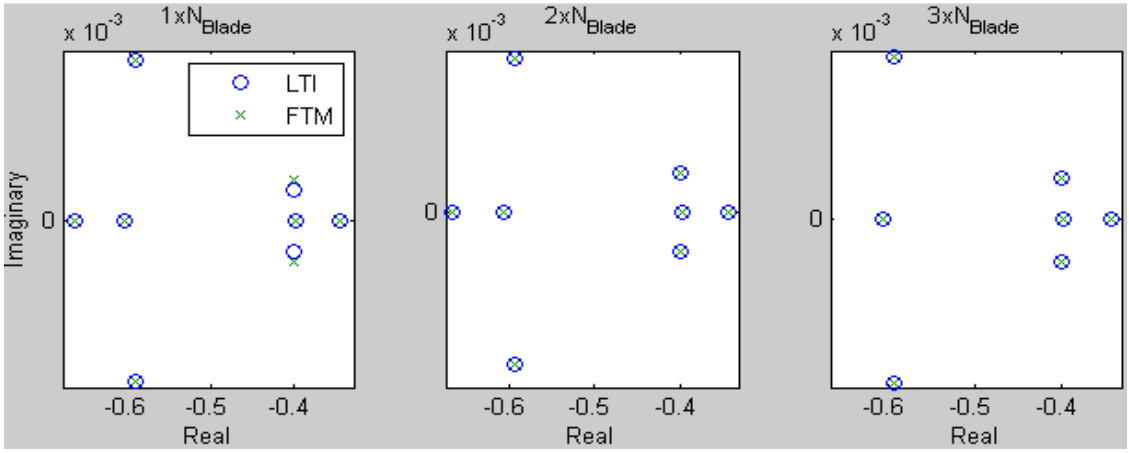

Figure 5. A zoom-in of Figure 4

3.6.3 Fidelity Estimations with Respect to Advance Ratio

In this section, average error is studied with 3 and 4 bladed analytical isolated rotor models. The trend of error is investigated against the use of the number of harmonics varying between 0 and $4.N_b$. In both Figure 6 and Figure 7, there is a very steep

increase in error with constant coefficient and N_b harmonic representations at the first interval between 0 and 0.1 advance ratios. In contrast with this behavior, higher harmonic representations starting at $2N_b$ show better error results and a more moderate increase in the error. This suggests that less than N_b harmonic representation is almost as crude an approximation as occurs with the constant coefficient and should not be used for stability purposes. This might also be interpreted as modeling only the modes that exist in the system equations is not sufficient. The highest frequency found in the state equations is $1N_b$/rev, but due to modulation of the frequencies in the state response can go up to $2N_b$/rev. Therefore, harmonics up to $2N_b$/rev have to be modeled in order to obtain a reliable stability characteristic.

Investigation shows that error lines with different numbers of harmonics tend to preserve the differences in error as the advance ratio increases, which leads to the conclusion that asymptotically, there should be a constant error difference between them. In other words, the modeling of each additional harmonic corresponds to a significant error improvement in the stability estimations. An important point to remember here is that analytical models are no longer valid in moderate and high advance ratios (roughly higher than 0.2). Therefore, these results should be considered in a mathematical form instead of as a physical assessment.

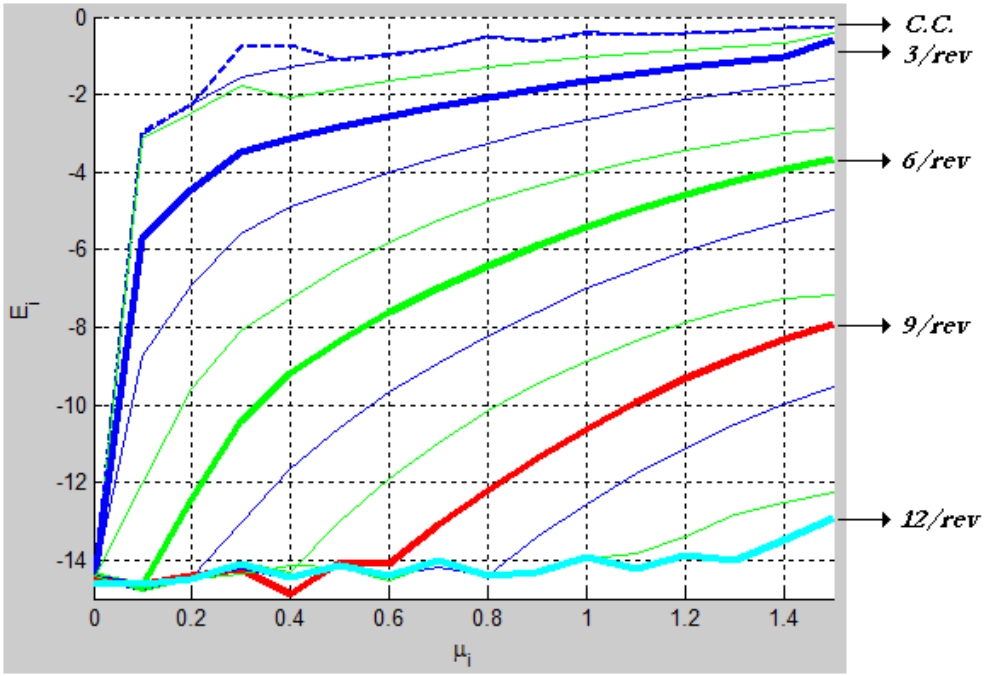

Figure 6. Error index of a 3 bladed isolated rotor (analytical model) as a function of advance ratio.

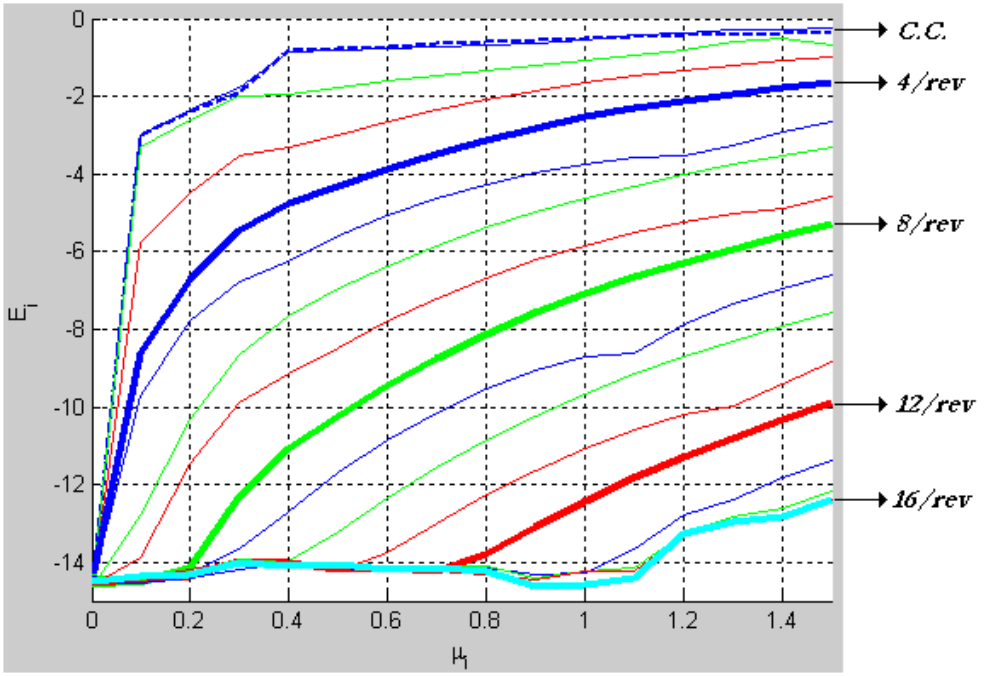

Figure 7. Error index of a 4 bladed isolated rotor (analytical model) as a function of advance ratio.

3.6.4 Fidelity Estimations with Respect to Model Parameters

In this section, the effect of model parameters other than the advance ratio is investigated. These are nondimensional frequency “ν” and Lock number “γ,” which represent the stiffness and aerodynamic effects, respectively. The non-dimensional frequency of the blade is a structural (blade stiffness) and mechanical property (hinge offset) of the blade that should not affect the required number of harmonics, while Lock number, the ratio of aerodynamic effects to the inertia effects, is more likely to produce periodic structures, and it can ultimately impact the required number of harmonics.

Figure 8 reveals that the practical Lock numbers of helicopter rotor blades are varied. The estimated errors are plotted against the number of harmonics used in the LTI, while other model properties such as advance ratio and non-dimensional frequency are shown to keep constant. There is a clear difference between the error levels when same number of harmonics are used in the LTI. In other words in order to capture the same level of fidelity, a different number of harmonics need to be used in the LTI.

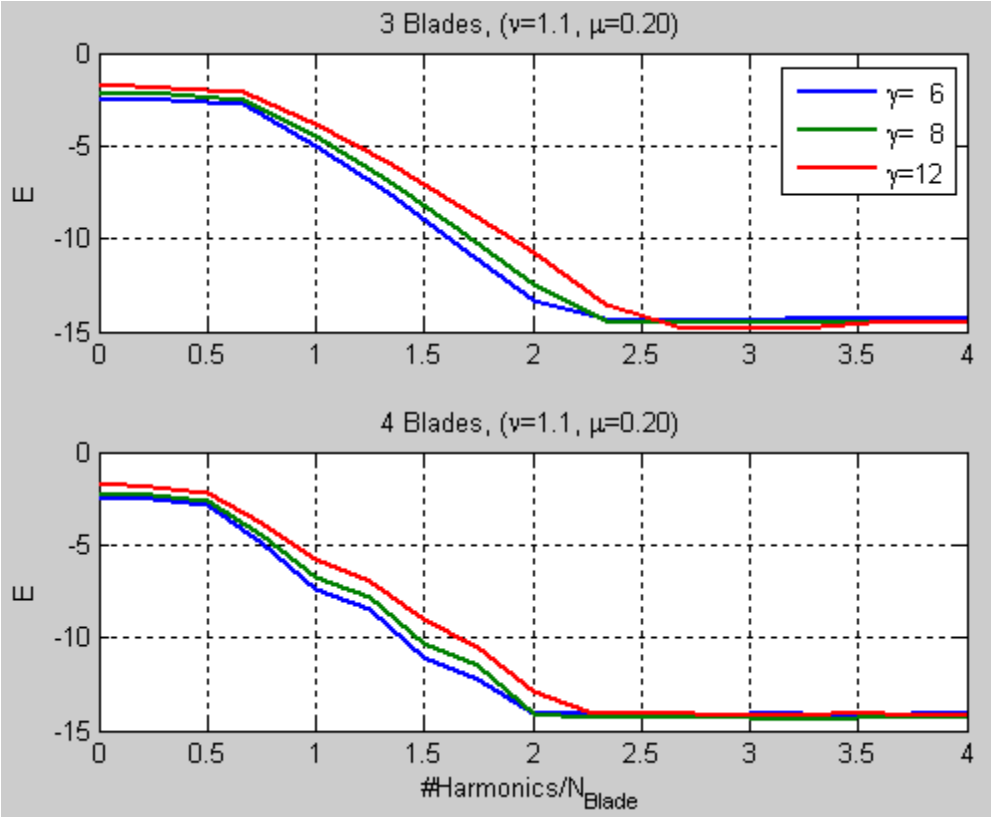

Figure 8. Error index as a function of number of harmonics with 3 different Lock numbers.

Figure 9 displays the results of a similar parametric study that was performed by interchanging the Lock number with non-dimensional frequencies. Non-dimensional frequencies, which varied here (0.9, 1.1, 1.3), are also practical values that can be found on operational helicopter rotor blades. In this case, all three lines associated with different parameters showed almost the same fidelity at every level of harmonics. This leads to the conclusion that for an LTI stability analysis, it is not the non-dimensional rotational frequency but rather only the Lock number and advance ratio that should be considered in order to determine the required number of harmonics.

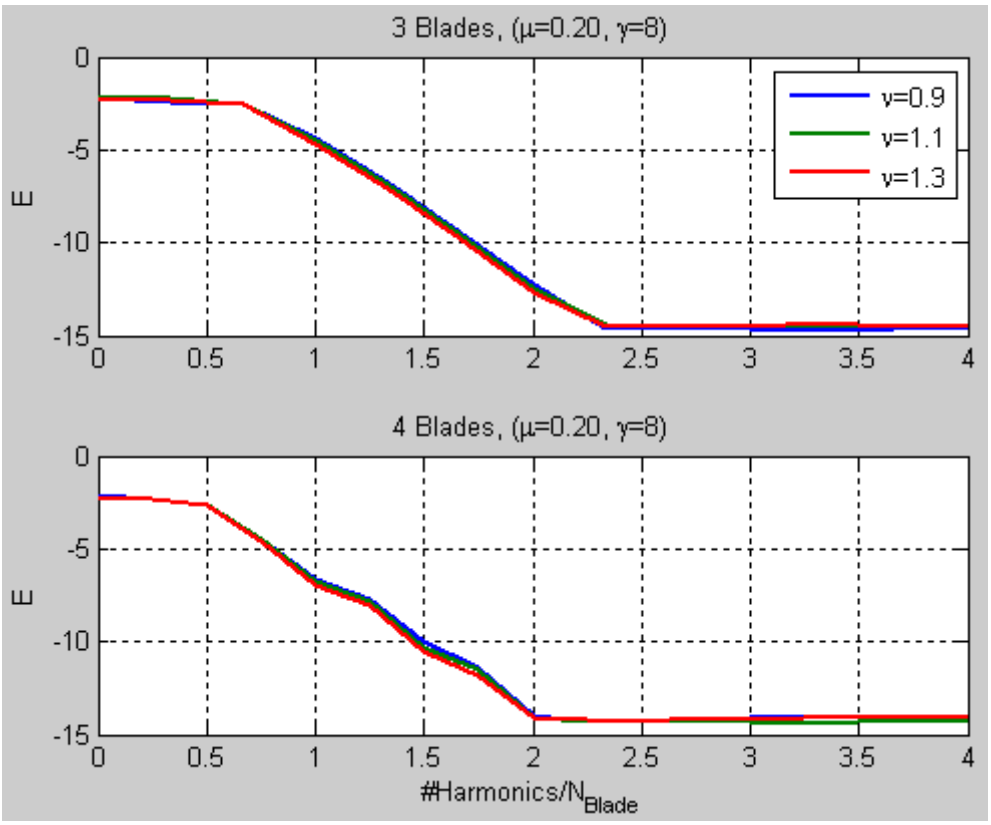

Figure 9. Error index as a function of number of harmonics with 3 non-rotating frequencies.

These results lead to the following question: "What is the combined effect of Lock number and advance ratio on the required number of harmonics?". These two parameters appear in the system equitation (see Eq. (63)) in product form. Therefore, as seen in Figure 10, this multiplication is kept constant while individual parameters composing the multiplication are varied. The same fidelity is observed with every case, and combining this with the earlier results shows that neither the Lock number nor the advance ratio has a sole effect on the required number of harmonics. What this does show is that their multiplication must be changed.

A physical reconsideration of these results suggests that given a rotor model, the advance ratio should be considered as the dominant effect on the required number of harmonics but that a change in the altitude can also effect the fidelity through the change

of density. Another aspect is that if comparisons need to be done between two helicopter models, one needs to carefully calibrate the advance ratio depending on the Lock number difference between those two models.

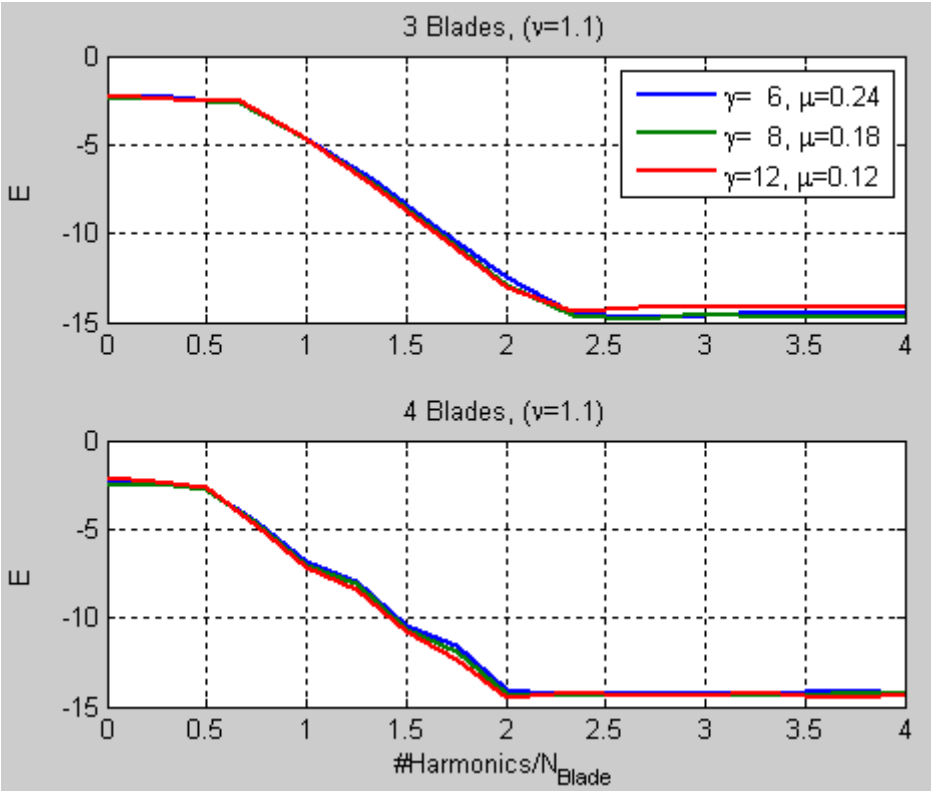

Figure 10. Error index as a function of the number of harmonics with 3 different combinations of Lock number and advance ratio for the same product.

3.7 Stability Assessment Using FLIGHTLAB Models

In this section, FLIGHTLAB models of both isolated rotor models and a full rotorcraft model with sufficient fidelity are investigated in order to assess the stability of LTI models. Model properties are given in the earlier section though it is important to note that for the full rotorcraft model, a model reduction occurs for the body states by focusing on the conventionally used states, i.e. if only pitch and roll attitudes are considered and

body yaw attitude is omitted. All the other states involving rotor and inflow are included in the model reduction.

The results are broken down into 3 subsections, which relate each section with a particular model at a single advance ratio of 0.15. In each section, the eigenvalues are studied individually, starting with their fidelity as a function of the number of harmonics included in the LTI, top subplot 'a'. The accuracy of the reference LTP eigenvalue is approximately 10^{-15}. This means that all the results presented here are above that threshold. In middle subplot 'b', the eigenvalue of mode of interest is indicated with bigger symbols; all other compared eigenvalues are plotted as well. The last figure, 'c', of the each individual eigenvalue study shows the associated eigenvectors as obtained from both FTM and LTI results, which were used for associating the eigenvalues between the two methods.

3.7.1 Isolated Rotor Model with Flap DOF Only

This is the simplest rotor model that could be achieved in FLIGHTLAB. The analytical isolated rotor model studied earlier is an approximation of this model using some assumptions such as uniform blade mass distribution. Thus, the FLIGHTLAB model is designed and used as a step between the analytical model and numerical rotorcraft model in order to understand issues that may arise due to numerical modeling, a discrete LTP model, and realistic rotor properties.

Figures 11 through 14 show respective results for each mode obtained with its fidelity with respect to number of harmonics, its eigenvalue indicated in the system domain, and its modeshape comparison between FTM and LTI. Similar trends with the earlier analytical model results are observed in all of the eigenvalues though the difference here is that adopted method based on eigenvector matching worked well for selecting the right eigenvalues between LTI and LTP. An important aspect that differs

from the analytical model results is that some harmonics (2, 4, 8, and 16 per rev) have a much bigger impact on the error and that other harmonics seem to have barely any or no effect at all on the accuracy of the LTI. Although this claim stands valid for the current model, it is known that an abundance of significant 1/rev harmonics in real-life rotors discourages the creation of less costly LTI models that are composed of these even harmonics only. A final abrupt decrease observed at the 32/rev harmonic is believed to be due to the analytical representation of the LTP in terms of harmonics up to this value. Finally, it is concluded so far that the numerical model and its results are valid and supports the direction of the study towards a rotorcraft model.

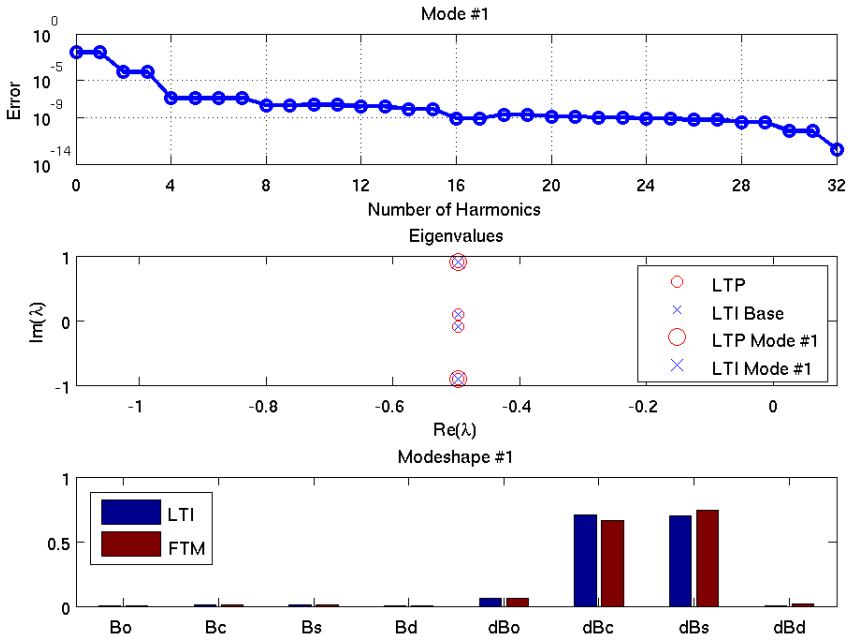

Figure 11. Isolated rotor 8-states. Mode 1 : a) Error Sensitivity of LTI, b) Eigenvalues on Imaginary Domain, LTP and LTI c) Modeshape 1, FTM and LTI

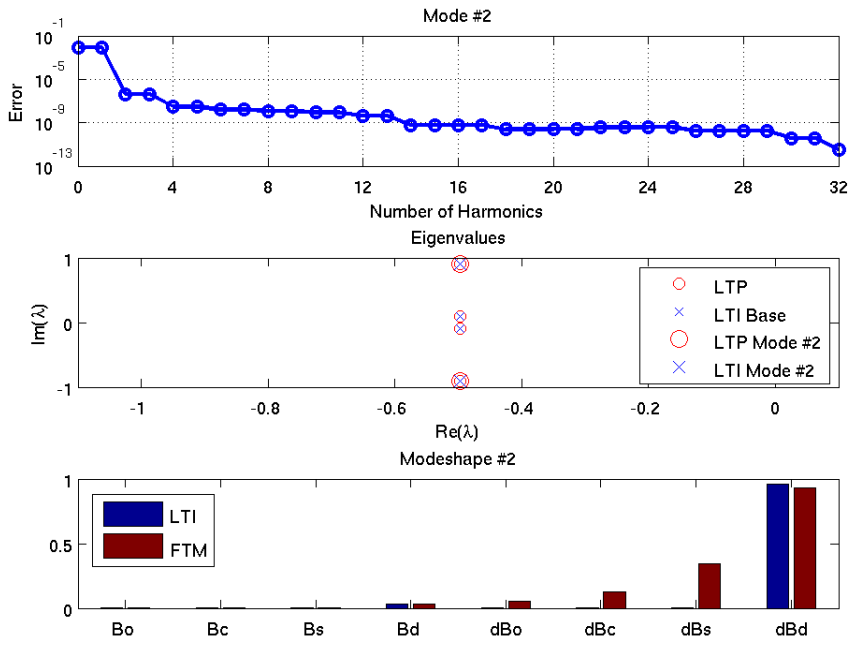

Figure 12. Isolated rotor 8-states. Mode 2 : a) Error Sensitivity of LTI, b) Eigenvalues on Imaginary Domain, LTP and LTI c) Modeshape 2, FTM and LTI

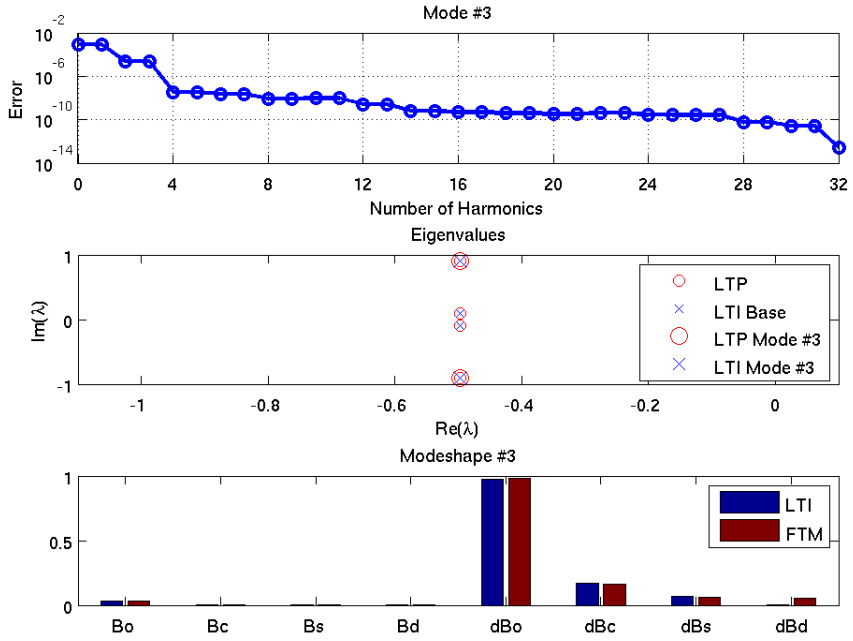

Figure 13. Isolated rotor 8-states. Mode 3 : a) Error Sensitivity of LTI, b) Eigenvalues on Imaginary Domain, LTP and LTI c) Modeshape 3, FTM and LTI

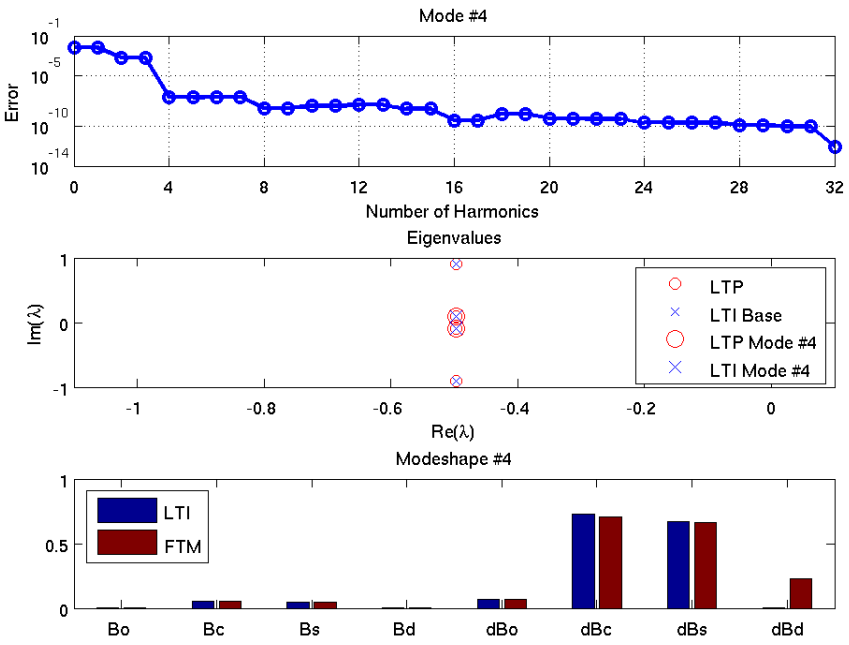

Figure 14. Isolated rotor 8-states. Mode 4 : a) Error Sensitivity of LTI, b) Eigenvalues on Imaginary Domain, LTP and LTI c) Modeshape 4, FTM and LTI

3.7.2 Isolated Rotor Model with Flap DOF and 3-State Inflow

In this section, the former isolated rotor model is enhanced with the 3-state inflow in order to study the effects of non-rotor states whose harmonic content is omitted in the LTI process. In order to keep this focus on the differences due to the presence of non-rotor states, only 2 modes are studied. Mode 1 of the isolated rotor model with 11-states is a mostly inflow dominated mode, whereas the other one (Mode 3) is a cyclic flapping mode that is strongly coupled with the inflow.

Figure 15 and Figure 16 show the results with the current LTI model. The eigenvector matching based method worked fine here as well in both modes. Although significant improvement in the error can be seen up to the 4/rev harmonic representation, after that value, sensitivity to the number of harmonics in the LTI is entirely lost. A combination of significant periodicity in the non-rotor states (inflow) and

the representation of those states with an average state is thought to be the source of such early saturation in the accuracy estimates of LTI. Therefore a hypothetical LTP model is extracted from this original one, where periodicity of the non-rotor related parts of the system matrix are suppressed. The LTP model and FTM obtained from this hypothetical case are called LTPo and FTMo, respectively; likewise, the LTI obtained from the LTPo is called LTIo. Figure 17 and Figure 18 show the results after that process, evidently revealing that even if there is no harmonic content in the portions of $A(\psi)$ corresponding to the non-rotor states, the stability characteristics are still sensitive to the harmonic representation of those states in the LTI. In order to examine this issue, an extended LTI (LTI*) model that includes same number of harmonics for both rotor and non-rotor states is constructed. Figure 19 and Figure 20 give example results with such an LTI model that includes an equal number of harmonics for all the states. Theoretically, this is the same level of modeling with the isolated rotor model with 8-state since within both models all the states decompose into the same number of harmonics. Consequently, similar results are observed here with the 11-state model as those in the 8-state model. One can use the LTI model with the non-rotor states treated with their average component only, as long as the stability properties are sufficiently accurate, as those obtained in Figure 17 and Figure 18 for the sake of low computational cost (lower size LTI due to lesser pseudo-states). In cases which require better accuracy, t one needs to switch to the extended version of the LTI model.

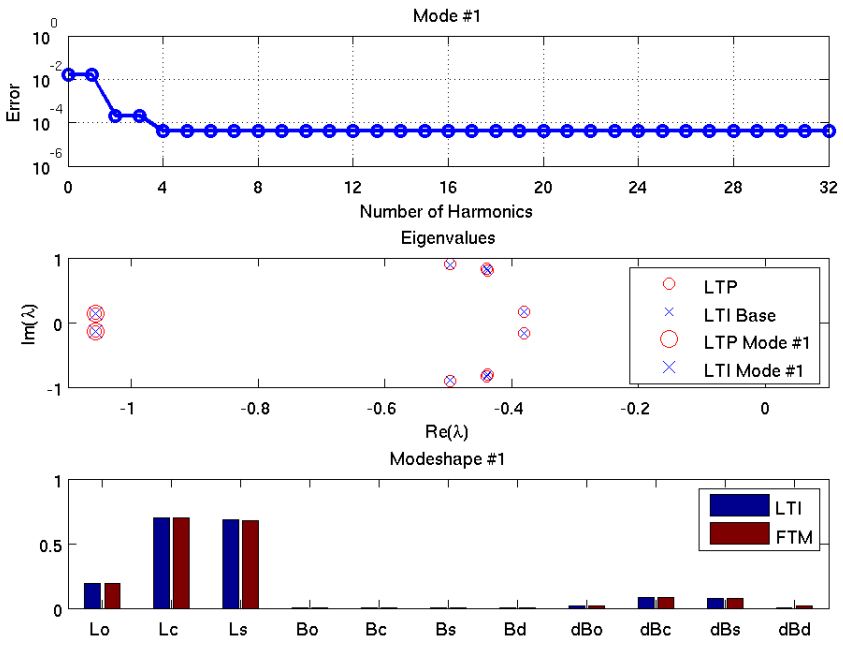

Figure 15. Isolated rotor 11-states. Mode 1 : a) Error Sensitivity of LTI, b) Eigenvalues on Imaginary Domain, LTP and LTI c) Modeshape 1, FTM and LTI

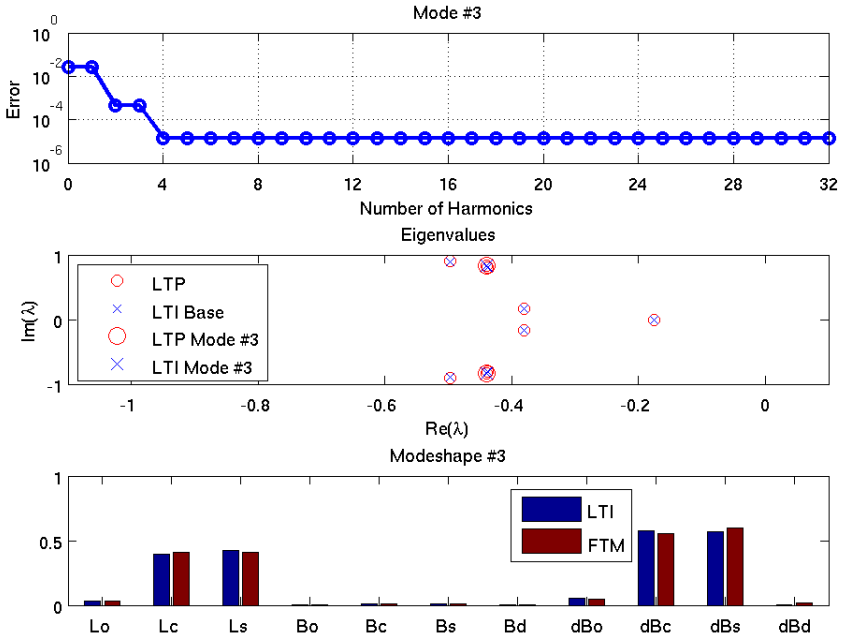

Figure 16. Isolated rotor 11-states. Mode 3 : a) Error Sensitivity of LTI, b) Eigenvalues on Imaginary Domain, LTP and LTI c) Modeshape 3, FTM and LTI

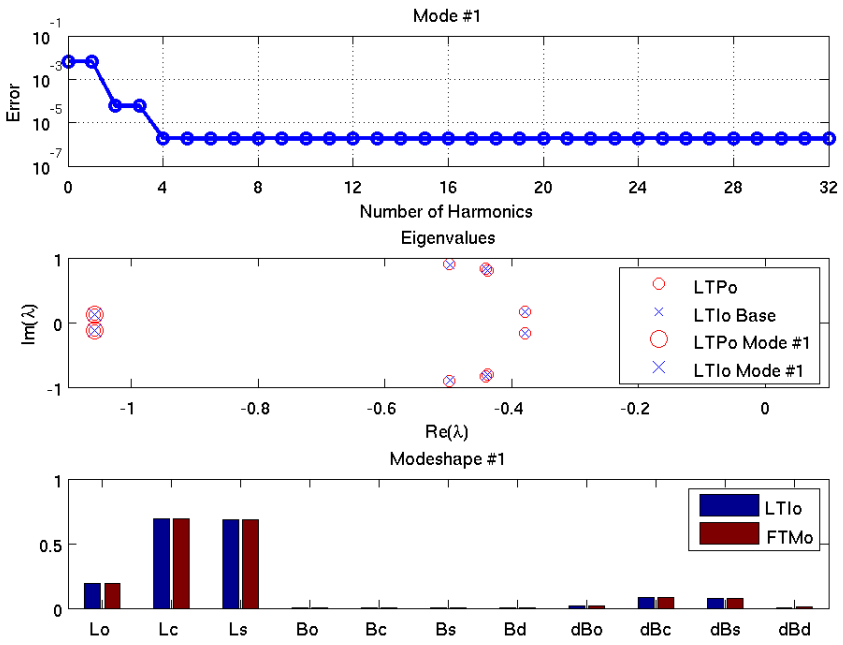

Figure 17. Isolated rotor 11-states. Mode 1 : a) Error Sensitivity of LTIo, b) Eigenvalues on Imaginary Domain, LTPo and LTIo c) Modeshape 1, FTMo and LTIo

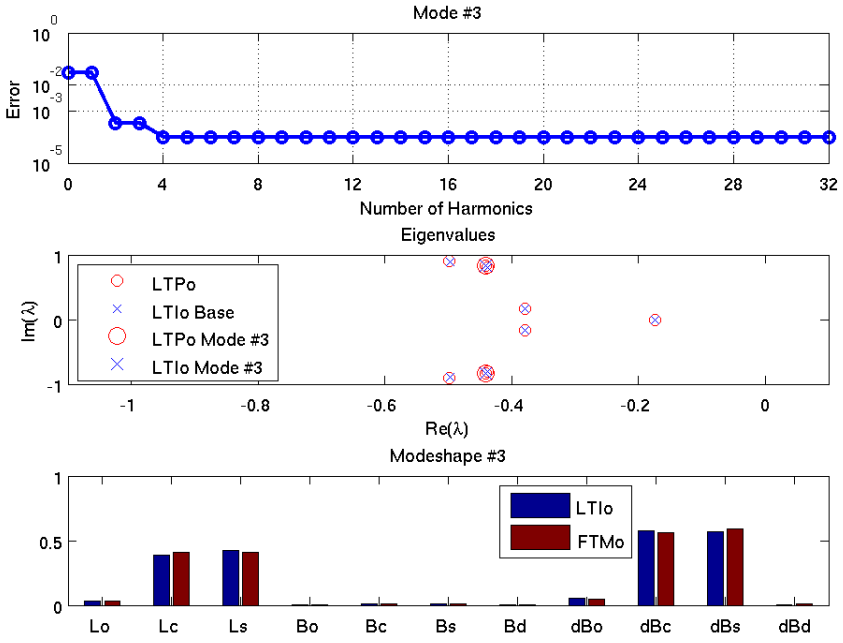

Figure 18. Isolated rotor 11-states. Mode 3 : a) Error Sensitivity of LTIo, b) Eigenvalues on Imaginary Domain, LTPo and LTIo c) Modeshape 3, FTMo and LTIo

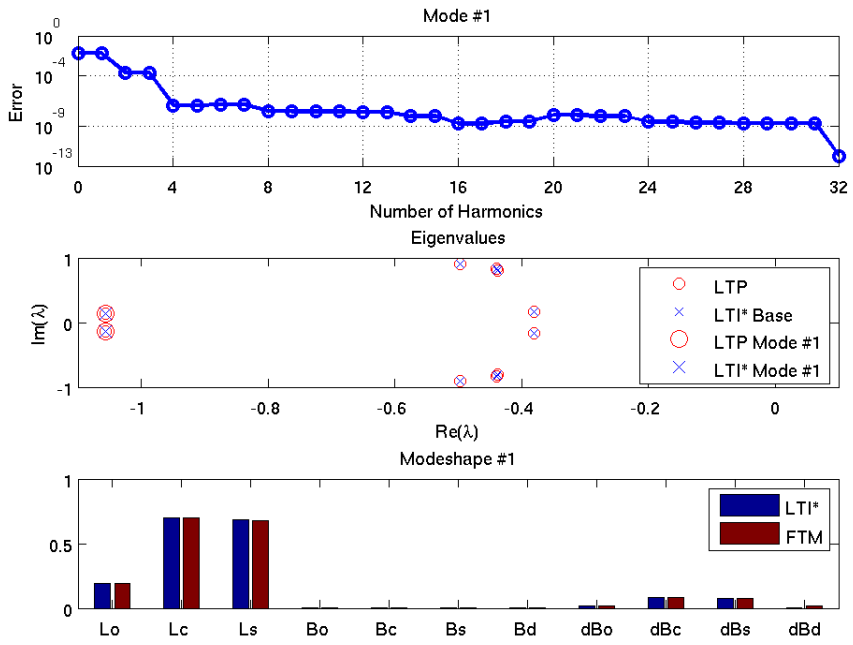

Figure 19. Isolated rotor 11-states. Mode 1 : a) Error Sensitivity of LTI*, b) Eigenvalues on Imaginary Domain, LTP and LTI* c) Modeshape 1, FTM and LTI*

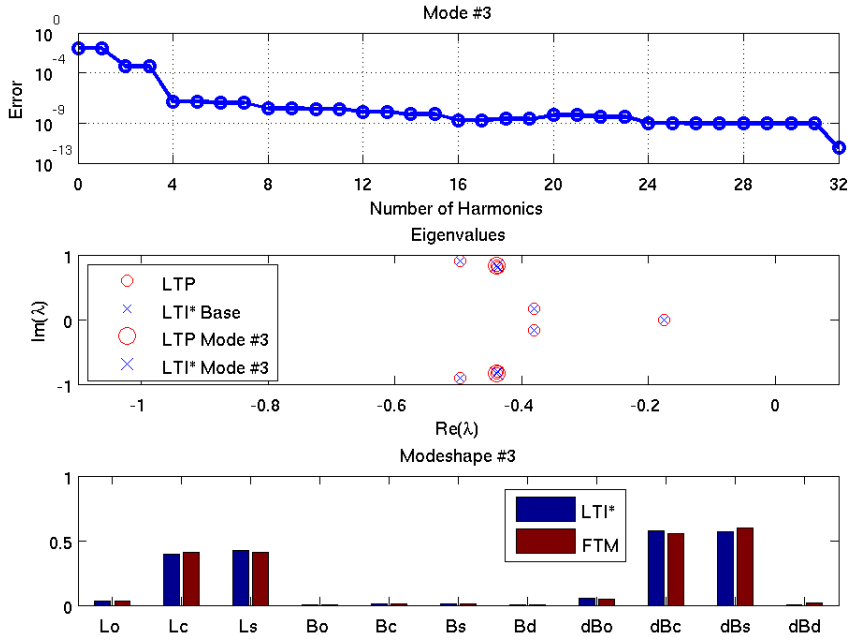

Figure 20. Isolated rotor 11-states. Mode 3 : a) Error Sensitivity of LTI*, b) Eigenvalues on Imaginary Domain, LTP and LTI*, c) Modeshape 3, FTM and LTI*

3.7.3 Full Rotorcraft Model

The full rotorcraft model studied here is the simplest representation of a full rotorcraft with sufficient fidelity. The modeling properties are explained in section 2.1 but it is important to note it here that during the process of linearization (LTP), not all of the states are included in the linear model. In other words, both the LTP and LTI models disregard states such as body yaw angle. The included states are the 8 body states (Φ, θ, Vx, Vy, Vz, p, q, r), the 3-state inflow (λ_o, λ_c, λ_s), and the 16 rotor states, which are the MBC transformation of the rigid flap and lag degrees of freedom for 4 blades. The proposed LTI model treats non-rotor states (body and inflow) with the average component only, and the rotor states are modeled up to the specified number of harmonics.

Figures 21 through 35 show the results with the LTI model proposed here and, Figures 36 through 50 show the results with the extension of the LTI model by representing all states up to the same number of harmonics. Although it was already shown in the section 3.7.2 that the former treatment of non-rotor states leads to a fundamental deficiency in the LTI stability properties, the accuracy obtained with that level of modeling might be sufficient depending on the purpose. Therefore, both results are presented here for the current objective rotorcraft model.

In the LTI model, accuracy saturated as early as 2/rev harmonics, as shown in Figures 21, 22, 26 and 27. Especially for the mode shown in Figures 22, 26 and 27 where there is coupling between rotor and non-rotor states, not only did accuracy saturate at 2/rev, but the obtained accuracy is also around 10% of the error when a constant coefficient approximation is made. This ratio is selected for the fidelity estimation purposes since the absolute error of a mode is dependent on the order of

magnitude of the eigenvalue of that mode. Therefore, such a scale can provide a more generic merit.

The absolute values obtained for these modes are on the order of 0.01 and 0.001, which might be sufficient for a particular study, but it is apparently not useful for a trade study due to the saturation regardless of its absolute value. On the plus side of this method, it is observed that all the modes that involved only body and inflow states in their modeshape profile showed progressively improving trend for their accuracy as the number of harmonics increased up to 8/rev where they saturated. Those saturated values are on the order of 10^{-5} and when compared to their error with constant coefficient representation the decrease ratio is about 0.001 which is an acceptable ratio.

Moreover all the estimations (Figures 21-35) performed using LTI method except for modes 2, 6 and 7 (Figures 22,26 and 27) showed excellent correlation between their eigenvectors and those tree comparisons match only the dominant component of the eigenvector. Therefore, overall statement for the eigenvector comparison is very good.

Considering the fidelity criteria together with the content of the modes it can be assessed that the LTI model can be used for vehicle stability and handling qualities requirements. Lack of accuracy for the other modes which all have rotor coupling would be a limiting factor for the use of the method for integrated flight and rotor control. Thus, these findings suggest that it is vital to extend the theory to include all the states (both rotor and non-rotor) in harmonic decomposition to further study the accuracy of eigenvalues.

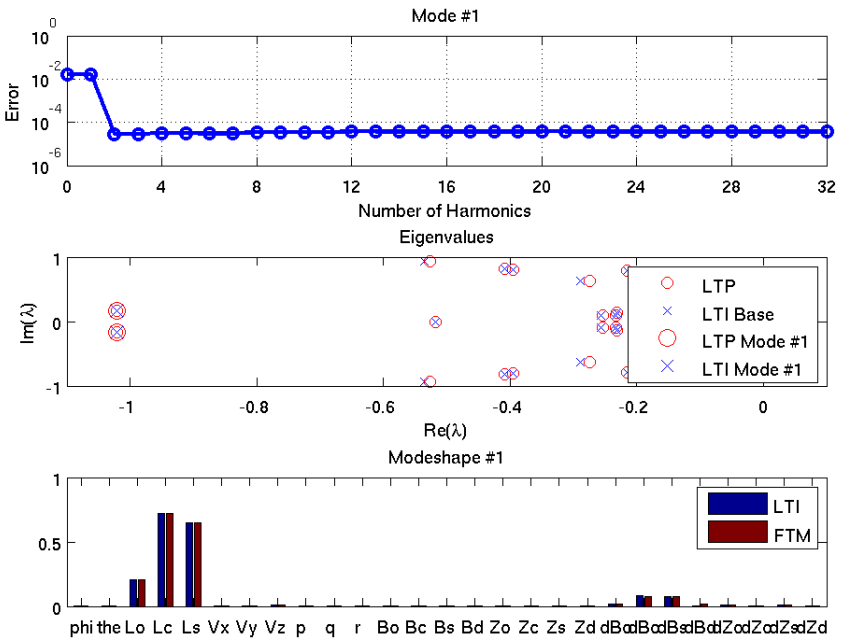

Figure 21. Rotocraft Model. Mode 1 : a) Error Sensitivity of LTI, b) Eigenvalues on Imaginary Domain, LTP and LTI c) Modeshape 1, FTM and LTI

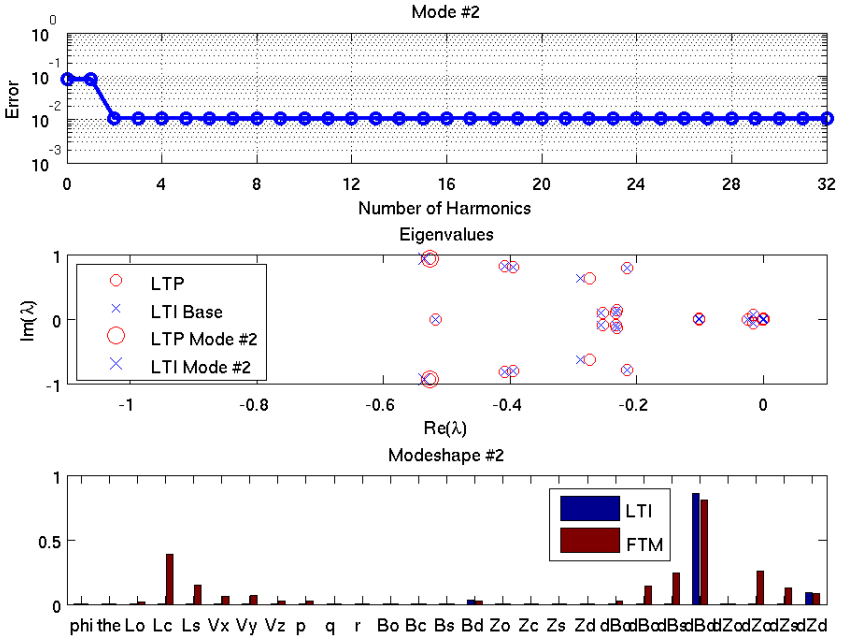

Figure 22. Rotocraft Model. Mode 2 : a) Error Sensitivity of LTI, b) Eigenvalues on Imaginary Domain, LTP and LTI c) Modeshape 2, FTM and LTI

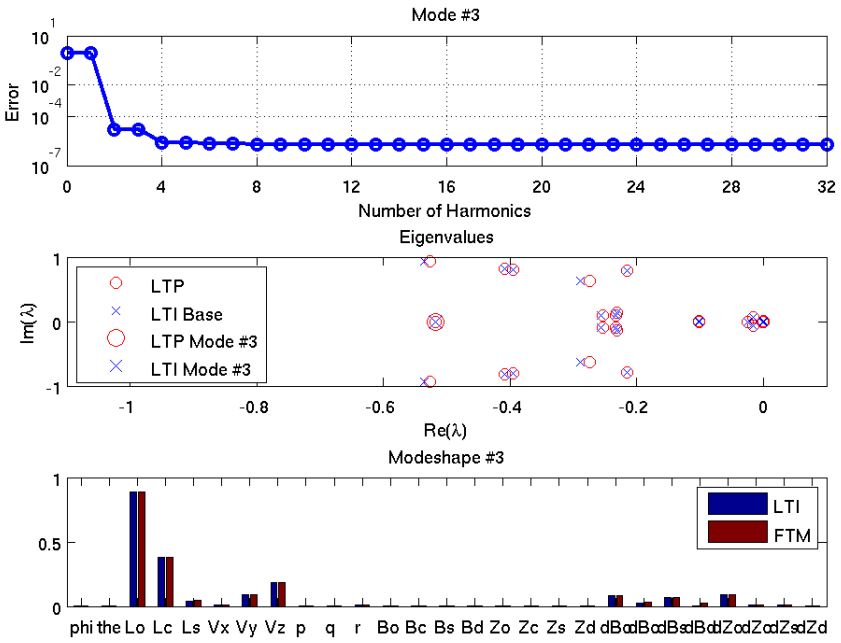

Figure 23. Rotocraft Model. Mode 3 : a) Error Sensitivity of LTI, b) Eigenvalues on Imaginary Domain, LTP and LTI c) Modeshape 3, FTM and LTI

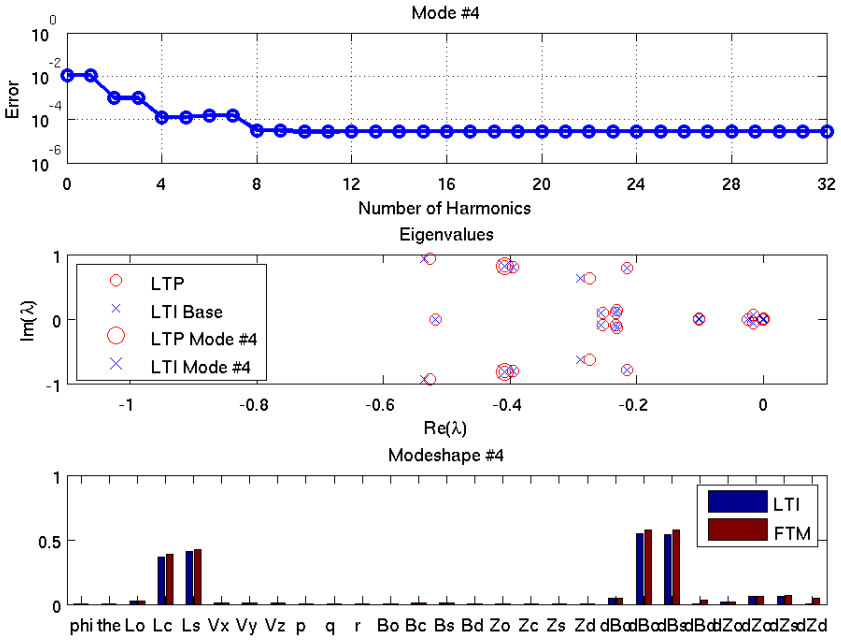

Figure 24. Rotocraft Model. Mode 4 : a) Error Sensitivity of LTI, b) Eigenvalues on Imaginary Domain, LTP and LTI c) Modeshape 4, FTM and LTI

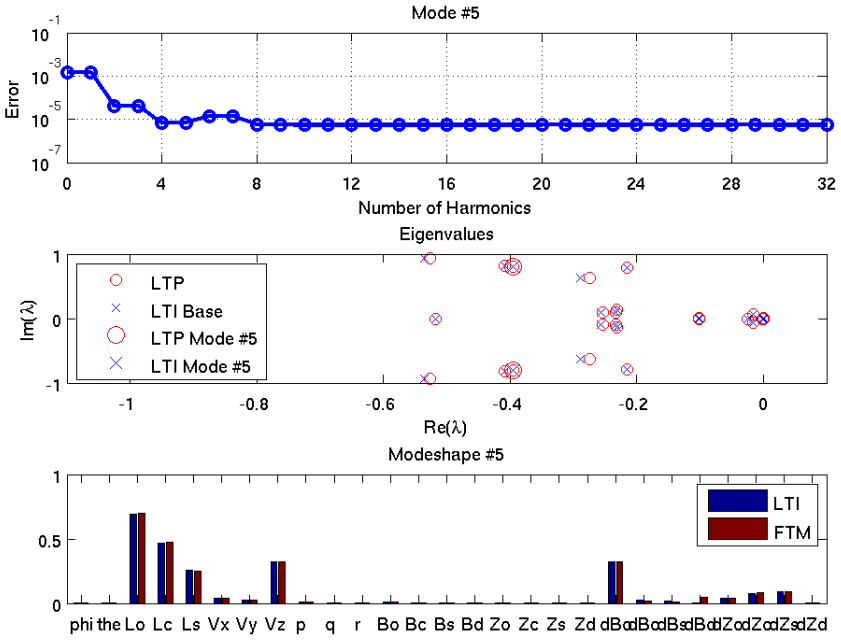

Figure 25. Rotocraft Model. Mode 5 : a) Error Sensitivity of LTI, b) Eigenvalues on Imaginary Domain, LTP and LTI c) Modeshape 5, FTM and LTI

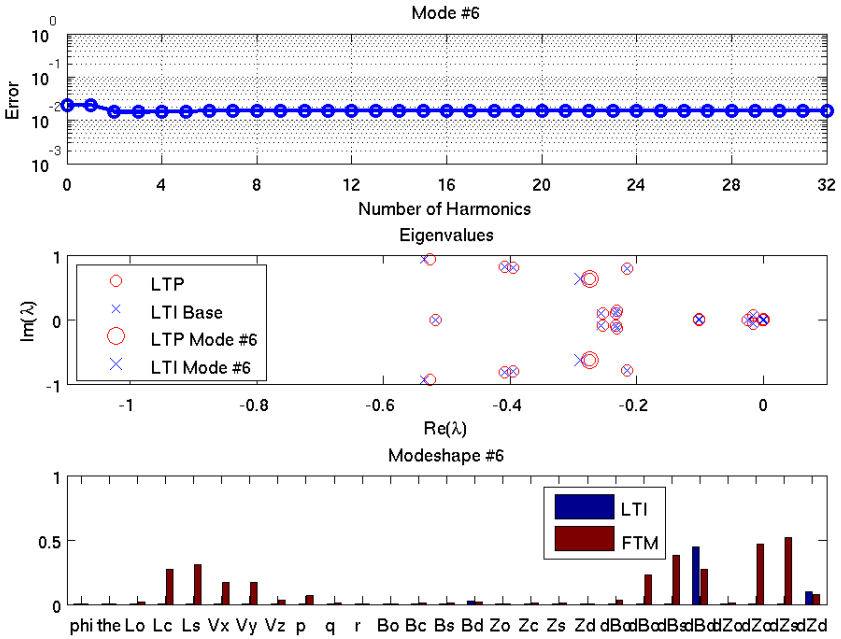

Figure 26. Rotocraft Model. Mode 6 : a) Error Sensitivity of LTI, b) Eigenvalues on Imaginary Domain, LTP and LTI c) Modeshape 6, FTM and LTI

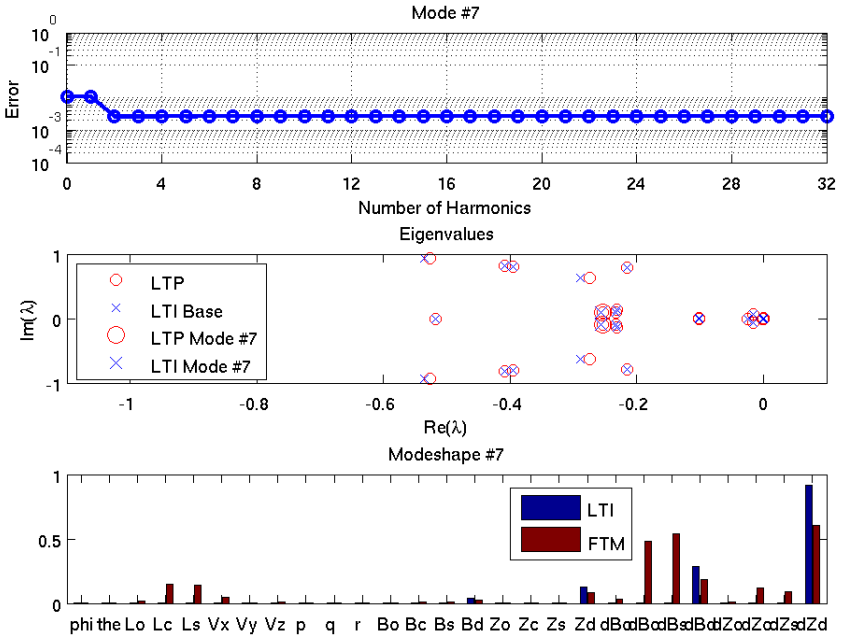

Figure 27. Rotocraft Model. Mode 7 : a) Error Sensitivity of LTI, b) Eigenvalues on Imaginary Domain, LTP and LTI c) Modeshape 7, FTM and LTI

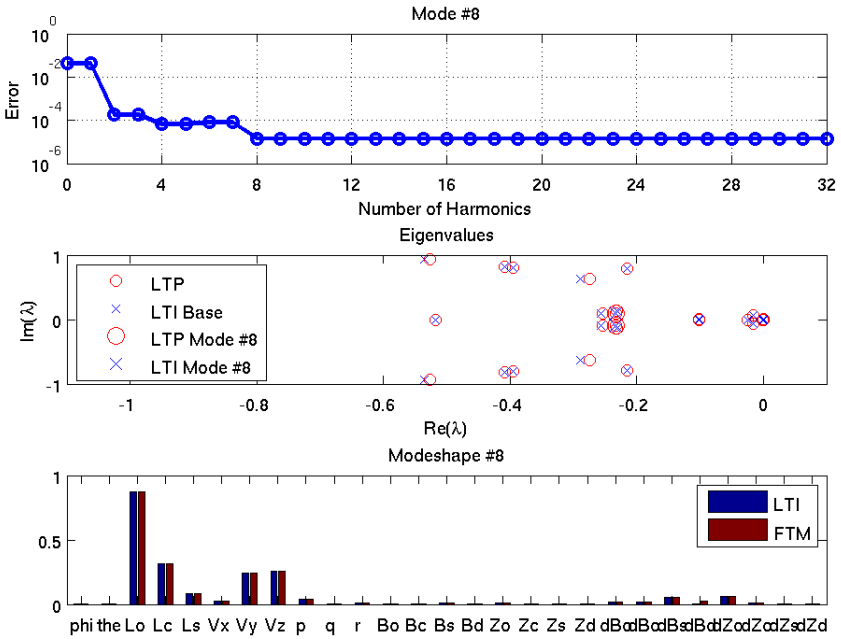

Figure 28. Rotocraft Model. Mode 8 : a) Error Sensitivity of LTI, b) Eigenvalues on Imaginary Domain, LTP and LTI c) Modeshape 8, FTM and LTI

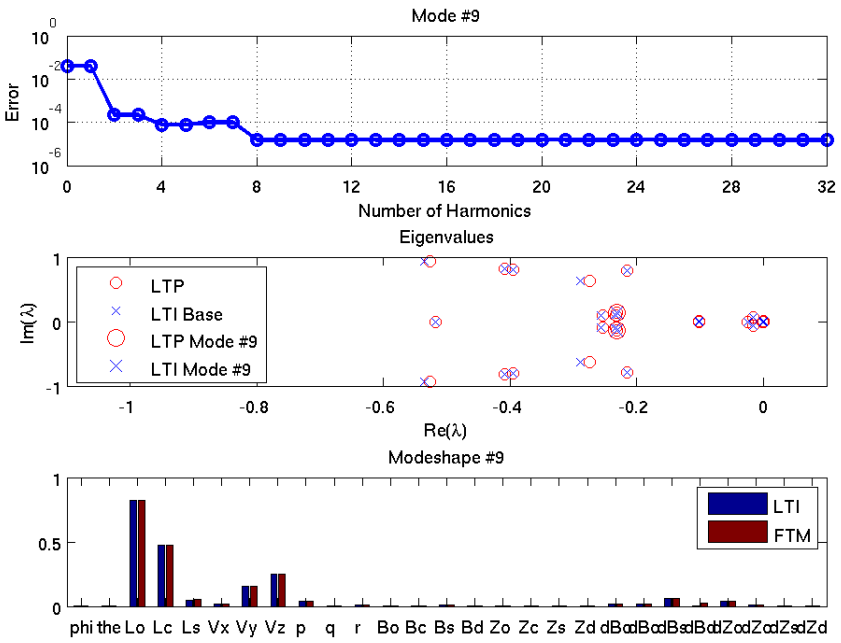

Figure 29. Rotocraft Model. Mode 9 : a) Error Sensitivity of LTI, b) Eigenvalues on Imaginary Domain, LTP and LTI c) Modeshape 9, FTM and LTI

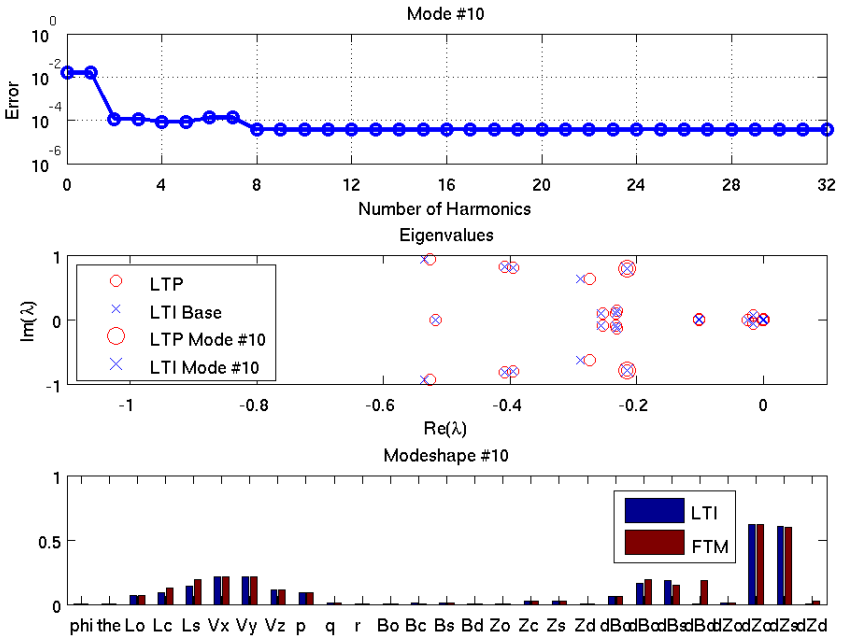

Figure 30. Rotocraft Model. Mode 10 : a) Error Sensitivity of LTI, b) Eigenvalues on Imaginary Domain, LTP and LTI c) Modeshape 10, FTM and LTI

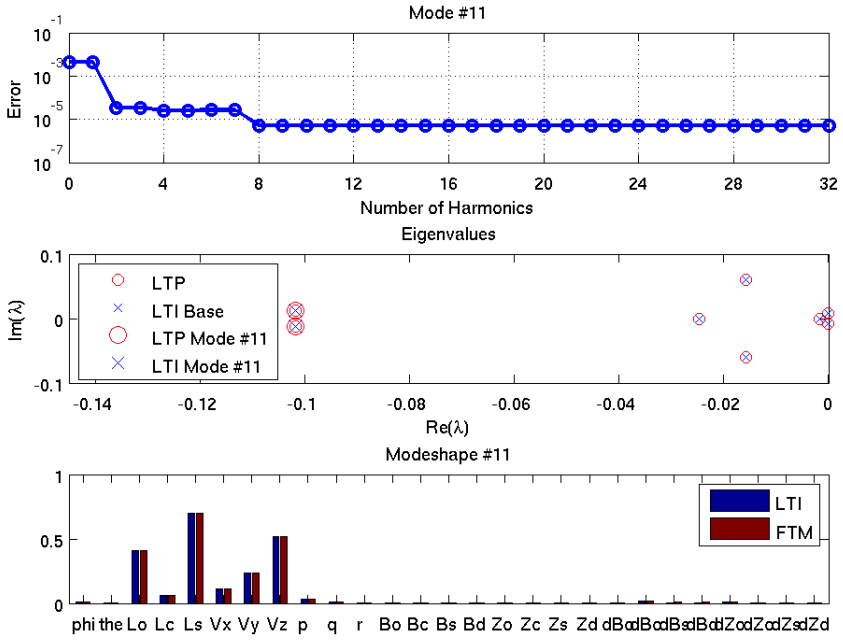

Figure 31. Rotocraft Model. Mode 11 : a) Error Sensitivity of LTI, b) Eigenvalues on Imaginary Domain, LTP and LTI c) Modeshape 11, FTM and LTI

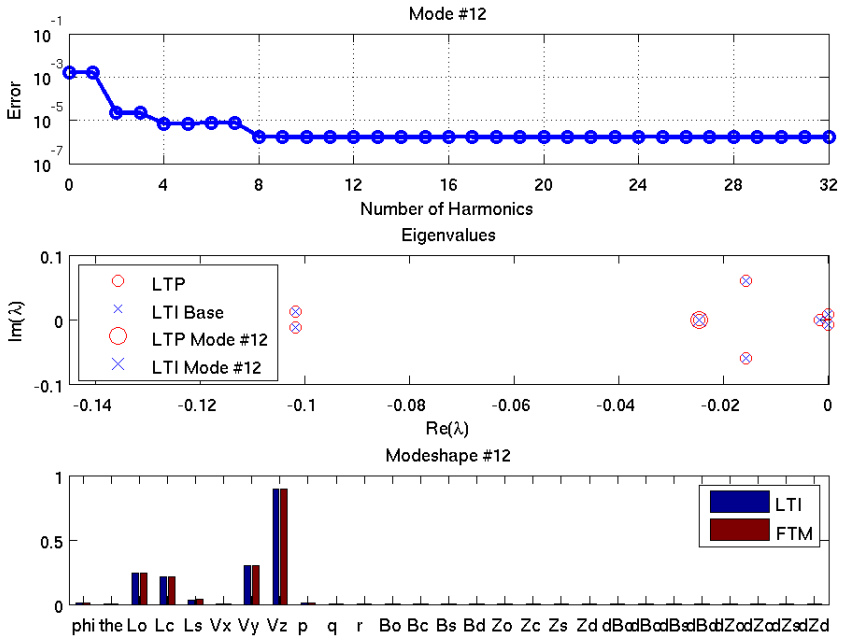

Figure 32. Rotocraft Model. Mode 12 : a) Error Sensitivity of LTI, b) Eigenvalues on Imaginary Domain, LTP and LTI c) Modeshape 12, FTM and LTI

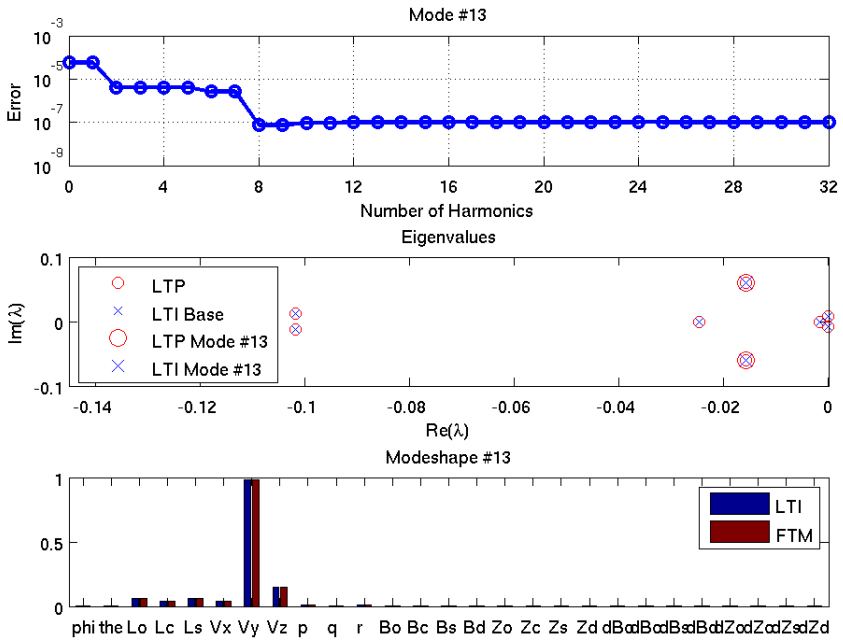

Figure 33. Rotocraft Model. Mode 13 : a) Error Sensitivity of LTI, b) Eigenvalues on Imaginary Domain, LTP and LTI c) Modeshape 13, FTM and LTI

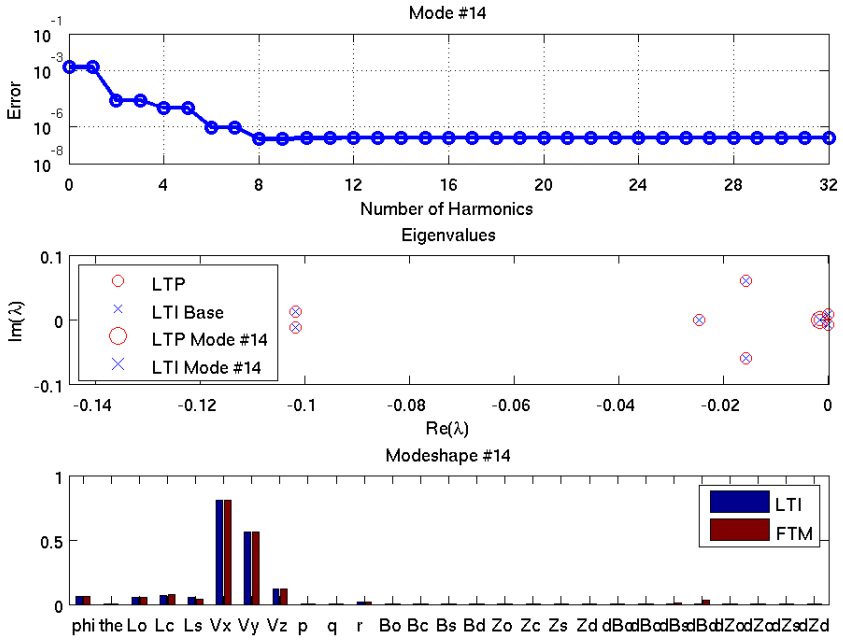

Figure 34. Rotocraft Model. Mode 14 : a) Error Sensitivity of LTI, b) Eigenvalues on Imaginary Domain, LTP and LTI c) Modeshape 14, FTM and LTI

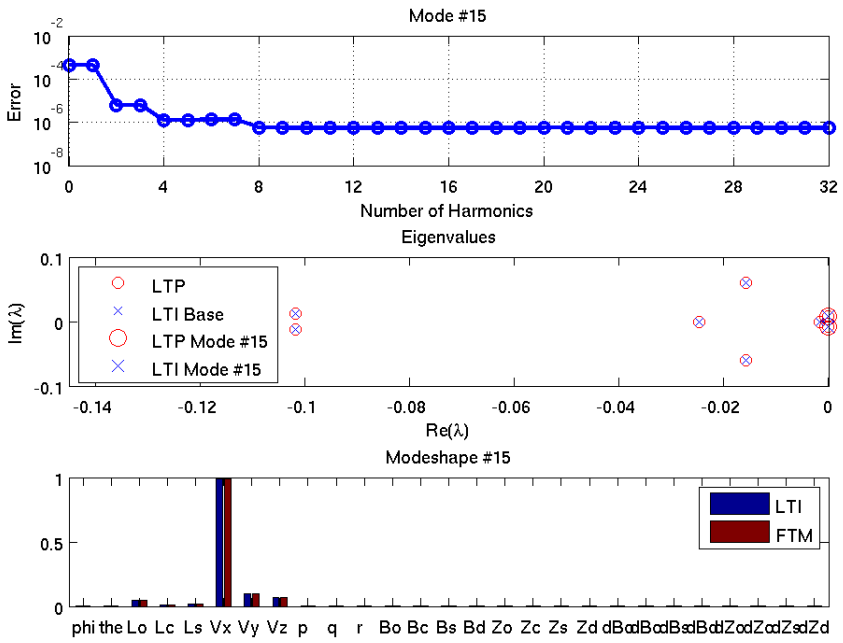

Figure 35. Rotocraft Model. Mode 15 : a) Error Sensitivity of LTI, b) Eigenvalues on Imaginary Domain, LTP and LTI c) Modeshape 15, FTM and LTI

The results for the extended LTI model (LTI*) presented in Figures 36 through 50. All of the results show a monotonic decrease in error for all modes except a few temporary situation explained later, whereas all of the results obtained with the former method saturated between 2/rev and 8/rev harmonics. Therefore, extended LTI model can be seen as a suitable tool for the parametric studies of stability properties.

Figures 39 through 42, there is an increase in error at 2/rev harmonics which can be explained as the increase in numerical error is much higher than the improvement of the eigenvalues due to 2/rev harmonics in those 4 modes,

Only one mode (Figure 38) shown did not have any change at that level of harmonic. In the higher number of harmonic representations rare increases in error is also seen but much lesser amounts which can be explained by the same rational. With the exception of this problem a monotonic decrease in error is seen mostly until the highest number of harmonic, 32/rev. As explained in earlier results abrupt decrease in

error at 32/rev can be related with the fact that LTP is represented with harmonics up to 32/rev.

Stability evaluation of LTI and LTI* had the same correlation at every mode for the eigenvector. This is an expected result since the reference modeshapes in both cases are identical as they were originated from the same LTP model. Even though LTI and LTI* evaluations are different, portion of the eigenvectors that extracted from each model for the comparison is the same, that corresponds to the 0^{th} harmonics of states. Therefore, improvement in the overall comparison between the LTP and LTI is only for the eigenvalues, yet eigenvector comparisons between LTP and LTI model were already found in a very good correlation.

With the improvement in the LTI estimation while switching from to LTI* not only saturation problem was resolved but also remarkable improvement in the error estimations is also seen at the number of harmonics is equal to the saturation point with the earlier method. Mode 9, as obtained from LTI and LTI* methods in Figrues 29 and 44, respectively, has the same error levels up to the 8/rev harmonics but when number of harmonics is reached up to this value where earlier method (LTI) saturated error is observed on the order of 10^{-5}, whereas error is even lower (10^{-6}) when LTI* method was used. This result suggest that decomposition of non-rotor states into their harmonics is vital even for the lesser number of harmonics.

When all of the modes are reviewed for their damping ratio least damped modes are grouped as translational velocity (Vx, Vy, and Vz) associated ones shown in Figures 48, 49 and 50. Then, in Figures 46 and 47, least damped modes are seen with coupling of inflow in addition to the same content (Vx, Vy, and Vz). It is interesting to experience the least damped modes with association of such states, body translational velocities

and inflow, which happen to be naturally damped states. This condition can be related to the aerodynamic modeling and lack of rotor wake interaction of the fuselage.

Figures 41 and 45 show the eigenvalues and eigenvectors for the modes least damped that involves states other than or in addition to the body translational velocities and inflow. Largest contribution within these modes is due to cyclic lag modes, which are also known regressive lag and progressive lag modes. Especially regressive lag mode is known for its part in the ground and air resonance phenomena.

As it was noticed in the sections 3.7.1, 3.7.2 and repeated in this section that progressive decrease in error can be observed only on particular number of harmonics, at 2/rev and higher even number of harmonics. This condition was contributed to the effect of 2/rev and 4/rev dominant dynamics of a four-bladed rotor. Since this behavior is also observed with the rotorcraft model in the current section of this study it can be stated that body dynamics do not alter this characteristic.

In all of the eigenvalues obtained using extended LTI (LTI*) very small error can be achieved (on the order of 10^{-9} or less), and it is possible to observe a progressive decrease in error as the number of harmonics is increased. Therefore, overall fidelity estimation can be made on these results in terms of the definition given in “Methodology” section 3.4. When the desired error decrease ratio is set to 10^{-3}, the minimum number of harmonics that needs to be used for good fidelity is 8/rev, and if this target value is decreased to $10^{-4,}$ then the requirement goes up to 10/rev.

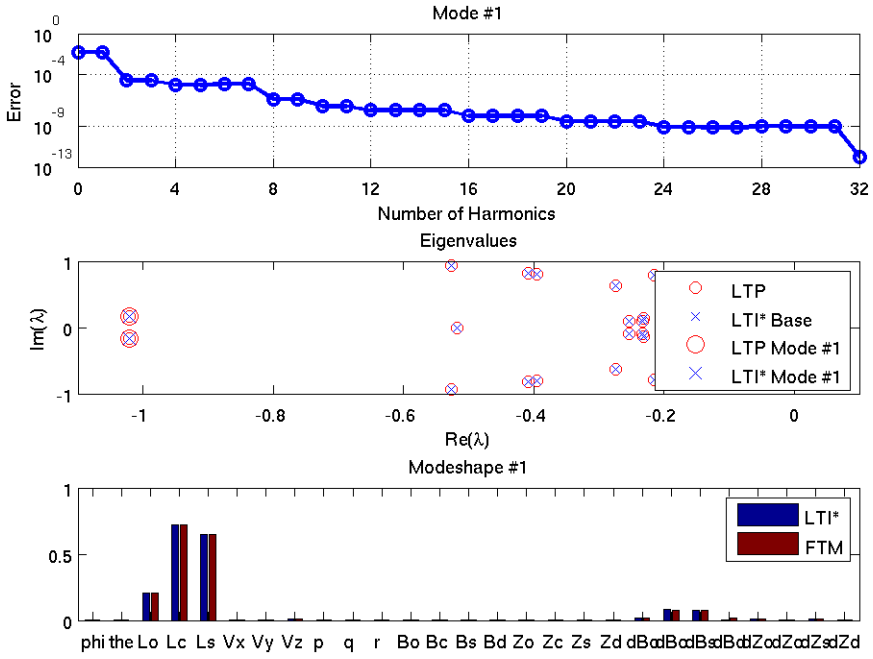

Figure 36. Rotocraft Model. Mode 1 : a) Error Sensitivity of LTI*, b) Eigenvalues on Imaginary Domain, LTP and LTI* c) Modeshape 1, FTM and LTI*

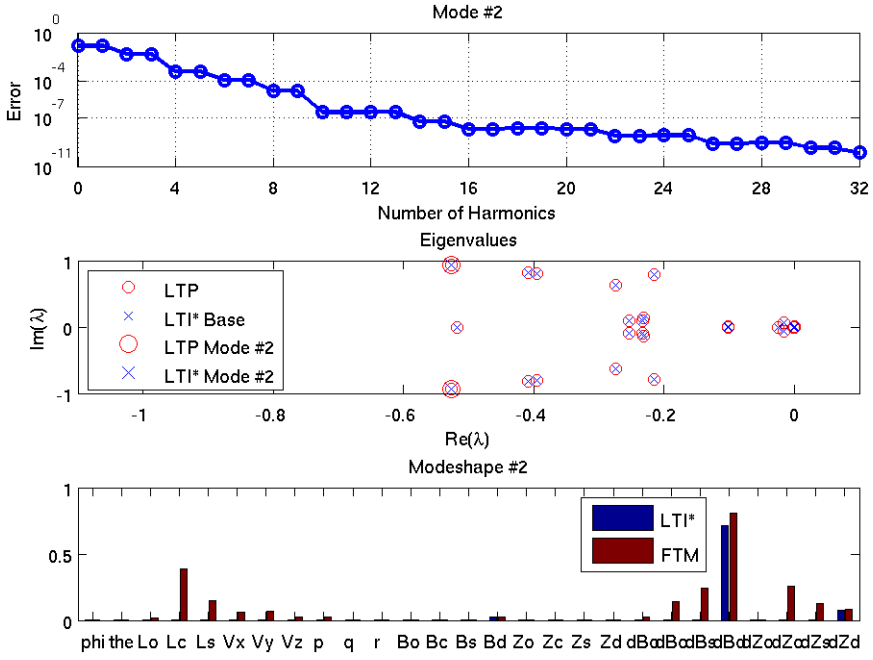

Figure 37. Rotocraft Model. Mode 2 : a) Error Sensitivity of LTI*, b) Eigenvalues on Imaginary Domain, LTP and LTI* c) Modeshape 2, FTM and LTI*

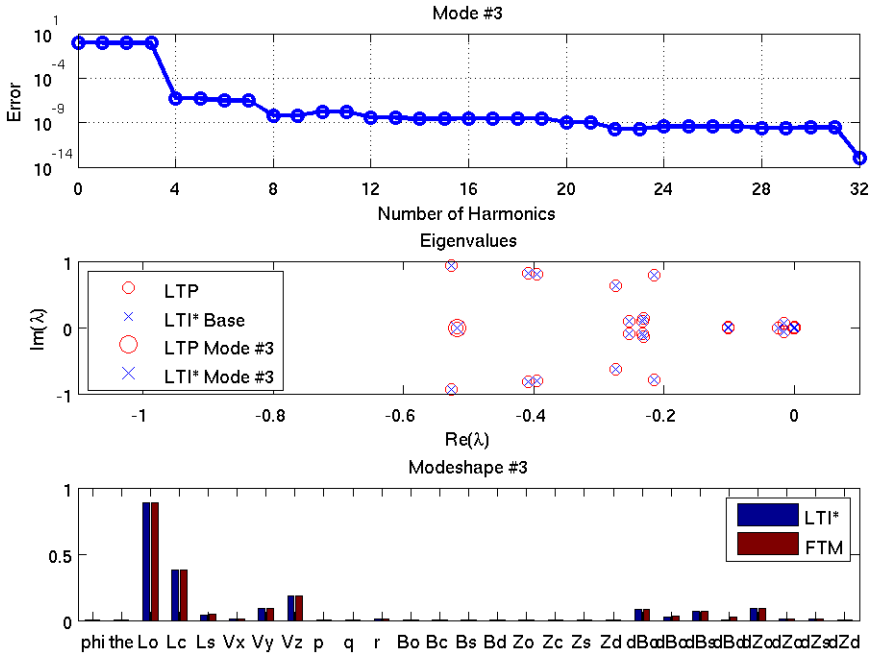

Figure 38. Rotocraft Model. Mode 3 : a) Error Sensitivity of LTI*, b) Eigenvalues on Imaginary Domain, LTP and LTI* c) Modeshape 3, FTM and LTI*

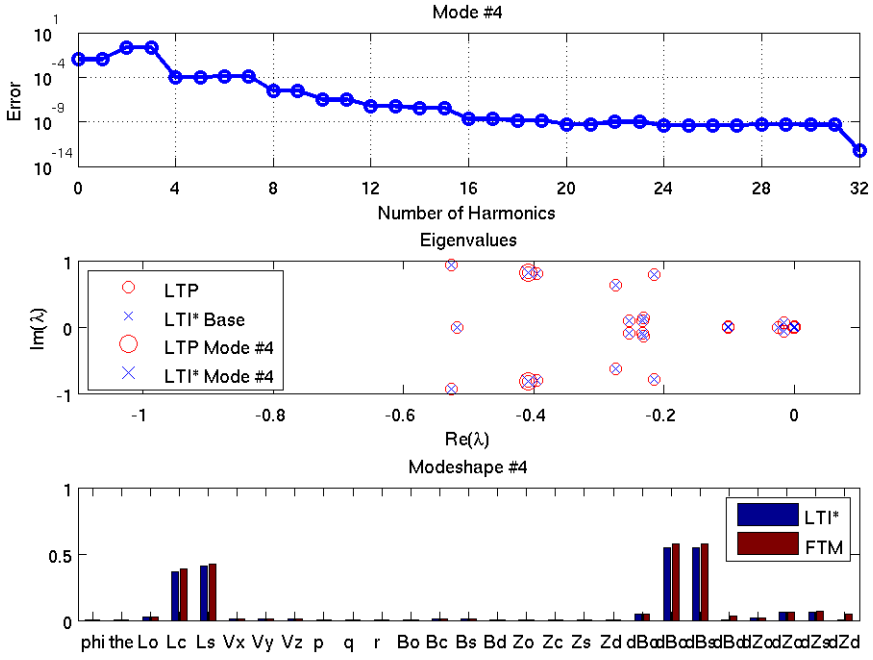

Figure 39. Rotocraft Model. Mode 4 : a) Error Sensitivity of LTI*, b) Eigenvalues on Imaginary Domain, LTP and LTI* c) Modeshape 4, FTM and LTI*

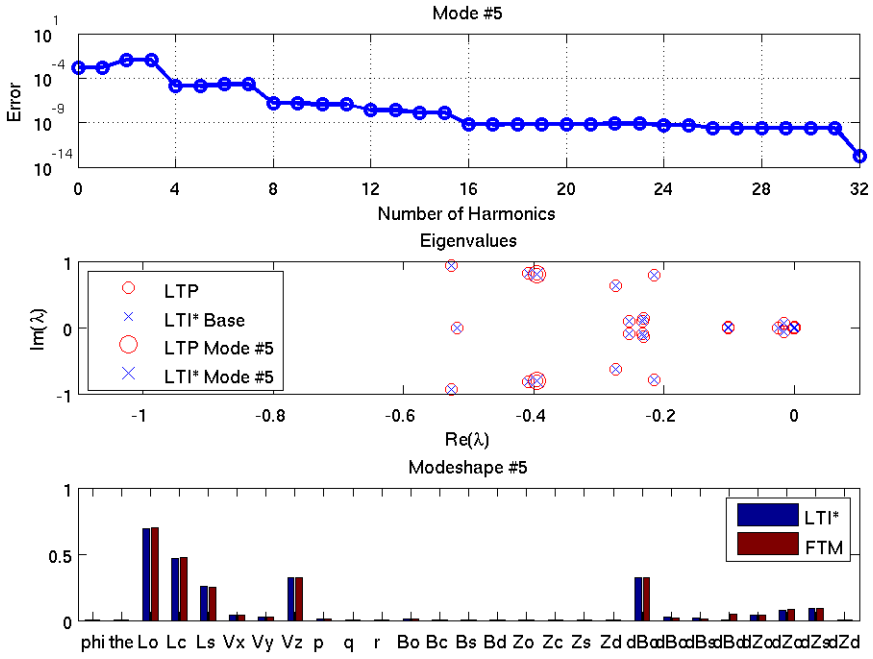

Figure 40. Rotocraft Model. Mode 5 : a) Error Sensitivity of LTI*, b) Eigenvalues on Imaginary Domain, LTP and LTI* c) Modeshape 5, FTM and LTI*

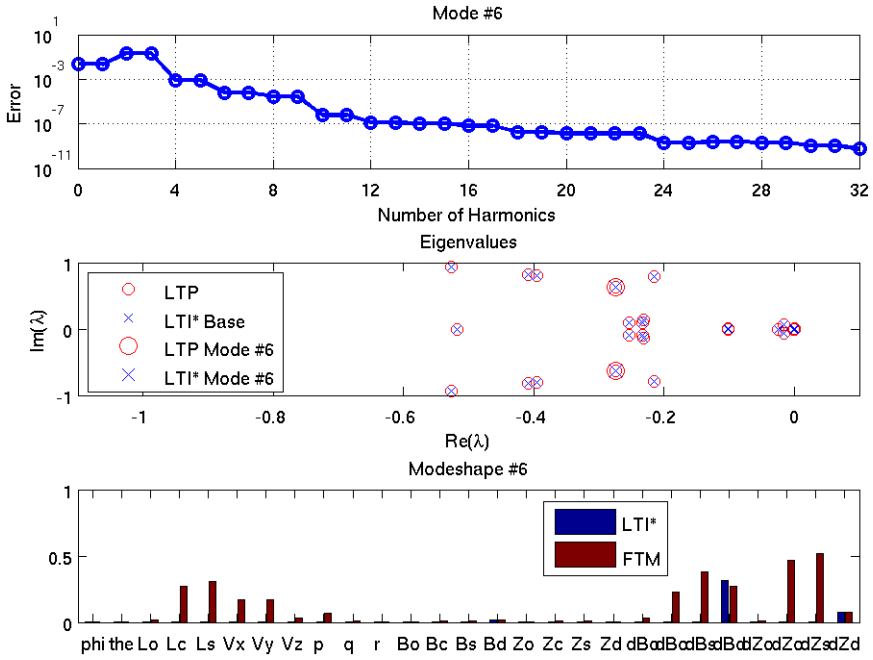

Figure 41. Rotocraft Model. Mode 6 : a) Error Sensitivity of LTI*, b) Eigenvalues on Imaginary Domain, LTP and LTI* c) Modeshape 6, FTM and LTI*

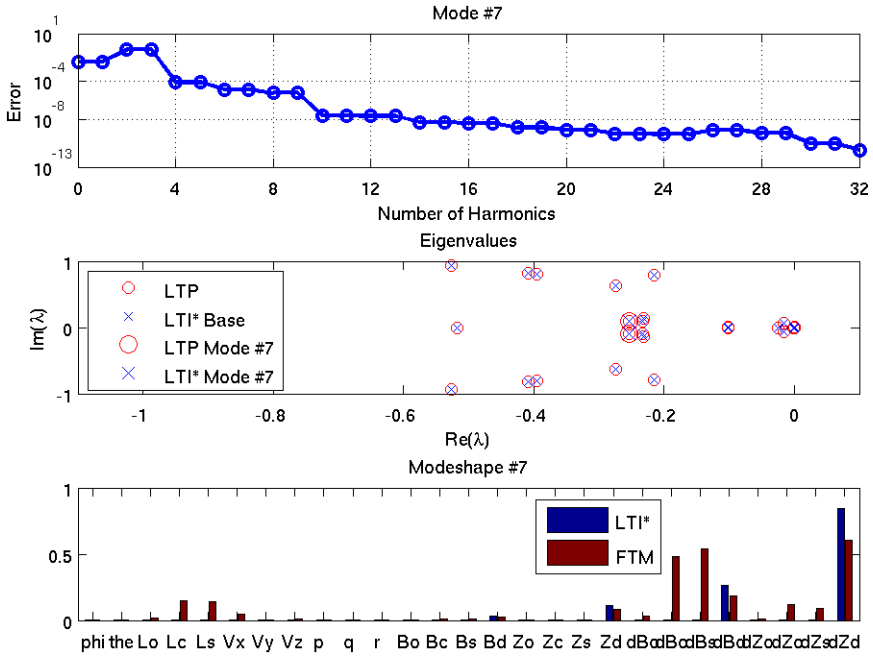

Figure 42. Rotocraft Model. Mode 7 : a) Error Sensitivity of LTI*, b) Eigenvalues on Imaginary Domain, LTP and LTI* c) Modeshape 7, FTM and LTI*

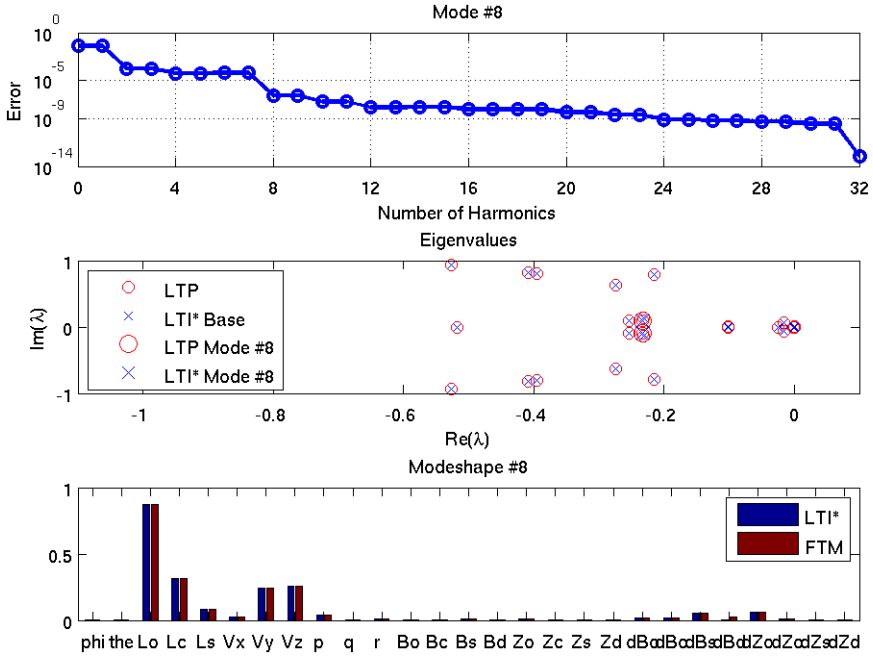

Figure 43. Rotocraft Model. Mode 8 : a) Error Sensitivity of LTI*, b) Eigenvalues on Imaginary Domain, LTP and LTI* c) Modeshape 8, FTM and LTI*

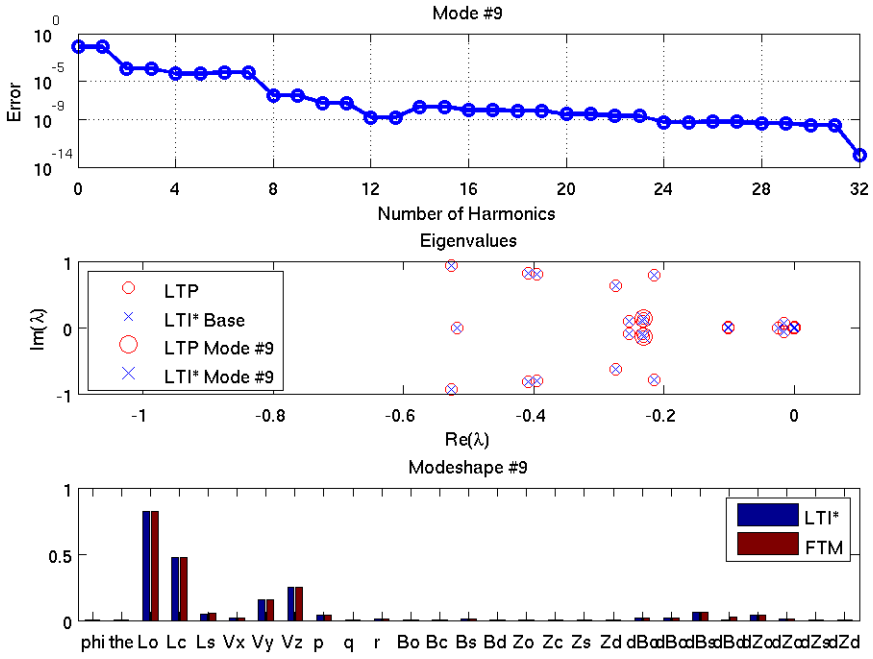

Figure 44. Rotocraft Model. Mode 9 : a) Error Sensitivity of LTI*, b) Eigenvalues on Imaginary Domain, LTP and LTI* c) Modeshape 9, FTM and LTI*

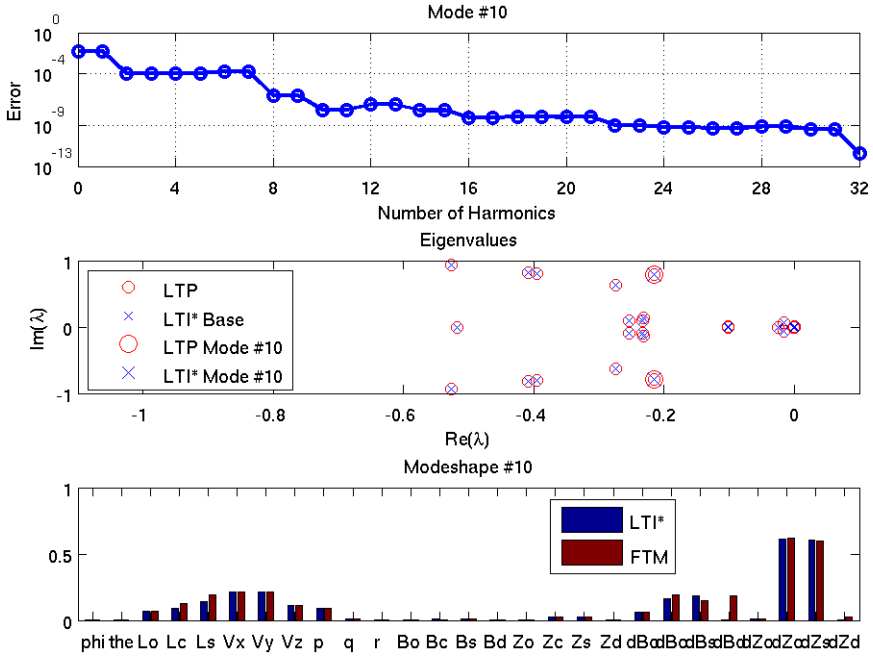

Figure 45. Rotocraft Model. Mode 10 : a) Error Sensitivity of LTI*, b) Eigenvalues on Imaginary Domain, LTP and LTI* c) Modeshape 10, FTM and LTI*

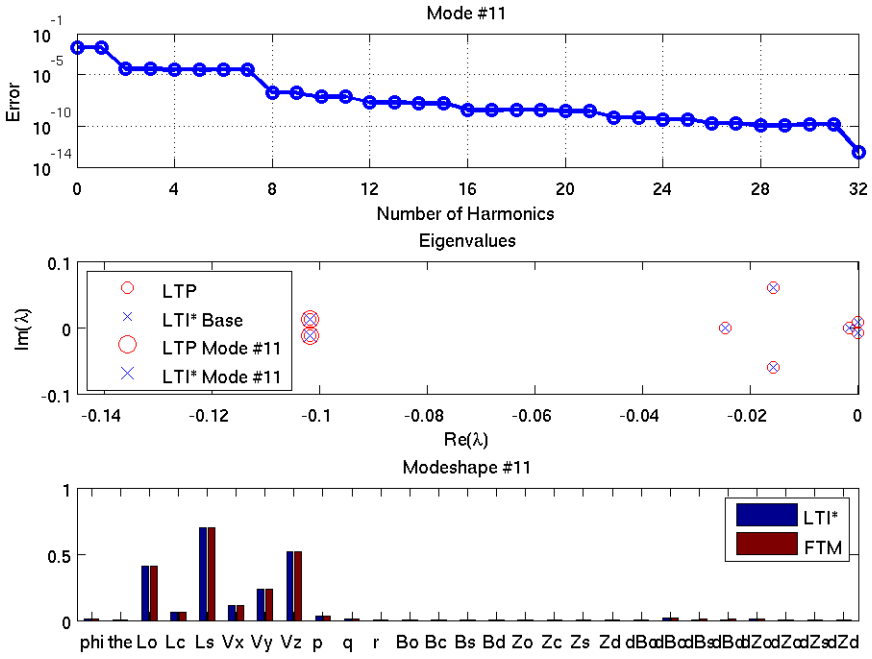

Figure 46. Rotocraft Model. Mode 11 : a) Error Sensitivity of LTI*, b) Eigenvalues on Imaginary Domain, LTP and LTI* c) Modeshape 11, FTM and LTI*

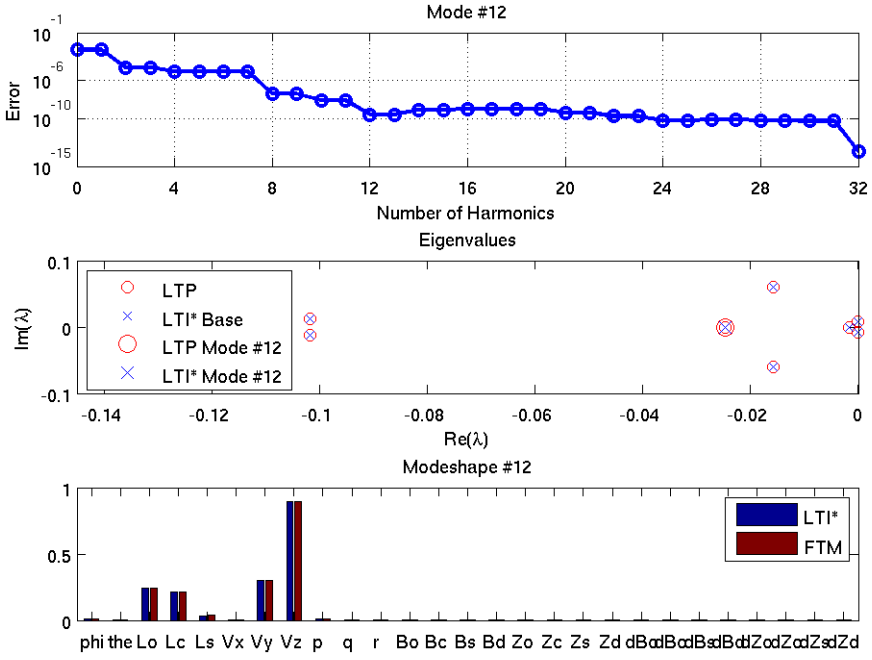

Figure 47. Rotocraft Model. Mode 12 : a) Error Sensitivity of LTI*, b) Eigenvalues on Imaginary Domain, LTP and LTI* c) Modeshape 12, FTM and LTI*

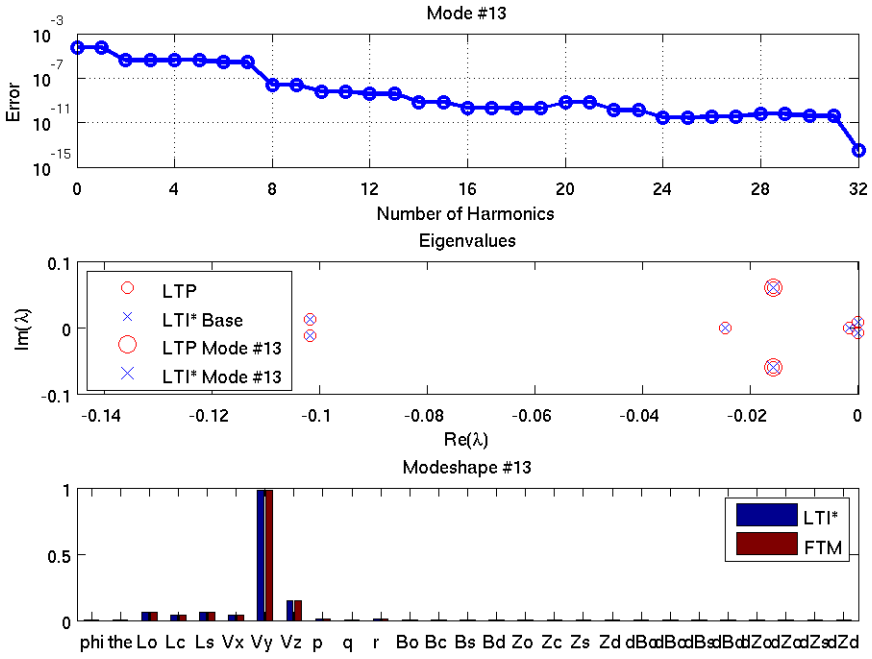

Figure 48. Rotocraft Model. Mode 13 : a) Error Sensitivity of LTI*, b) Eigenvalues on Imaginary Domain, LTP and LTI* c) Modeshape13, FTM and LTI*

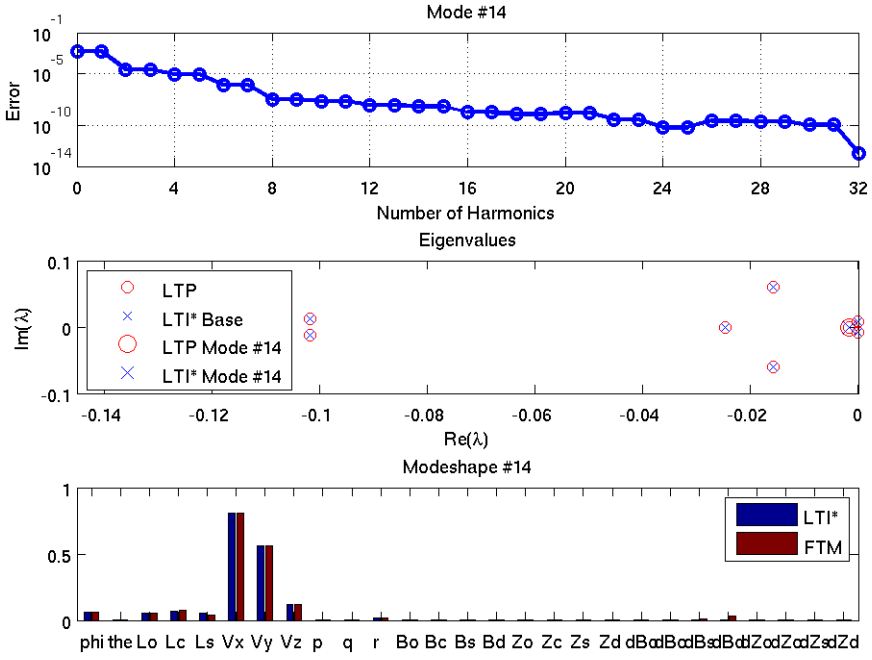

Figure 49. Rotocraft Model. Mode 14 : a) Error Sensitivity of LTI*, b) Eigenvalues on Imaginary Domain, LTP and LTI* c) Modeshape 14, FTM and LTI*

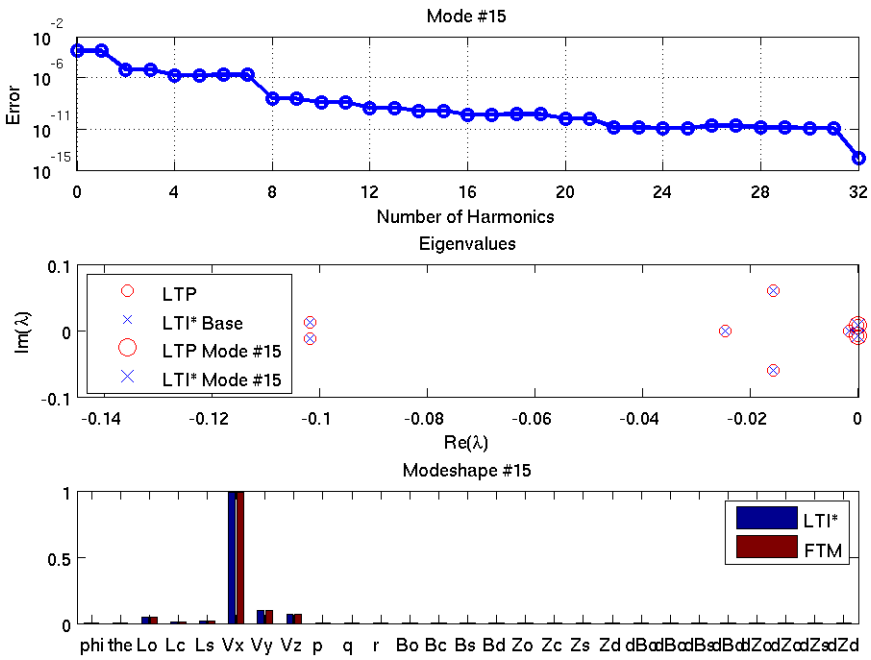

Figure 50. Rotocraft Model. Mode 15 : a) Error Sensitivity of LTI*, b) Eigenvalues on Imaginary Domain, LTP and LTI* c) Modeshape 15, FTM and LTI*

CHAPTER 4 LTI MODEL RESPONSE EVALUATIONS FOR IBC INPUTS

This chapter provides evaluation results for the method developed for the extraction of LTI models from a nonlinear model of a generic helicopter when an IBC input channel is used for excitation. The metrics used in the LTI model fidelity evaluations are introduced first. Next, the fidelity evaluation results for response characteristics are provided for the case of individual blade control applications. An evaluation of the response characteristics is presented in two sections for the time and frequency domain responses.

4.1 Metrics for Evaluation of Model Fidelity

Tischler and Remple [64] suggested the use of the metrics used here for checking the fidelity of flight mechanics models identified from test data in time and frequency domains.

The metrics below are adapted in this study by treating y_{data} as the response from the nonlinear model and y as the response from the LTI model. Δy in Eq. (67) is the perturbation time history of response from trim, n_t is the number of response points and n_o is the number of outputs. In Eq. (68), "T_c" is the transfer function from the nonlinear model, "T" is the transfer function from the LTI model, "γ_{xy}" is the coherence function, and "n_ω" is the number of discrete frequency points used.

The normalized fixed system hub forces and moments are used as outputs for model evaluations in this study as expressed in Eq. (66).

$$y = \left[\frac{F_x}{m} \quad \frac{F_y}{m} \quad \frac{F_z}{m} \quad \frac{M_x}{I_{xx}} \quad \frac{M_y}{I_{yy}} \quad \frac{M_z}{I_{zz}} \right]^T \tag{66}$$

It is suggested in [64] that 1 deg/s error is equivalent to 1 ft/s or 1 ft/s^2. Here, this equivalence is extended to 1 deg/s^2 as well. Hence, the fixed system hub forces and moments are normalized by the vehicle mass and the corresponding mass moments of inertia, respectively, as shown in Eq. (66). The elements of the weighting matrix "W" in "J" of Eq. (67) are appropriately selected to achieve this equivalency. It is suggested in [64] that for good model fidelity, the value of the time domain error index ($J^{(1)}$) needs to be less than 1 ~ 2 and that the value of the frequency domain error index ($J^{(2)}$) needs to be less than 100.

$$J^{(1)} = \sqrt{\frac{1}{n_t . n_o} \sum_{i=1}^{n_t} \left[(\Delta y_{data} - \Delta y)_i^T \, W \, (\Delta y_{data} - \Delta y)_i \right]} \tag{67}$$

$$J^{(2)} = \frac{20}{n_\omega} \sum_{\omega_1}^{\omega_{n_\omega}} W_\gamma \left[W_g \left(|T_c| - |T| \right)^2 + W_p (\angle T_c - \angle T)^2 \right] \tag{68}$$

$$\begin{aligned} where \;\; & W_\gamma(\omega) = [1.58 \cdot (1 - e^{-\gamma_{xy}^2})]^2, \\ & W_g = 1.0 \\ & W_p = 0.01745 \end{aligned} \tag{68.a}$$

4.2 Validation Studies for Response Characteristics

The following two sections investigate the response characteristics of the LTI models. Time and frequency domain responses to known practical input types and profiles are tried in the time domain, whereas a conventionally sine sweep is used for gathering the required time history for frequency domain validation studies.

The number of average states in the LTI model is 55, including 15 inflow and 8 body states (vehicle mass center velocity components, angular velocity components, body pitch and roll attitudes).It has 32 Multi Blade Coordinate (MBC) rotor states (16 for the rigid flap and lead-lag motions and 16 for the elastic flap and lag motions). The number of harmonic components of the rotor MBC states is 256 for the case when 1/rev to 4/rev sine and cosine harmonic components are included (64 for rigid mode flap, 64 for elastic mode flap, 64 for rigid mode lead-lag and 64 for elastic mode lead-lag) resulting in an LTI model order of 311. When the 1/rev to 8/rev sine and cosine harmonics of rotor MBC states are included, the resulting LTI model order becomes 567, which includes 55 average states and 512 harmonic sine and cosine components of the rotor MBC states. In the case of an isolated rotor representation, the body states are absent, thus reducing the LTI model order by 8. In general the number of states "N_s" for the extracted LTI model is given by Eq. (69)

$$N_s = ns_o + ns_r\left(2 \cdot n_h + 1\right) \tag{69}$$

where n_h is the number of harmonics, ns_o is the number of non-rotor (body and inflow) states, and ns_r is the number of rotor MBC states.

4.2.1 Time Domain Validation

This section uses the generic helicopter model (GHM) available in FLIGHTLAB with the enhancements mentioned earlier is used for the LTI model fidelity evaluations. The vehicle weighs 15,000 lbs and has a four bladed articulated rotor, a conventional tail rotor, a horizontal stabilizer, and a vertical fin. The analog and digital SAS portions of the control system are disabled in this study. The nonlinear model includes one rigid plus one elastic mode per flap as well as the lead-lag motions of each blade and a 15-state dynamic inflow model. The blade feathering is assumed to be rigid.

The LTI model fidelity evaluations are carried out for a forward flight case of a 0.15 advance ratio. The types of IBC inputs used are assumed to be similar to those used in the literature for vibration and noise control applications (for example, see [2, 3, 7]). In the time domain evaluations, the simulation time is set at 5 seconds for all cases. In each case, the simulation begins at trim, and the selected input is applied at 1 sec into the simulation. The input is turned off at 3 seconds into the run, and the simulation continues until 5 seconds.

Higher harmonic inputs (2/rev, 3/rev, 4/rev, etc.) are used in the literature for reductions in vibration, noise, and rotor power [2, 3, 7]. For reducing rotor power, a 2/rev individual blade control (IBC) input is suggested in [1]. In order to evaluate the fidelity of the extracted LTI models for their use in active rotor power reduction studies, a 2/rev IBC input of 2^o magnitude (similar in magnitude to what has been tried in [2]) and (an arbitrarily selected) 125^o phase is used in the LTI model fidelity evaluations. The resulting fixed hub load variations with time (as predicted from FLIGHTLAB and from the extracted LTI model) are compared in Figure 51. The LTI model includes up to 4/rev harmonic components of the rotor MBC states. Figure 52 is a zoom-in of the results from Figure 51. The time-domain error index computed using Eq. (67) is obtained as 0.316, indicating good fidelity of the extracted LTI model. Expected results are observed when 2/rev IBC inputs beneficially impact the steady state components of rotor thrust and torque as evident from the response predictions of F_z and M_z in Figure 51.

It is well known that N/rev vibration in the fixed system arises from blade force variations in the rotating frame at (N-1)/rev, N/rev and (N+1)/rev vibrations, where N is the number of blades [29]. Hence, as suggested from several studies in the literature (for example, [2]), it is expected that the IBC inputs at these frequencies can be used for vibration control. An IBC input consisting of 3/rev, 4/rev and 5/rev components is used

as a way to test the fidelity of the extracted LTI models for their use in active vibration control studies. The magnitudes of the harmonic components of the IBC are selected to be 1.5^o of 3/rev, 1^o of 4/rev and 0.5^o of 5/rev. These values are similar to the IBC harmonic component magnitudes used in [2]. The phases of the individual harmonic components of the IBC are selected arbitrarily. The extracted LTI model includes up to 4/rev harmonic components of rotor states. The fixed system hub load responses to the selected IBC input as predicted from FLIGHTLAB are compared with those predicted using the LTI model in Figure 53 with a zoom-in of the results shown in Figure 54. The time-domain error index computed using Eq. (67) is obtained as 0.612, indicating good model fidelity of the extracted LTI model, suggesting that the proposed LTI model extraction process can be used in active vibration control studies.

It is suggested in [3] that a combination of 6/rev and 7/rev may be used for simultaneous vibration and noise control. In order to verify the LTI model fidelity for its use in active vibration and noise control studies, a test case IBC input with 6/rev and 7/rev components of magnitudes (0.5^o of 6/rev and 0.5^o of 7/rev) similar to those considered in [3] is used. Two different orders of LTI model approximations are used, one that includes up to 4/rev harmonic components of rotor states and one that includes up to 8/rev harmonic components of rotor states. The predicted fixed system hub load responses from FLIGHTLAB are compared with those from the LTI model predictions in Figure 55 with a zoom-in of the results shown in Figure 56. The figures reveal that the inclusion of up to 8/rev harmonic components of rotor states in the LTI model improves the LTI model fidelity significantly (error index of 0.037) when compared to that of the LTI model with only up to 4/rev harmonic components of rotor states (error index 0.71). The higher frequency variations in the fixed hub load responses seen in the FLIGHTLAB

results are well captured in the predictions from the LTI model that includes up to 8/rev harmonic components of rotor states (see Figure 56).

Next, the LTI model fidelity is evaluated using pulse inputs of the IBC when a blade is passing through a selected azimuthal range. This input has been suggested in the literature [7] for avoidance of blade vortex interactions (BVI) by using a trailing edge flap actuation. A similar type of input is used with the IBC in the present study. The selected IBC input as a function of rotor azimuth angle is shown in Figure 57. The isolated rotor with the elastic blade and 15-state dynamic inflow model is used in this case in order to focus on the accuracy of the method. The predicted flapping response is shown in Figure 58 in terms of vertical deflection from the hub (shown in inches) at three different locations along the radius of a reference blade. A visual comparison of the isolated rotor elastic blade flapping responses from FLIGHTLAB and those from the LTI model indicates that the fidelity of the extracted LTI model is good, suggesting that the proposed LTI model extraction process can be used in active BVI control studies.

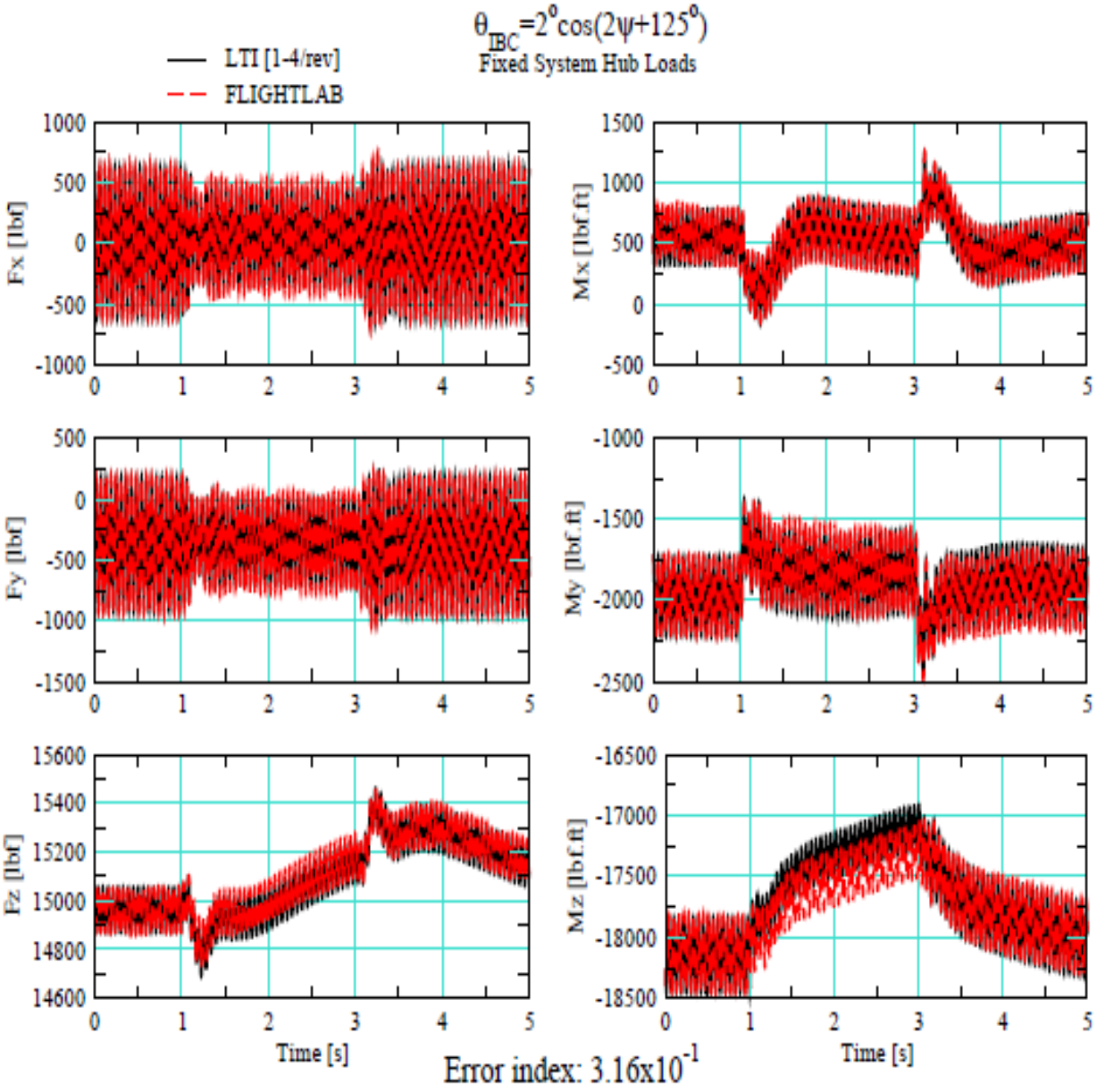

Figure 51. Predicted Fixed System Hub Load Variations to 2/rev IBC Input.

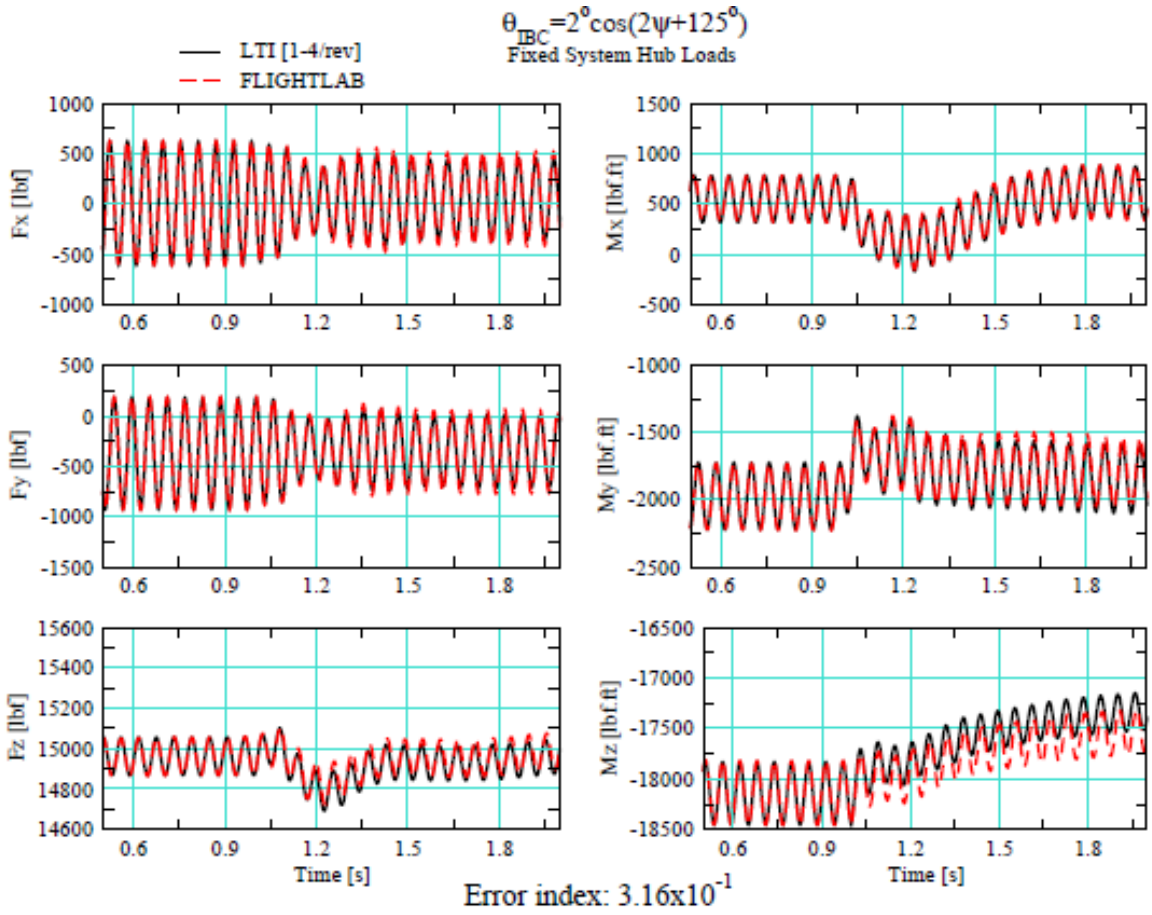

Figure 52. A zoom-in of Figure 51.

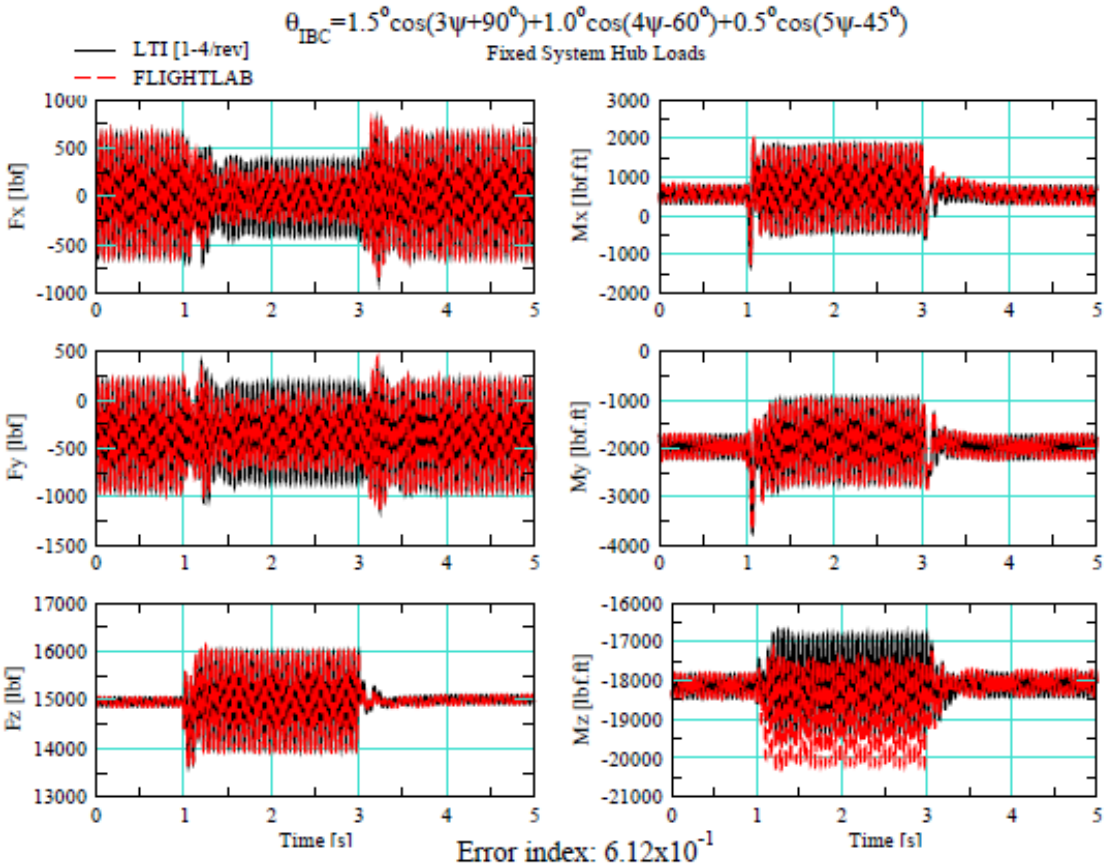

Figure 53. Predicted Fixed Stem Hub Load Variations to IBC Inputs with 3/rev, 4/rev and 5/rev Components.

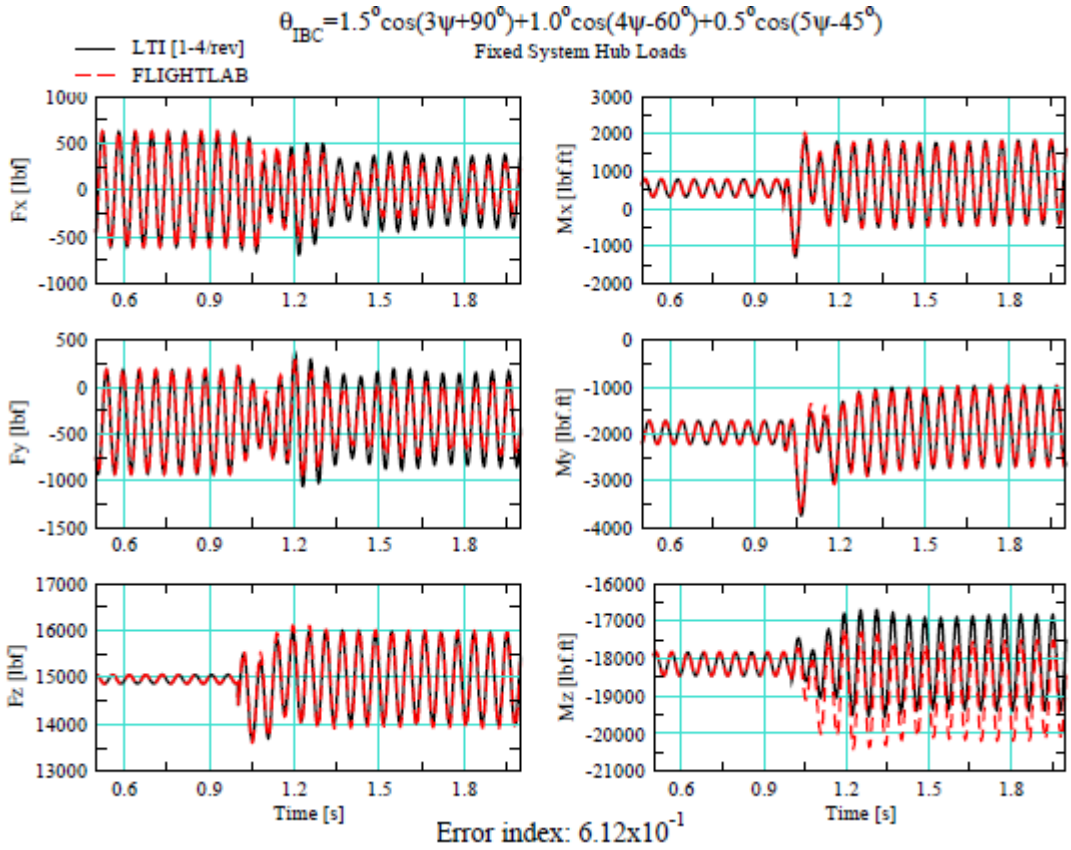

Figure 54. A zoom-in of Figure 53

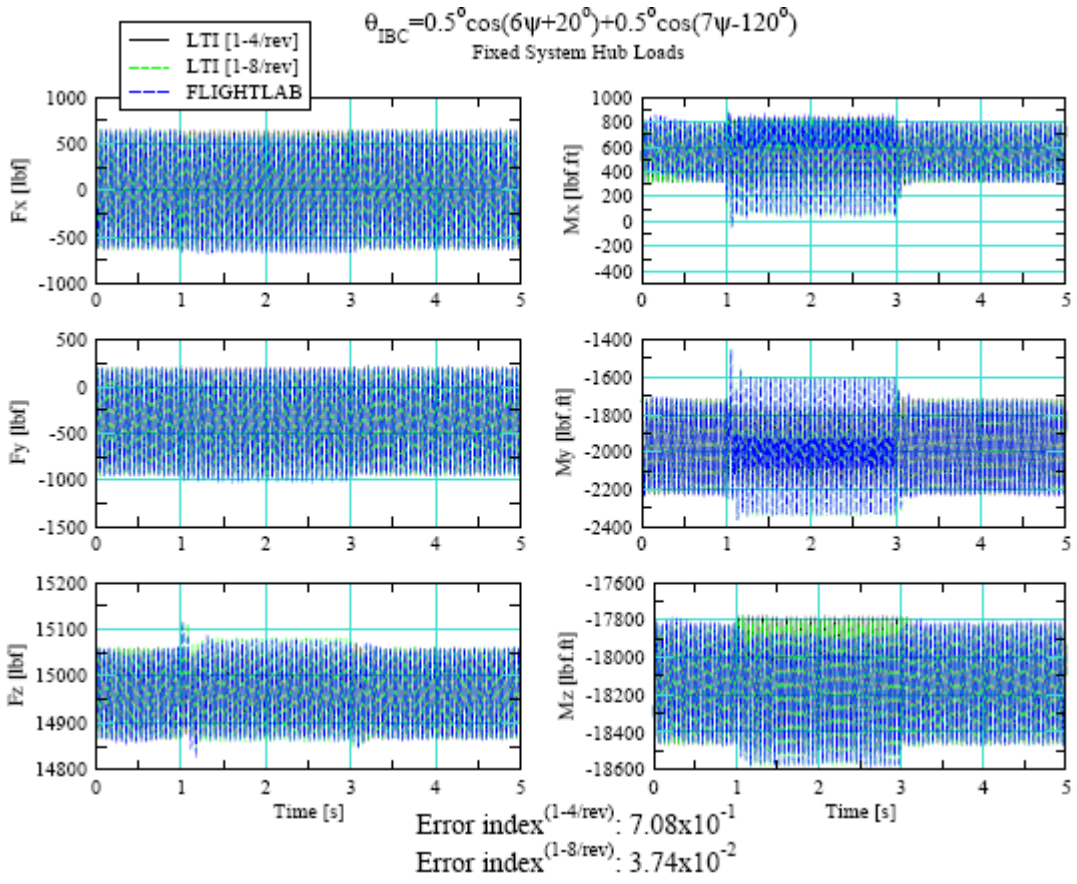

Figure 55. Predicted Fixed Stem Hub Load Variations to IBC Inputs with 6/rev and 7/rev Components.

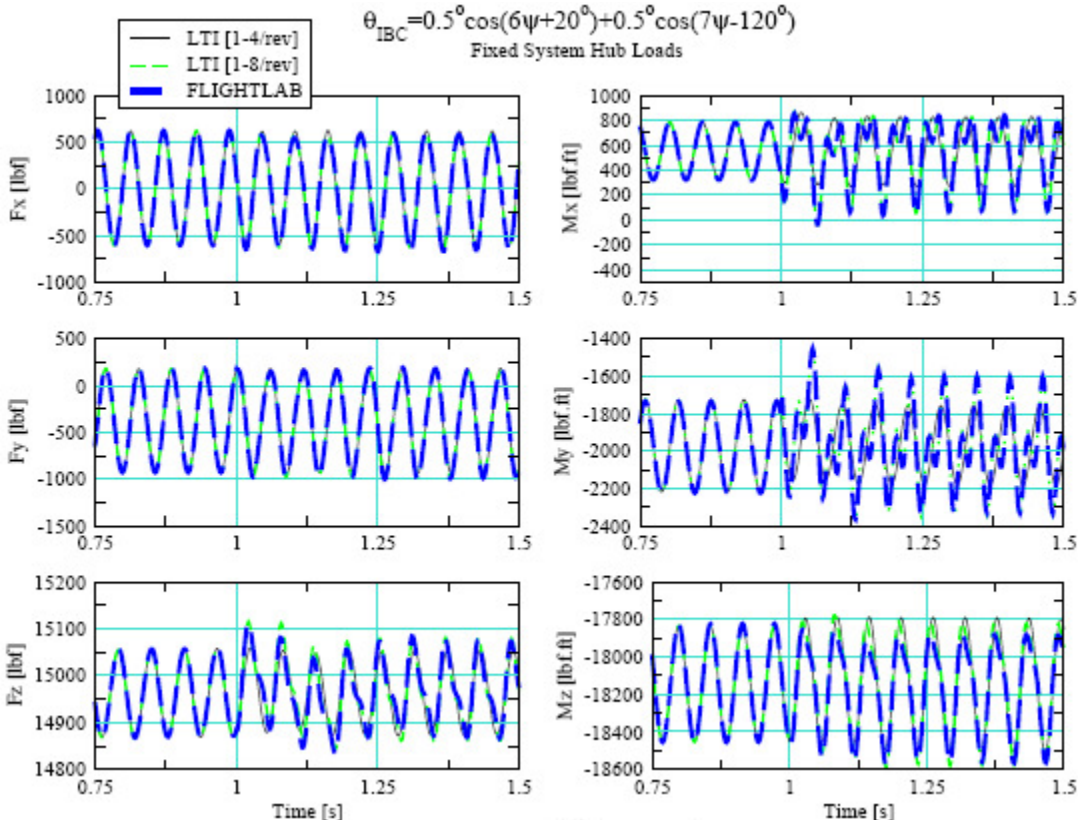

Figure 56. A zoom-in of Figure 55

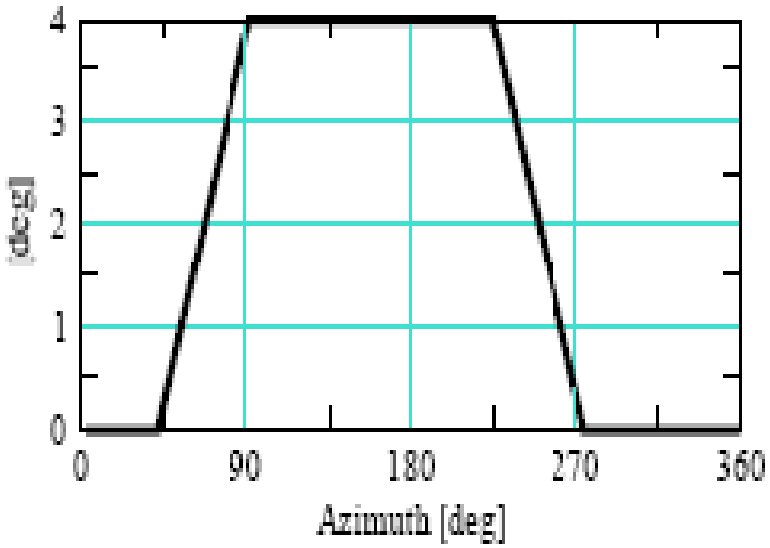

Figure 57. Selected Azimuth Dependent IBC Input.

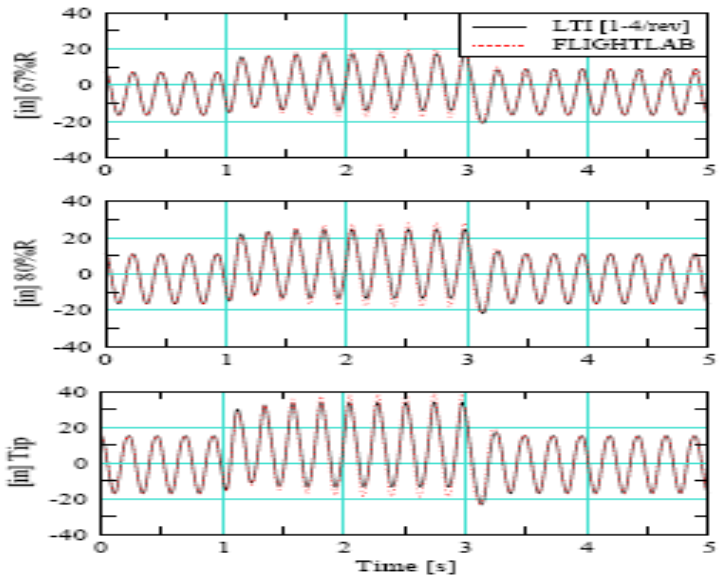

Figure 58. Predicted Elastic Blade Vertical Deflection (inches) in Response to the Selected IBC Pulse Input.

4.2.2 Frequency Domain Validation

The Comprehensive System Identification from Frequency Responses (CIFER) [64] is used to obtain frequency responses between the fixed system hub loads and the respective input channels, IBC or OBC. For frequency domain evaluations, time response is extracted using a sine sweep excitation with varying frequency in the respective input channel in order to obtain a frequency response. The initial and final frequencies are selected to obtain a broad band of frequency response. The starting frequency is assumed to be close to the lowest body mode, and the final frequency is assumed to be N_b/rev harmonic, where N_b is the number of blades. The duration of the signal is based on the CIFER guideline [64] as 2.5 times the highest period. The tabulated time data is transferred as an input to CIFER [64]. CIFER performs frequency response analyses using up to 5 different window sizes within its FRESPID module. Each FRESPID result with a different window size becomes an input to the COMPOSITE module in order to obtain a frequency response from a set of input/output data.

Both the FLIGHTLAB and LTI (up to 8/rev harmonics) models are excited through a single blade IBC frequency sweep input. The frequency sweep magnitude is set at 1 deg, and the frequency is linearly varied from 0.3 rad/sec to 135 rad/sec (=5Ω) with time. The duration of the frequency sweep is set at 120 seconds and the azimuthal increment (sampling rate) is set at $\Delta\psi=2.5^{o}$. Five different sizes of moving windows (24 sec, 12sec, 8 sec, 2 sec and 1 sec) are used in the construction of a composite frequency response from the frequency sweep input and output data. The generic helicopter with enhancements, elastic blade, and 15-state dynamic inflow model is used as in the time domain studies with the IBC input channel.

The predicted frequency responses between the fixed system rotor thrust (F_z) and rotor torque (M_z) to single blade IBC input are shown in Figure 59 and Figure 60, respectively. The frequency domain error indices for model fidelity in Figure 59 and Figure 60 are computed using Eq. (68), which are obtained as 17.6 and 16.8 for F_z and M_z outputs, respectively. These values are well within the bound of 100 suggested in [64], indicating a good fidelity of the extracted LTI model.

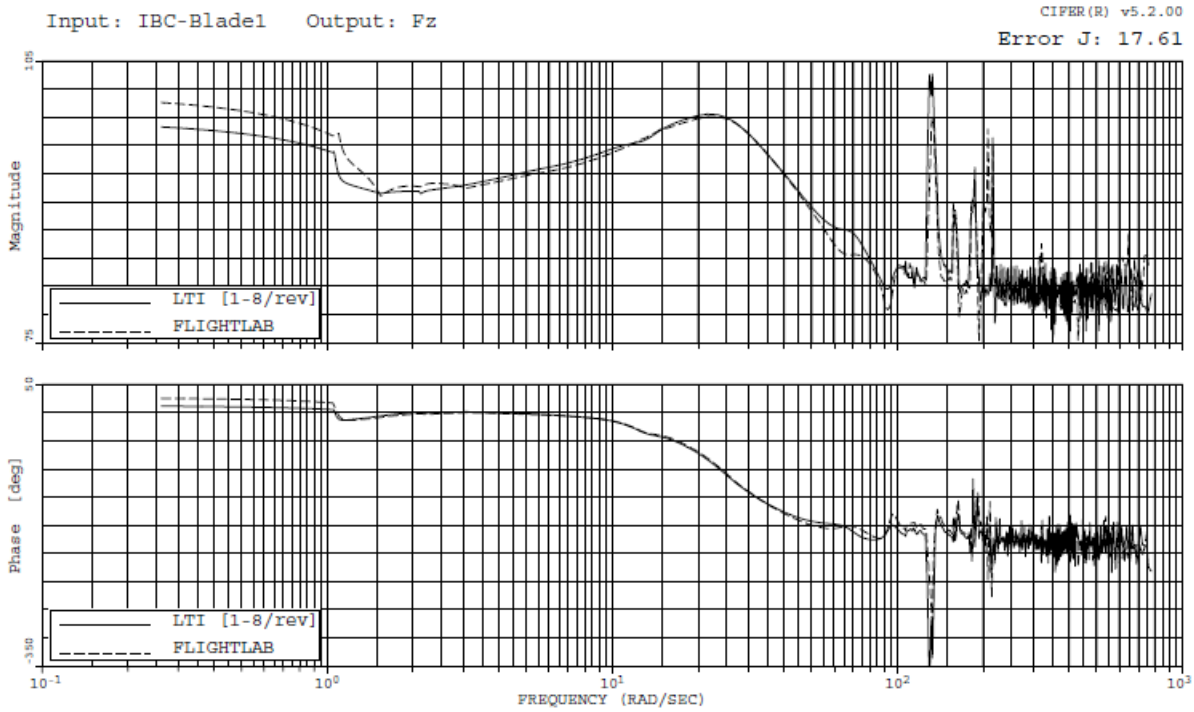

Figure 59. Predicted Frequency Response of Rotor Thrust to a Single Blade IBC Input.

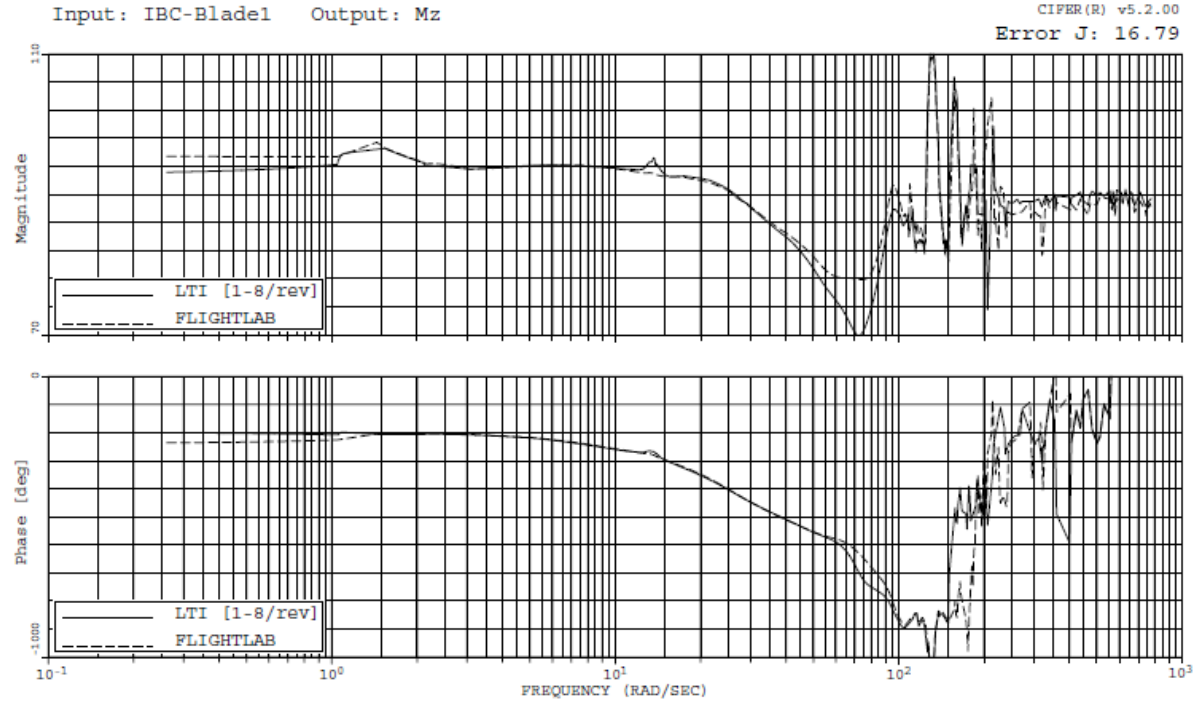

Figure 60. Predicted Frequency Response of Rotor Torque to a Single Blade IBC Input.

CHAPTER 5 LTI MODEL RESPONSE EVALUATIONS FOR OBC INPUTS

This chapter first explains the reduced order aerodynamic modeling of a flap actuator. In order to model the sensitivity of the aerodynamics of blade sections due to actuation of the trailing edge flap elements, adaptive neural networks are trained using extensive CFD data. These models are tested before being integrated into the FLIGHTLAB model. Then various scenarios are tested in the FLIGHTLAB environment to extract time and frequency response data. LTI model of FLIGHTLAB model incorporating reduced order aerodynamic model is extracted, and the time and frequency responses are evaluated for validation purposes.

5.1 NNET Model for Unsteady Aerodynamics

The current study adopts the development of a NNET based reduced order model for capturing the unsteady aerodynamic effects of a trailing edge flap actuator presented in the literature [65, 66]. The reduced order model is arrived at by first obtaining the changes that result from a trailing edge flap deflection on 2D airfoil data through CFD analysis. The compressible Navier-Stokes solver OVERFLOW version 2.0y is used in [67]. These changes are combined with existing baseline 2D airfoil data without a trailing edge flap. The changes in 2D airfoil data due to the deflection of a trailing edge flap are captured using a pre-trained NNET model from extensive CFD analysis data. Even for a limited range of inputs (see Table 1), a large amount of CPU time is required to produce

all the training data required for the NNET model. However, this is needed only once for a given airfoil and TEF configuration.

For the selected distribution of the input parameters of Table 1, CFD runs are designed for an airfoil (SC1095) with an integral quarter chord trailing edge flap (TEF) concept. Both airfoil and TEF angle are defined as sinusoidal functions as

$$\alpha = \alpha_o + \alpha_c \sin(\omega \cdot t) \tag{70.a}$$

$$\delta = \delta_c \sin(\omega_\delta \cdot t + \psi_\delta) \tag{70.b}$$

where ω is the oscillation frequency of the airfoil angle of attack, ω_δ is the oscillation frequency of the trailing edge flap deflection, and ψ_δ is the phase angle between the angle of attack and the TEF angle. The reduced frequency of the airfoil angle of attack and the trailing edge flap deflection are obtained using

$$k_\alpha = \frac{\omega b}{V} \tag{71.a}$$

$$k_\delta = \frac{\omega_\delta b_\delta}{V} \; where \; 4b_\delta = b \tag{71.b}$$

Reduced frequency, defined in general is a measure of unsteadiness (see [70] for rotorcraft applications and [71] for general unsteady aerodynamics) such that flow can be assumed steady only if the reduced frequency is below 0.05. Under this consideration, review of the reduced frequency numbers presented in Table 1 reassures the requirement of unsteady aerodynamic modeling in case of OBC applications.

The discrete sets of parameter values considered in the CFD analysis are given in Table 1. Each CFD run is conducted with a combination of these input parameters for a complete cycle. The values of the NNET input variables and the computed aerodynamic coefficients from the CFD analysis are extracted at each of the integration steps used.

Table 1. Parameters for CFD runs

Mach Number	Airfoil AoA	OBC Angle
M=[0.3 0.4]	α_o=[15 10 5 0 -6]	δ_c=[7 4 0]
	α_c=[10 5 2.5]	φ_δ=[0 90 180]
	k=[0 0.03 0.05 0.10]	k_δ=[0.5 1.0]k
M=[0.5 0.6]	α_o=[7 3 0 -3]	δ_c=[5 3 0]
	α_c=[4 2]	φ_δ=[0 90 180]
	k=[0 0.03 0.05 0.10]	k_δ=[0.5 1.0]k
M=[0.7]	α_o=[5 2 0 -2]	δ_c=[3 1.5 0]
	α_c=[2 1]	φ_δ=[0 90 180]
	k=[0 0.03 0.05 0.10]	k_δ=[0.5 1.0]k

The baseline aerodynamic coefficient values are subtracted from the CFD data in order to obtain the changes that result from the effect of a TEF deflection. Separate databases are recorded for each aerodynamic coefficient since individual training for each set is found to be computationally more efficient as each set may require different settings for the NNET training. Construction of the developed ROM is given in a generic equation form as

$$[c_d \quad c_l \quad c_m]_{base} = f_{table}(\alpha, M) \tag{72.a}$$

$$[c_d \quad c_l \quad c_m]_{cfd} = f_{cfd}(\alpha, \dot{\alpha}, M, \delta, \dot{\delta}) \tag{72.b}$$

$$\Delta[c_d \quad c_l \quad c_m] = [c_d \quad c_l \quad c_m]_{cfd} - [c_d \quad c_l \quad c_m]_{base} \tag{72.c}$$

$$\Delta[c_d \quad c_l \quad c_m] \cong \Delta[c_d \quad c_l \quad c_m]_{nnet} \tag{72.d}$$

where

$$\Delta[c_d \quad c_l \quad c_m]_{nnet} = f_{nnet}(\alpha, \dot{\alpha}, M, \delta, \dot{\delta}) \tag{72.e}$$

$$[c_d \quad c_l \quad c_m]_{rom} = f_{nnet} + f_{base} \tag{72.f}$$

The NNET model training is performed with a dedicated module within the FLIGHTLAB [55]. The NNET training makes use of the Levenberg-Marquardt algorithm [55] for the training of all three coefficients, i.e., ΔCl, ΔCm, and ΔCd. The selected values of various parameters such as the number of neurons, type of basis function, error tolerance, etc., for the NNET training are shown in Table 2. The number of neurons is selected to be much higher for the drag coefficient as compared to those for the lift and moment coefficients since the drag coefficient data from the CFD analysis shows significantly higher nonlinearity when compared to lift or pitching moment coefficients.

Table 2. Parameters for NNET training

	ΔC_d	ΔC_l	ΔC_m
Hidden Neurons	34	17	17
Hidden Activation Function	Tangent Hyperbolic	Tangent Hyperbolic	Tangent Hyperbolic
Output Activation Function	Linear $(-\infty,+\infty)$	Linear $(-\infty,+\infty)$	Linear $(-\infty,+\infty)$
Error Tolerance	10^{-6}	10^{-6}	10^{-6}
Maximum number of iterations	10	10	10

In order to make use of the reduced order model component of the trailing edge flap element in the form of the baseline plus the NNET airfoil data, the aerodynamic modules within the FLIGHTLAB are modified to include the effects of trailing edge flaps at user defined locations along a rotor blade. The selected baseline component in FLIGHTLAB makes use of Mach number and angle of attack as inputs. The NNET component makes use of the TEF deflection, TEF deflection rate, local value of the Mach number, angle of attack and its time rate as inputs in order to run the NNET model for evaluating incremental changes of aerodynamic coefficients due to TEF deflections.

5.2 Fidelity of the Reduced Order Model

The accuracy of the reduced order model was evaluated through comparisons with the CFD results from which the ROM was extracted. Sample results for the case of an SC-1095 airfoil with a trailing edge flap are shown in Figures 61 through 64. Figure 61 compares the ROM prediction of the lift coefficient of an SC-1095 airfoil with zero flap

deflection in a deep dynamic stall. The ROM result correlates well with the CFD simulation in terms of regarding both trend and magnitude. The ROM prediction also closely follows the trend of the secondary oscillation of lift coefficient during the early stage of the stall recovery as shown in the CFD results, but it is not as oscillatory as the CFD data. This could be improved by refining the NNET neuron structure. However, such a minor discrepancy is not a concern for practical applications. Similarly, good correlation of the pitch moment coefficient prediction by ROM with CFD was also achieved (See Figure 62). Figure 63 and Figure 64 compare ROM results with the CFD data for the case of SC-1095 plus flap combination. After the model was trained using CFD data, it was tested for additional data sets that were not used in the training. In general, very good agreement was found as shown in Figure 61 and Figure 62.

The fidelity of the trained NNET model in capturing the individual components of airloads, i.e., lift, drag and pitching moment, is evaluated after it is integrated with the baseline model within FLIGHTLAB. Example cases of CFD runs from Table 1 are used in the NNET fidelity evaluations. Figure 65 through Figure 67 show example comparisons between the CFD results and results from the NNET plus the baseline model. These results indicate that the lift and moment coefficient comparisons show very good correlation, while the drag coefficient comparisons show similar trends with a larger relative error.

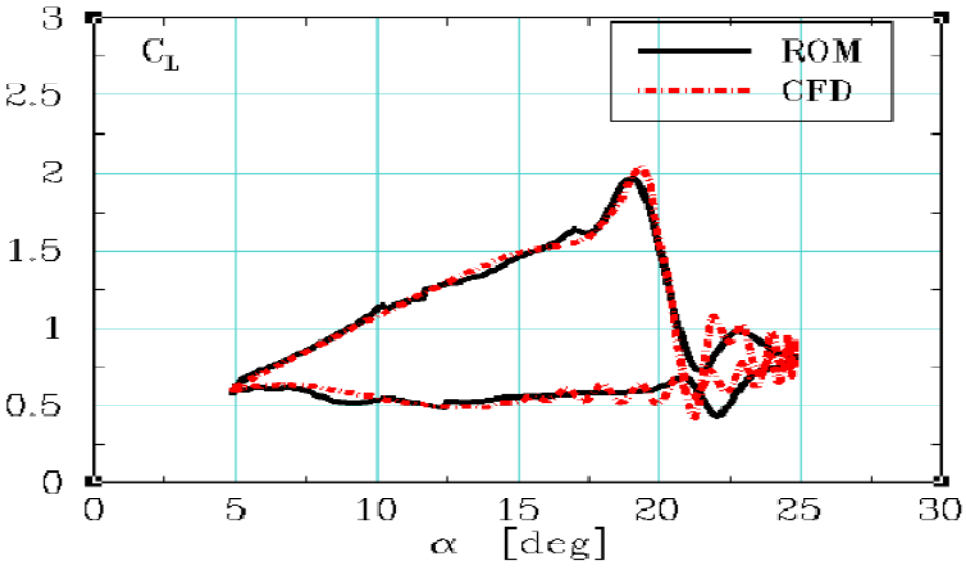

Figure 61. Computed and Predicted Lift Hysteresis Loops for a SC-1095 Airfoil in Deep Stall

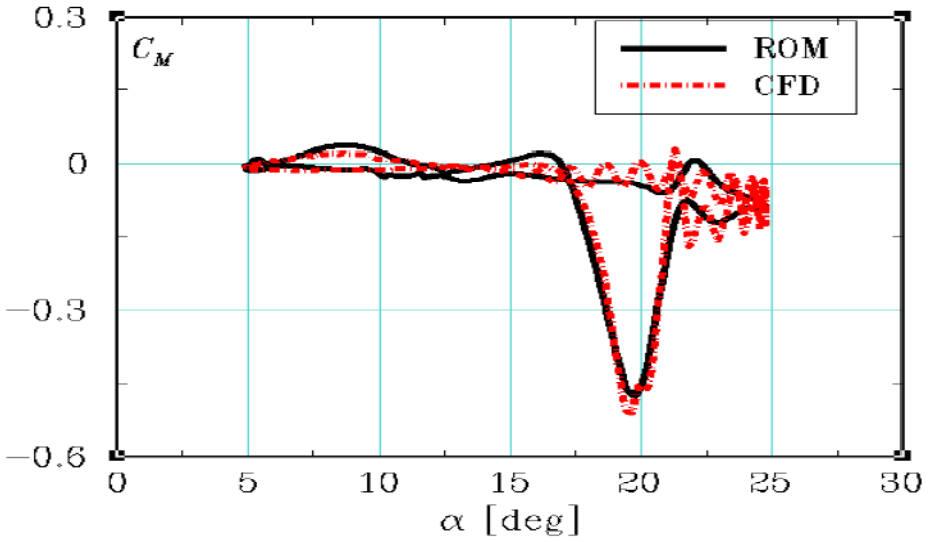

Figure 62. Computed and Predicted Moment Hysteresis Loops for a SC-1095 Airfoil in Deep Stall

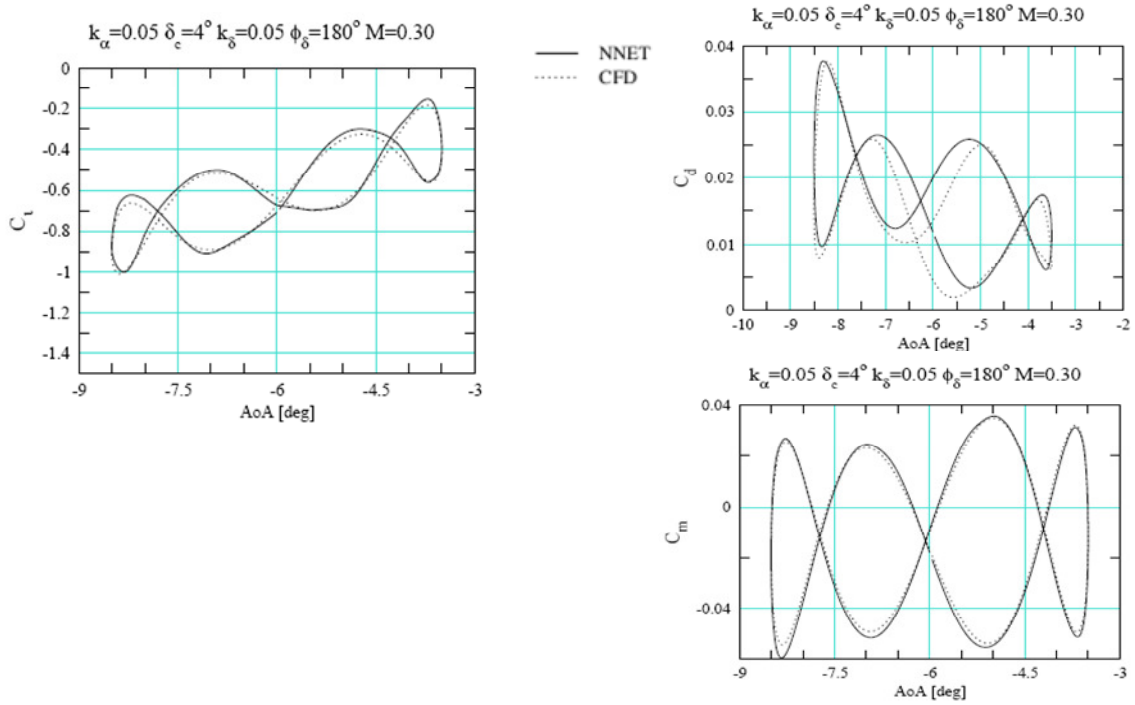

Figure 63. Computed and Predicted Lift Hysteresis Loops for a SC-1095 Airfoil +Flap Combination

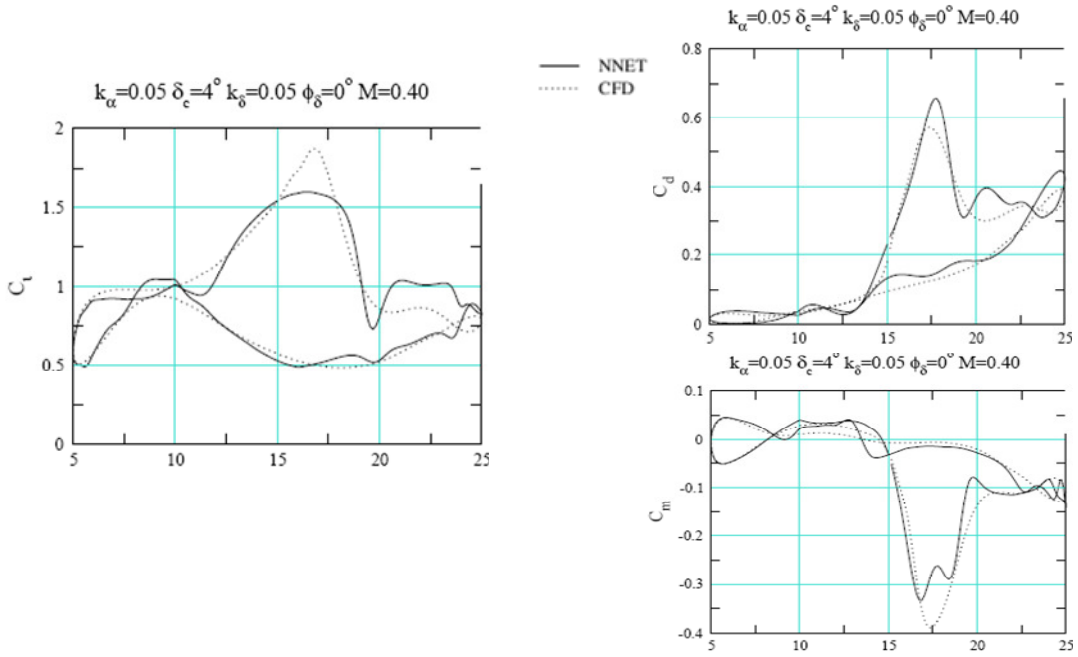

Figure 64. Computed and Predicted Moment Hysteresis Loops for a SC-1095 Airfoil +Flap Combination

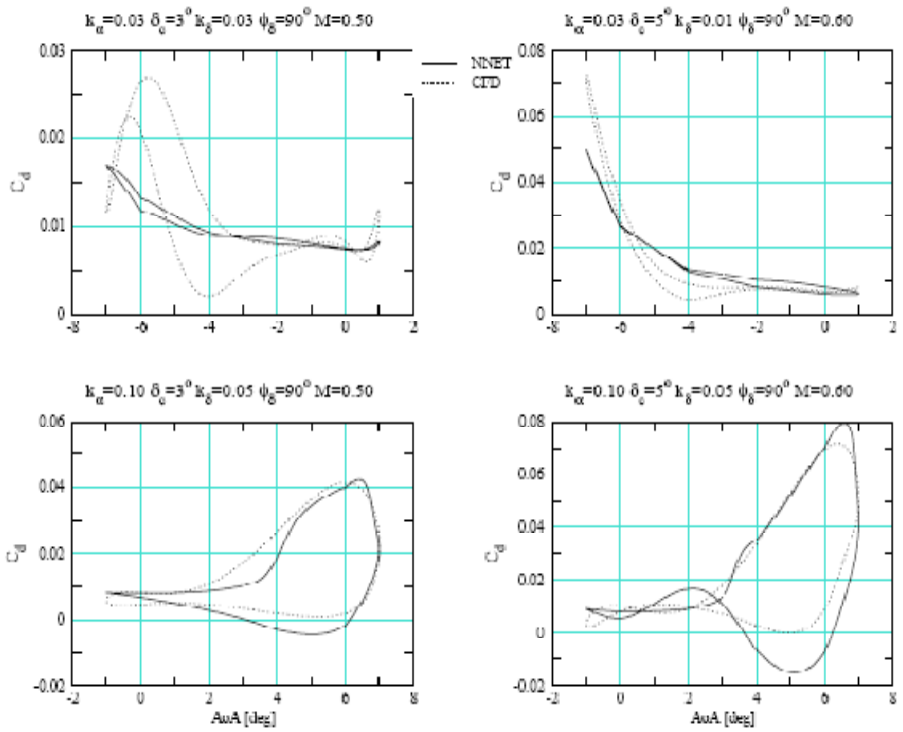

Figure 65. Drag Coefficient NNET Estimations Compared to CFD Data

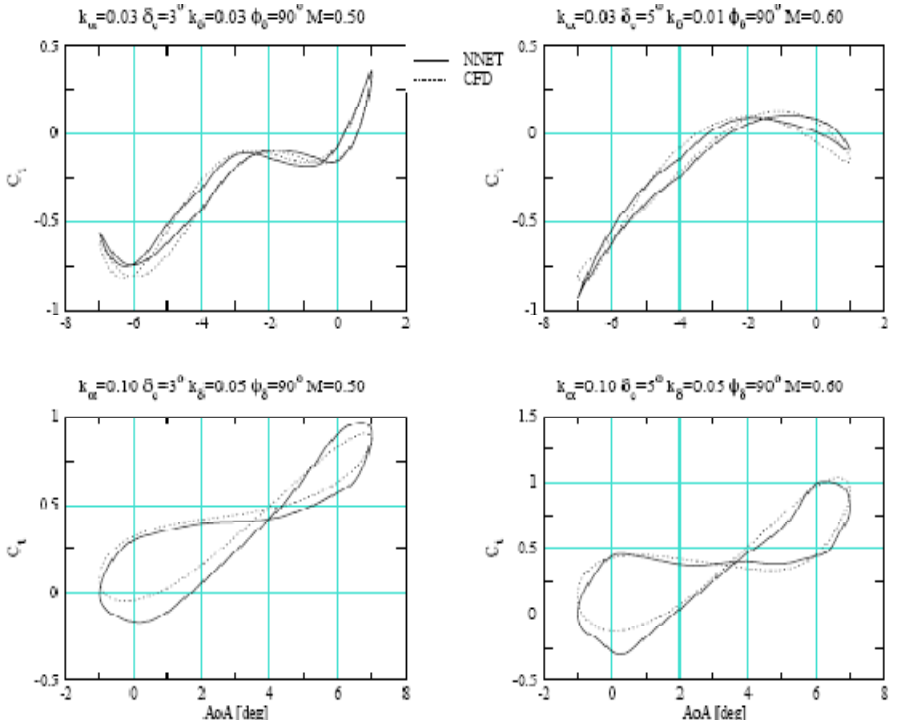

Figure 66. Lift Coefficient NNET Estimations Compared to CFD Data

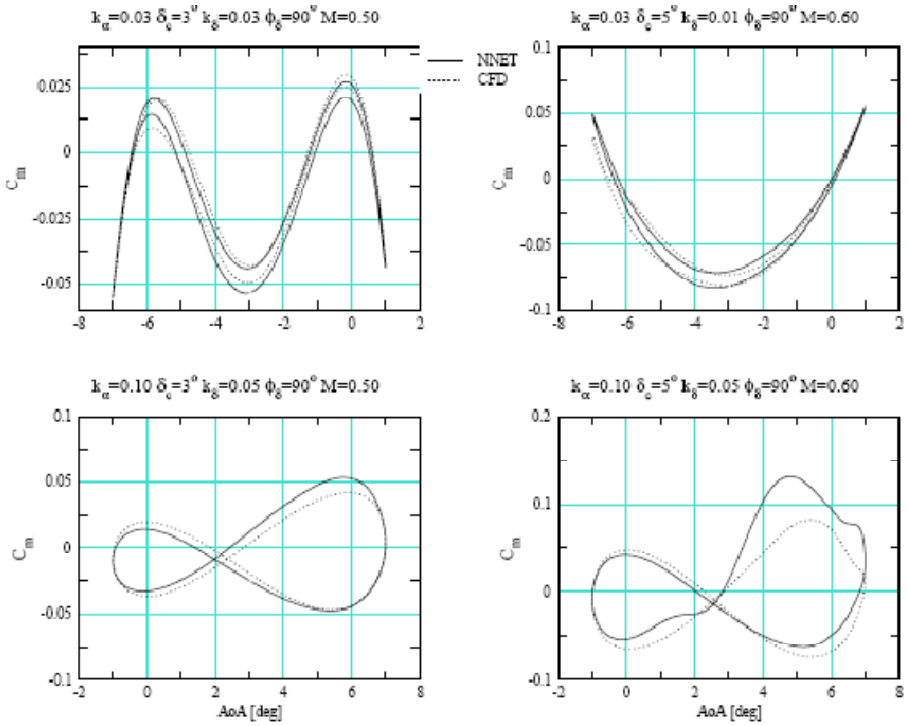

Figure 67. Moment Coefficient NNET Estimations Compared to CFD Data

5.3 LTI Model Response Evaluations for OBC Inputs

LTI model fidelity evaluations are carried out for an advance ratio of 0.15 TEF type OBC inputs. The types of inputs used in this study are taken from vibration and performance enhancement studies from the literature. In all cases considered, each simulation is carried out for 2.5 seconds with the selected TEF input turned on for 1 second from the 0.5 second to 1.5 second interval. The predicted fixed system hub forces and moments are shown for each evaluation case. As the scope of this study is limited to validation of LTI models and not necessarily to determine the optimum input needed for vibration reduction etc., arbitrary phasing is used for the harmonic input, while the magnitudes of the inputs are taken to be relatively similar to those used in past experimental studies.

All fidelity evaluations in this study are carried out using the modified version of a generic helicopter model with an elastic blade representation and a 33-state inflow model.

5.3.1 Time Response to On-Blade Control

Due to the nature of the aerodynamic effects from TEF deflections, higher harmonic excitations are expected, and hence, up to 8/rev harmonic representation is used in all of the evaluations. Similar to those used in the IBC applications, higher harmonic OBC inputs (2/rev, 3/rev, 4/rev, etc. where 1/rev is approximately 4.3 hertz) are also used in the literature for reductions in vibration, noise and rotor power [7, 4]. The TEF input "δ" tried for every case is embedded in the figures (Figure 68 - Figure 73) as a function of azimuth position "ψ".

For reducing rotor power, a 2/rev excitation is suggested in [2]. In order to evaluate the fidelity of the extracted LTI models for their use in active rotor power reduction studies, a 2/rev TEF input of 0.5° magnitude and (an arbitrarily selected) 70° phase is used in the LTI model fidelity evaluations. The resulting fixed hub load variations with time, as predicted from FLIGHTLAB and from the extracted LTI model, are compared in Figure 68. The LTI model includes up to 8/rev harmonic components of the rotor MBC states. These include rigid (flap & lag) and elastic modes (first elastic flap and first elastic lag), both. Figure 69 is a zoom-in of the results from Figure 68. The time-domain error index computed using Eq. (67) is less than 0.001, indicating good fidelity of the extracted LTI model.

As suggested from several studies in the literature (for example, [2]) and likewise inChapter 5, where IBC inputs were considered, it is expected that OBC inputs at these frequencies can be used for vibration control. A TEF input consisting of 3/rev, 4/rev and 5/rev components is used as a way to test the fidelity of the extracted LTI models for their use in active vibration control studies. The magnitudes of the harmonic components

of the TEF inputs are selected to be 1.0° of 3/rev, 0.5° of 4/rev and 0.25° of 5/rev. The phases of the individual harmonic components are selected arbitrarily. The extracted LTI model includes up to 8/rev harmonic components of the rotor states. The fixed system hub load responses to the selected TEF input as predicted from FLIGHTLAB are compared with those predicted using the LTI model in Figure 70, with a zoom-in of the results shown in Figure 71. Even though there is slight deviation in terms of both magnitude and phase visible in the zoom-in plot in Figure 71, the computed time-domain error index of 0.0135 indicates good model fidelity of the extracted LTI model.

Following the same background with the IBC applications, 6/rev and 7/rev may be used for simultaneous vibration and noise control. In order to verify the LTI model fidelity for its use in active vibration and noise control studies, a test case TEF input with 6/rev and 7/rev components of magnitudes (0.25° of both 6/rev and 7/rev) similar to those considered in [2] is used. The predicted fixed system hub load responses from FLIGHTLAB are compared with those from the LTI model predictions in Figure 72, with a zoom-in of the results shown in Figure 73. Once again, these results demonstrate the fidelity of the extracted LTI models.

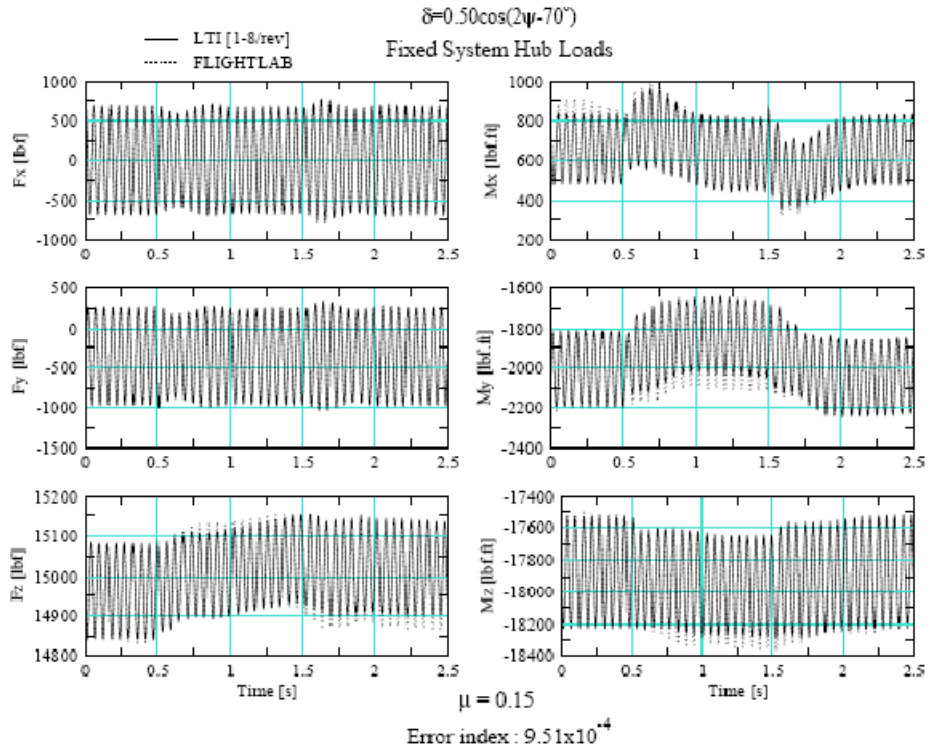

Figure 68. Predicted Fixed System Hub Load Variations to 2/rev TEF Input.

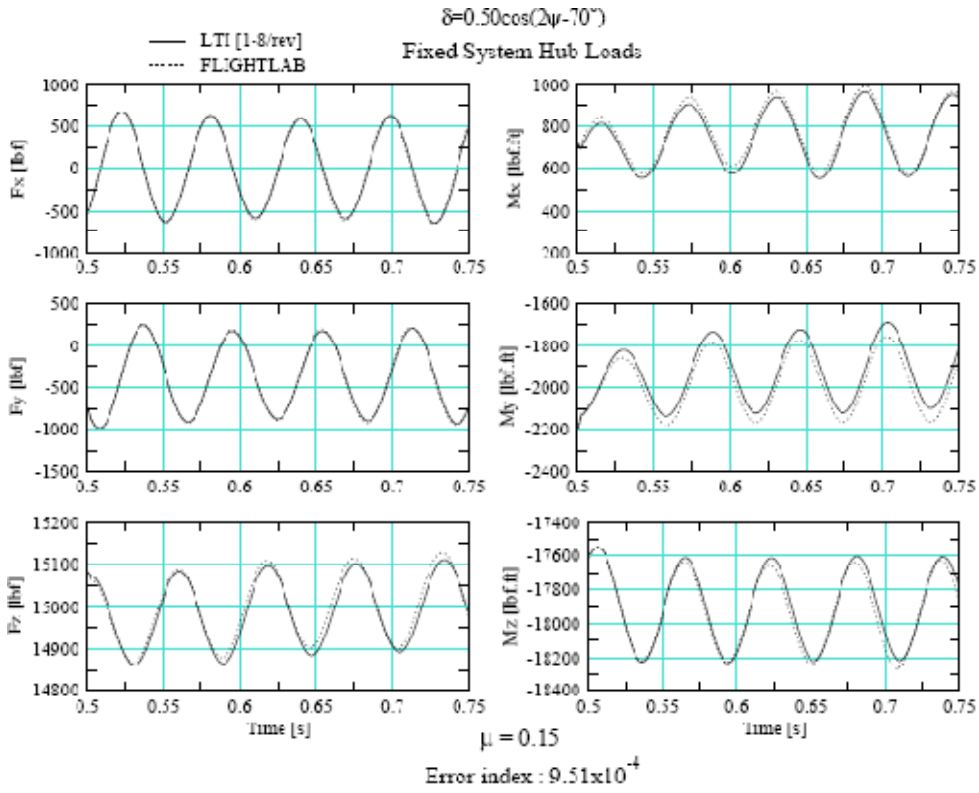

Figure 69. A zoom-in of Figure 68.

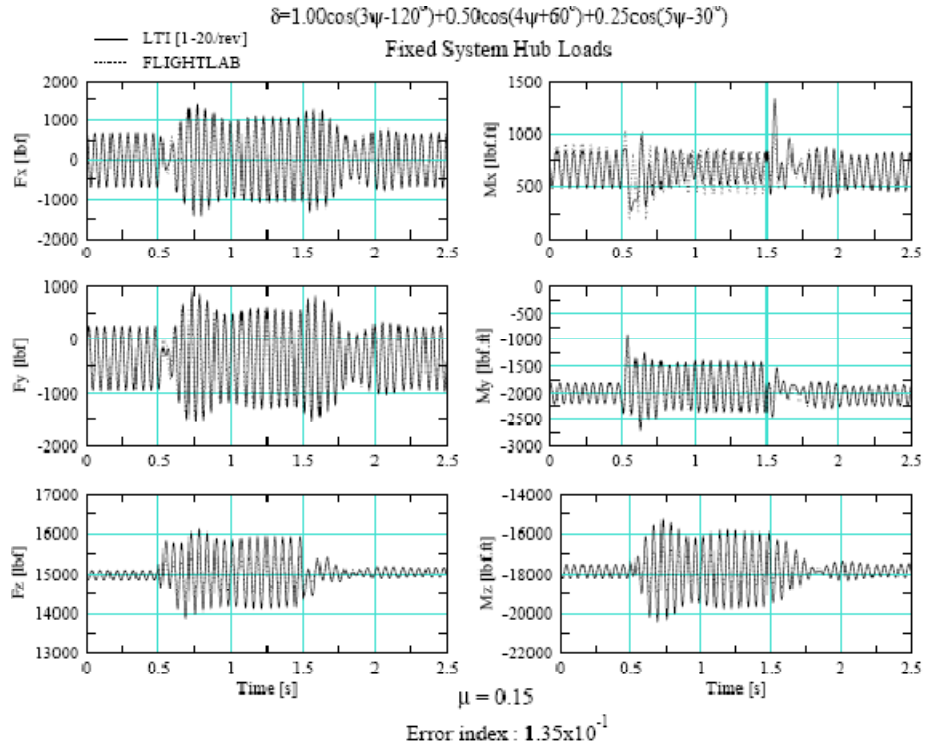

Figure 70. Predicted Fixed System Hub Load Variations to Combination of 3,4 & 5/rev TEF Input.

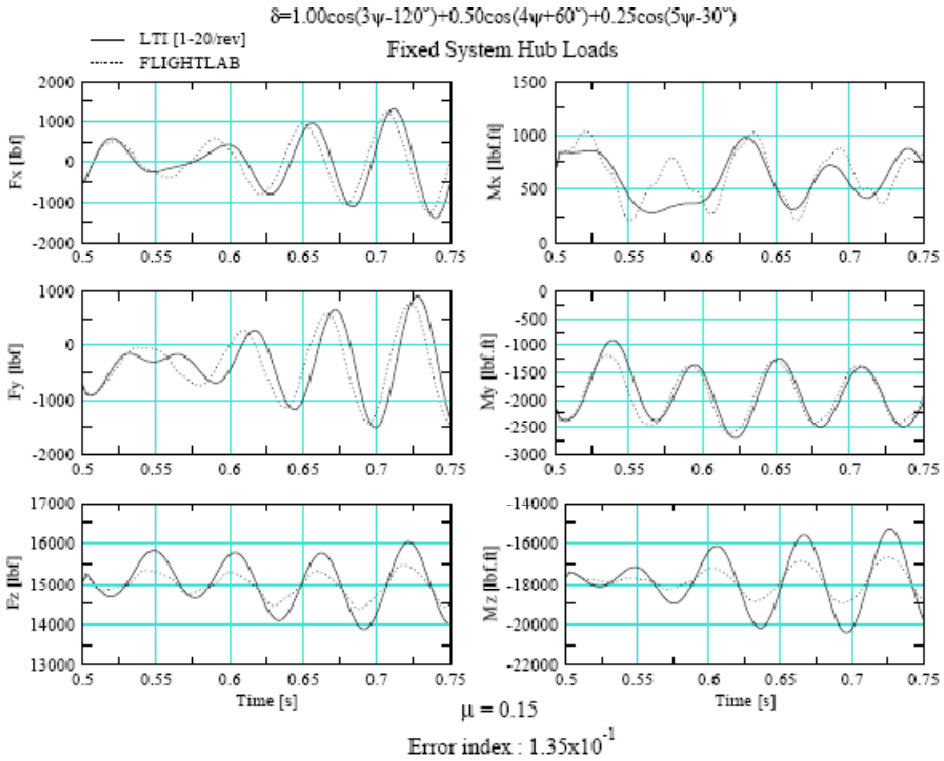

Figure 71. A zoom-in of Figure 70.

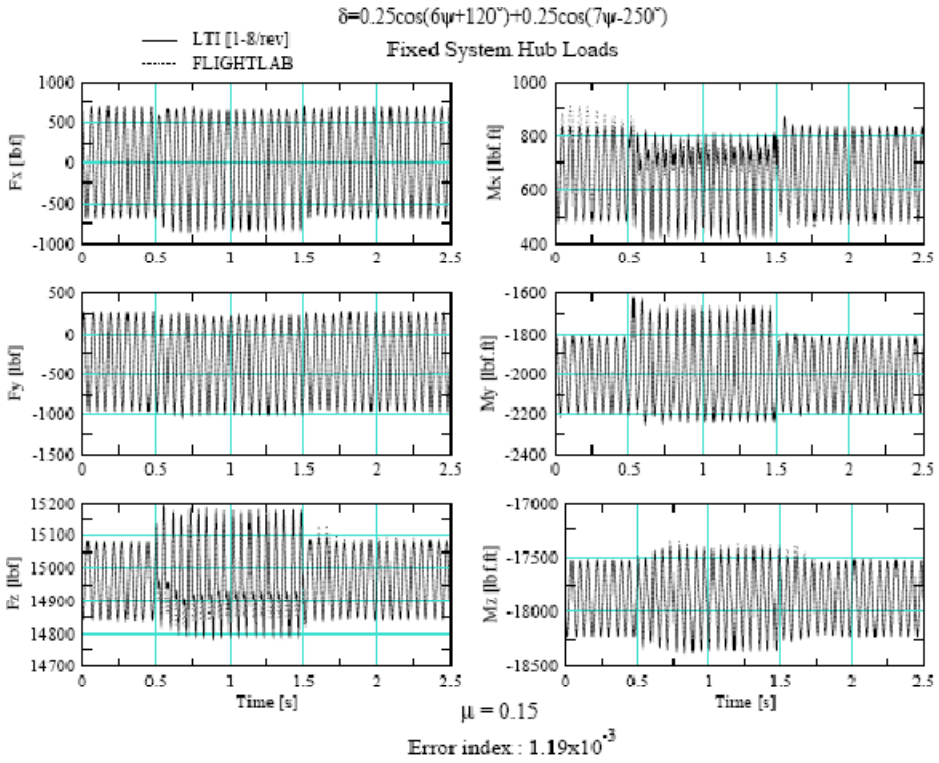

Figure 72. Predicted Fixed System Hub Load Variations to Combination of 6 & 7/rev TEF Input (1-8/rev).

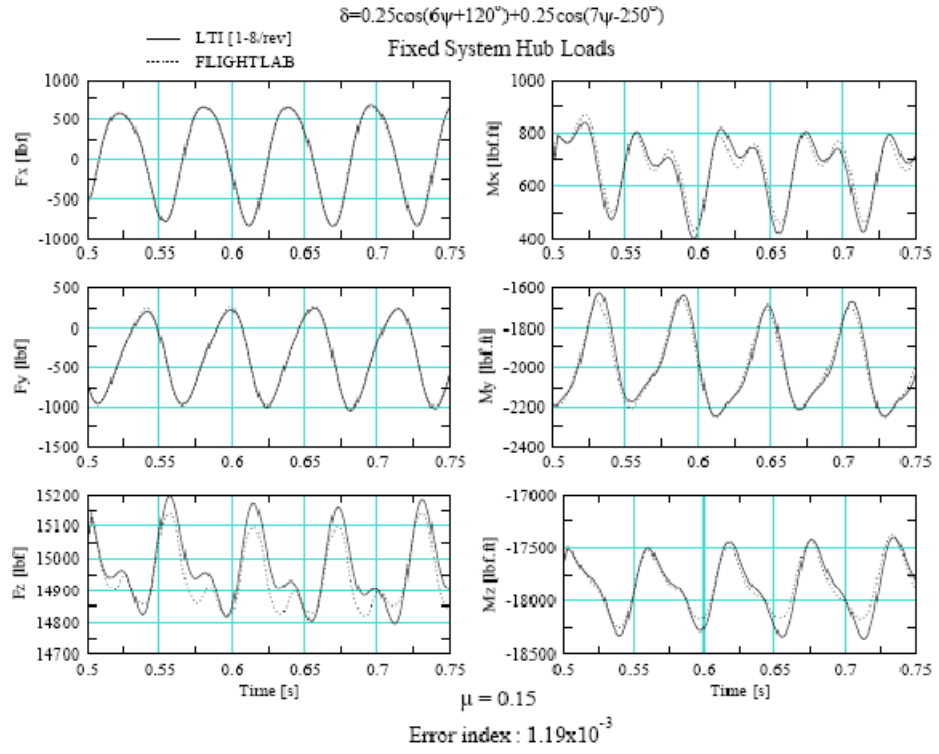

Figure 73. A zoom-in of Figure 72.

5.3.2 Frequency Response to On-Blade Control

Figure 74 and Figure 75 show the computed frequency responses of rotor thrust and torque due to TEF inputs. The selected TEF deflection magnitudes and rates considered as inputs are adjusted to ensure that the resulting aerodynamic effects due to TEF deflections stay within the linear range of the trained NNET. The composite responses of rotor thrust and torque along with the TEF inputs are used in CIFER [64] to arrive at frequency responses from the TEF input to rotor thrust and the TEF input to rotor torque. Figure 74 and Figure 75 provide frequency response comparisons between the FLIGHTLAB and LTI model results. The value of the frequency domain error index computed using Eq. (68) is 22.86 for the rotor thrust frequency response results (Figure 74) and 4.57 for the rotor torque response results (Figure 75). These values are well within the suggested value of less than 100 for good model fidelity [64].

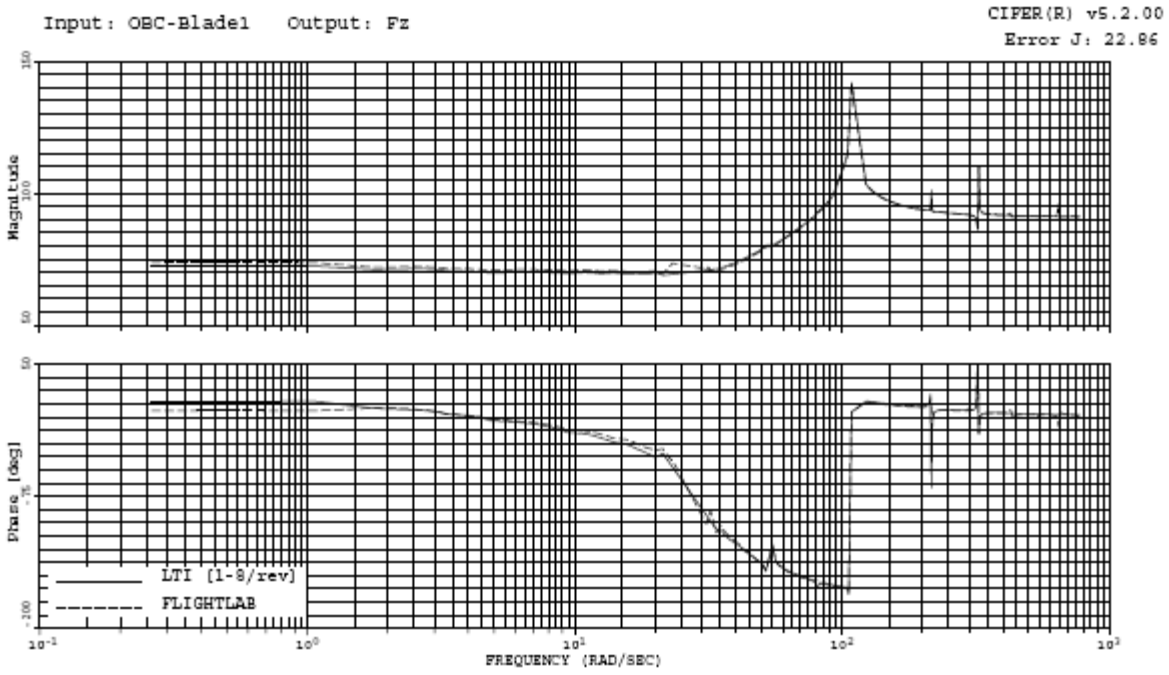

Figure 74. Predicted Frequency Response of Rotor Thrust to a Single Blade TEF Input.

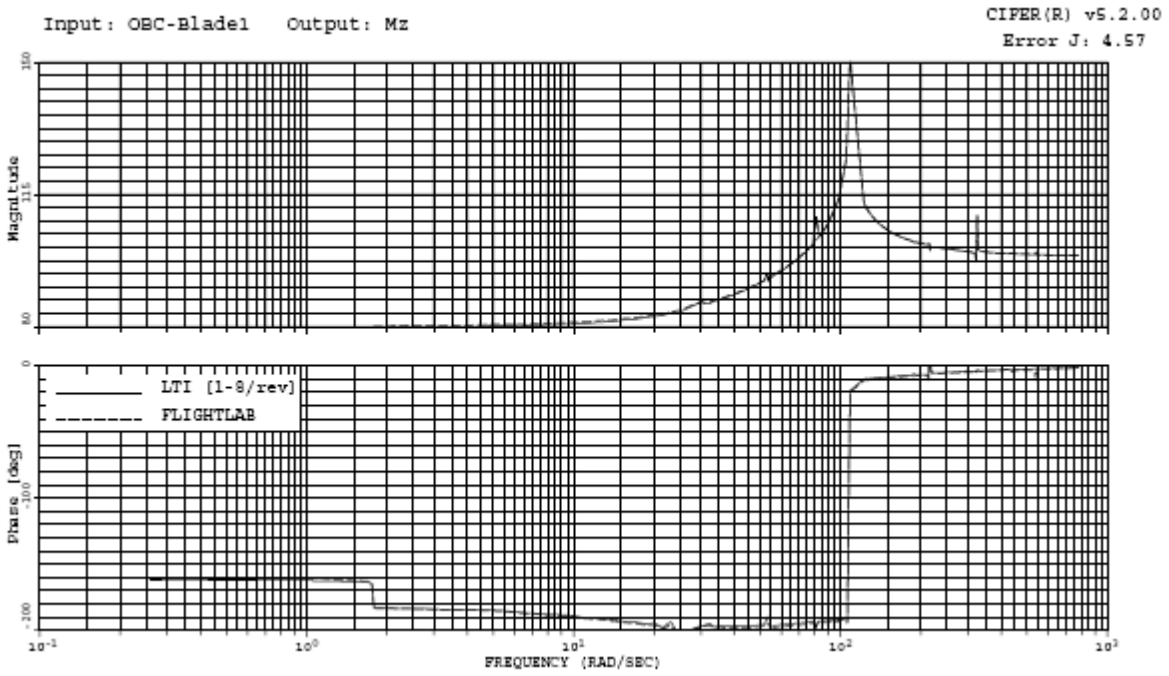

Figure 75. Predicted Frequency Response of Rotor Torque to a Single Blade TEF Input.

CHAPTER 6 CONCLUSION AND RECOMMENDATIONS

The formulation of linear time invariant (LTI) models of a nonlinear system about a periodic equilibrium using the harmonic domain representation is well established in the literature. A computationally efficient scheme for extraction of linear time invariant (LTI) models of a nonlinear helicopter model about a periodic equilibrium is developed during this study and presented in the literature [47, 56]. The developed computational approach makes use of closed form expressions relating various elements of an LTI model with the harmonic components of a corresponding linear time periodic (LTP) model. The developed numerical scheme is seen as improving computational speed by an order of magnitude when it is compared with the numerical scheme from the literature involving perturbations of individual harmonic components of state/control.

The developed computational scheme is implemented within FLIGHTLAB^{TM} and is used to extract LTI models of a generic helicopter nonlinear model in forward flight. The fidelity of the extracted LTI models is evaluated for stability properties against a self claimed error criterion, and response characteristics are verified in both time and frequency domains against the error metrics from the literature [64, 68]. Stability properties are compared in terms of the eigenvalues of the LTI and LTP models. Simulation comparisons are made between the nonlinear model and the extracted linear models using predicted fixed system hub load responses to typical individual blade control (IBC) and On-Blade Control (OBC) inputs that have been suggested in the literature for vibration, noise control, and BVI avoidance applications. The evaluation results demonstrate the fidelity of the extracted LTI models for response characteristics, but the fidelity is limited for the stability characteristics. Although LTI can be used with

this limited fidelity, extension of the method is found to be vital for the fidelity of the stability properties in order to make use of the LTI model in integrated flight and rotor control studies. For this reason, an extended LTI model is also proposed in this study.

A methodology for assessing the fidelity of reduced order LTI models that include different number of harmonic rotor states is also presented. The methodology is rooted in the assumption that when periodicity is mild, which is typical of advance ratios in the range of 0.1, the composition of eigenvector components, at least with respect to the dominant motions, does not significantly deviate from the corresponding composition obtained from the constant coefficient approximation. The methodology is evaluated using two types of isolated rotor rigid blade flapping dynamic models (an analytical model and a generic model available in FLIGHTLAB). The methodology is also evaluated using the generic helicopter model available in FLIGHTLAB, which includes body, rigid blade flapping and lead-lag, and three-state inflow dynamics. The evaluation results presented indicate that the proposed methodology provides a framework for assessing the fidelity of reduced order LTI model formulations in capturing the stability properties of a time periodic system with mild periodicity.

A methodology for developing reduced order airload models of on-blade control concepts based on artificial neural networks (NNET) is also described in this study. It is evaluated for a selected case of airfoil and trailing edge flap combination to validate the ROM of airloads. It is successfully integrated into FLIGHTLAB to model the Trailing Edge Flap type On-Blade Control concepts, and LTI validity studies are performed on GHM, which is enhanced with such OBC concepts.

6.1 Conclusions

Specific conclusions of this study are numbered as follows,

1. This computationally efficient method for generating LTI models from the nonlinear model made it possible to arbitrarily change the number of harmonics, hence, facilitating the parametric studies.
2. It is assessed that the minimum number of harmonics of the LTI model needs to be twice the number of the rotor blades (8 for GHM studied here) in order to achieve the best results for time and frequency domain response characteristics as well as for the stability properties if only vehicle's stability is considered.
3. Increasing the number of harmonics beyond 8/rev does not improve the LTI results for the stability properties due to the saturation of the fidelity which was contributed to the average component based modeling of non-rotor states. Therefore, for a complete fidelity achievement extended LTI model must be used with harmonics up to at least 10/rev.
4. LTI model is observed to have overall good fidelity if the interest in the stability properties is limited to the vehicle's stability and handling qualities, leaving the rotor portion out.
5. Overall good fidelity can be achieved only with the extension of the LTI model to LTI* such that it includes the harmonics of all states up to the same level. Overall good fidelity for all characteristics is obtained when harmonics up to 8/rev are included in LTI*.
6. The increment in the number of harmonics to obtain better fidelity should be performed by half the number of rotor blades for even bladed rotors.

Although it was seen in the analytical model studies that each harmonic included increased the fidelity (or decreased the error), the conclusion was limited to the analytical models since it was not repeated in the FLIGHTLAB model results. The fundamental difference between the analytical and the numerical models is that there are many more harmonics in the numerical model than the analytical representation used here.

7. It was noticed during this study that the combination of an elastic blade, a higher state inflow model, and unsteady aerodynamics has a significant effect on the vibration levels. A study [44] conducted for this purpose showed that this effect is in the positive direction to capture the actual vibration levels.

8. The computational cost of an LTI model linearly increases with the number of harmonics. This cost is driven by the harmonic decomposition of the LTP model. The cost of algebraic manipulations, such as one half of "n^{th}" sine harmonic component of $K(\psi)$, is a small fraction of the cost of obtaining that component itself through harmonic analysis.

9. It is noticed that even though the reference model has very good accuracy (10^{-15} in this study), it was not possible to reach that accuracy in the eigenvalue estimation of the LTI models since the absolute error of the eigenvalue analysis of the A_{LTI} (10^{-10} in this study) is much higher when a high number of harmonics is used in the LTI.

10. A large number of neurons is required for the training of drag coefficient data compared to the number of neurons needed for the training of lift

and moment coefficient. Therefore, NNET training of airfoil coefficients should be performed separately in order to create ROM aerodynamics.

11. Although successful response characteristics could be achieved using LTI models with respect to the available criteria, it is also important to note that expected trends could be captured as well using the LTI model. These trends include power reduction due to 2/rev inputs, control over N_b/rev vibrations through N_b-1, N_b, N_b+1 excitations of IBC or OBC input channels, and blade deflection using azimuth dependent input in order to avoid Blade Vortex Interaction (BVI).

12. In the analytical model studies of the LTI stability properties, it is understood that in order to achieve the same order of fidelity at the same number of harmonics, the multiplication of the advance ratio and Lock number should be kept constant. This finding can be generalized to the studies of GHM in terms of amplitudes of the A_{LTP} matrix such that same order of fidelity can be achieved with the same level LTI models if the amplitudes of the A_{LTP} matrices are matched.

13. Even if the portions of A_{LTP} corresponding to the non-rotor states are time invariant, treating those non-rotor states with their average components only leads to an error that cannot be corrected by increasing the number of harmonics used for the rotor states. This result can also be verified with the LTI model presented in the Appendix. Assuming all the cosine and sine components of A11, A12 and A13 to be zero, the time derivative of the harmonic components of non-rotor states (left hand side of the equation) will still have non-zero values (on the right hand side of the equation) due to multiplication of average components of A12 and A13

with the harmonic components of rotor states; hence, there will always be a harmonic component of the non-rotor states as long as there exists a harmonic component of rotor states. Briefly, there is always coupling between the rotor harmonic states and the non-rotor harmonic states as long as coupling between rotor and body is present.

6.2 Recommendations

Recommendations for future work are listed in this section.

1. Depending on the fidelity requirement, either LTI or its extension LTI* can be used for integrated flight and rotor controller synthesis and design.
2. Fidelity studies of stability properties rely on matching the eigenvectors of FTM to the dominant portion of the LTI eigenvectors. This method is limited by the low periodicity of the eigenvectors. Thus, it is expected to fail at high advance ratios even though LTI models still can be constructed with a finite number of harmonics without additional penalty. Therefore, more generic tools are needed to make the comparison between the eigenvalues.
3. Further extension of the proposed methodology is needed using modal participation factors suggested in the literature to address cases involving higher levels of periodicity.

APPENDIX: LTI* EXAMPLE

An example generic LTI* model in purely analytical form is shown here. Number of harmonics is limited to 2, 4, 6 and 8 per rev. This example is intended to guide for programming of the analytical equations given in this thesis and to show a compact form of the LTI in terms of harmonics of the LTP as they appear in the LTI.

$$\dot{x} = A_{LTP}x \qquad where$$

$$A_{LTP} = \begin{bmatrix} A11(\psi) & A12(\psi) & A13(\psi) \\ 0 & 0 & I \\ A31(\psi) & -K(\psi) & -C(\psi) \end{bmatrix}$$

$$x = \begin{bmatrix} x_b & x_r & \dot{x}_r \end{bmatrix}^T, \qquad x_b : Body\ \&\ Inflow\ States, x_r : Rotor\ States$$

$$x_b = (x_b)_o + \sum_{i=2,4,6,8} \left[(x_b)_{ic} \cos(i\psi) + (x_b)_{is} \sin(i\psi) \right]$$

$$x_r = (x_r)_o + \sum_{i=2,4,6,8} \left[(x_r)_{ic} \cos(i\psi) + (x_r)_{is} \sin(i\psi) \right]$$

$$A11(\psi) = A11_o + \sum_{i=2,4,6,8} \left[A11_{ic} \cos(i\psi) + A11_{is} \sin(i\psi) \right]$$

$$A12(\psi) = A12_o + \sum_{i=2,4,6,8} \left[A12_{ic} \cos(i\psi) + A12_{is} \sin(i\psi) \right]$$

$$A13(\psi) = A13_o + \sum_{i=2,4,6,8} \left[A13_{ic} \cos(i\psi) + A13_{is} \sin(i\psi) \right]$$

$$A31(\psi) = A31_o + \sum_{i=2,4,6,8} \left[A31_{ic} \cos(i\psi) + A31_{is} \sin(i\psi) \right]$$

$$K(\psi) = K_o + \sum_{i=2,4,6,8} \left[K_{ic} \cos(i\psi) + K_{is} \sin(i\psi) \right]$$

$$C(\psi) = C_o + \sum_{i=2,4,6,8} \left[C_{ic} \cos(i\psi) + C_{is} \sin(i\psi) \right]$$

$$(\dot{x}) = A_{LTI}(x) \qquad where$$

$$A_{LTI} = \begin{bmatrix} A11_{LTI} & A12_{LTI} & A13_{LTI} \\ 0 & 0 & I \\ A31_{LTI} & -K_{LTI} & -C_{LTI} \end{bmatrix}$$

$$(x) = \begin{bmatrix} (x_b) & (x_r) & (\dot{x}_r) \end{bmatrix}^T,$$

$$(x_b) = \begin{bmatrix} (x_b)_o & (x_b)_{2c} & (x_b)_{2s} & (x_b)_{4c} & (x_b)_{4s} & (x_b)_{6c} & (x_b)_{6s} & (x_b)_{8c} & (x_b)_{8s} \end{bmatrix}$$

$$(x_r) = \begin{bmatrix} (x_r)_o & (x_r)_{2c} & (x_r)_{2s} & (x_r)_{4c} & (x_r)_{4s} & (x_r)_{6c} & (x_r)_{6s} & (x_r)_{8c} & (x_r)_{8s} \end{bmatrix}$$

$$(\dot{x}_r) = \begin{bmatrix} (\dot{x}_r)_o & (\dot{x}_r)_{2c} & (\dot{x}_r)_{2s} & (\dot{x}_r)_{4c} & (\dot{x}_r)_{4s} & (\dot{x}_r)_{6c} & (\dot{x}_r)_{6s} & (\dot{x}_r)_{8c} & (\dot{x}_r)_{8s} \end{bmatrix}$$

$$A11_{LTI} = \begin{bmatrix} A11_o & \frac{1}{2}A11_{2c} & \frac{1}{2}A11_{2s} & \frac{1}{2}A11_{4c} & \frac{1}{2}A11_{4s} \\ A11_{2c} & A11_o + \frac{1}{2}A11_{4c} & \frac{1}{2}A11_{4s} & \frac{1}{2}(A11_{6c} + A11_{2c}) & \frac{1}{2}(A11_{6s} + A11_{2s}) \\ A11_{2s} & \frac{1}{2}A11_{4s} & A11_o - \frac{1}{2}A11_{4c} & \frac{1}{2}(A11_{6s} - A11_{2s}) & \frac{1}{2}(A11_{2c} - A11_{6c}) \\ A11_{4c} & \frac{1}{2}(A11_{6c} + A11_{2c}) & \frac{1}{2}(A11_{6s} - A11_{2s}) & A11_o + \frac{1}{2}A11_{8c} & \frac{1}{2}A11_{8s} \\ A11_{4s} & \frac{1}{2}(A11_{6s} + A11_{2s}) & \frac{1}{2}(A11_{2c} - A11_{6c}) & \frac{1}{2}A11_{8s} & A11_o - \frac{1}{2}A11_{8c} \end{bmatrix}$$

$$+ \begin{bmatrix} 0 & 0 & 0 & 0 & 0 \\ 0 & 0 & -2 \cdot \Omega I & 0 & 0 \\ 0 & 2 \cdot \Omega I & 0 & 0 & 0 \\ 0 & 0 & 0 & 0 & -4 \cdot \Omega I \\ 0 & 0 & 0 & 4 \cdot \Omega I & 0 \end{bmatrix}$$

$$A12_{LTI} = \begin{bmatrix} A12_o & \frac{1}{2}A12_{2c} & \frac{1}{2}A12_{2s} & \frac{1}{2}A12_{4c} & \frac{1}{2}A12_{4s} \\ A12_{2c} & A12_o + \frac{1}{2}(A12_{4c}) & \frac{1}{2}A12_{4s} & \frac{1}{2}[(A12_{6c} + A12_{2c})] & \frac{1}{2}[(A12_{6s} + A12_{2s})] \\ A12_{2s} & \frac{1}{2}A12_{4s} & A12_o - \frac{1}{2}(A12_{4c}) & \frac{1}{2}[(A12_{6s} - A12_{2s})] & \frac{1}{2}[(A12_{2c} - A12_{6c})] \\ A12_{4c} & \frac{1}{2}[(A12_{6c} + A12_{2c})] & \frac{1}{2}[(A12_{6s} - A12_{2s})] & A12_o + \frac{1}{2}(A12_{8c}) & \frac{1}{2}A12_{8s} \\ A12_{4s} & \frac{1}{2}[(A12_{6s} + A12_{2s})] & \frac{1}{2}[(A12_{2c} - A12_{6c})] & \frac{1}{2}A12_{8s} & A12_o - \frac{1}{2}(A12_{8c}) \end{bmatrix}$$

$$+ \begin{bmatrix} 0 & 0 & 0 & 0 & 0 \\ 0 & \frac{1}{2}(-2\Omega \cdot A13_{4s}) & +2\Omega \cdot \left(A13_o + \frac{1}{2}A13_{4c}\right) & \frac{1}{2}[-4\Omega(A13_{6s} + A13_{2s})] & \frac{1}{2}[+4\Omega(A13_{6c} + A13_{2c})] \\ 0 & -2\Omega \cdot \left(A13_o - \frac{1}{2}A13_{4c}\right) & -\frac{1}{2}(-2\Omega \cdot A13_{4s}) & \frac{1}{2}[-4\Omega(A13_{2c} - A13_{6c})] & \frac{1}{2}[+4\Omega(A13_{6s} - A13_{2s})] \\ 0 & \frac{1}{2}[-2\Omega(A13_{6s} - A13_{2s})] & \frac{1}{2}[+2\Omega(A13_{6c} + A13_{2c})] & +\frac{1}{2}(-4\Omega \cdot A13_{8s}) & +4\Omega \cdot \left(A13_o + \frac{1}{2}A13_{8c}\right) \\ 0 & \frac{1}{2}[-2\Omega(A13_{2c} - A13_{6c})] & \frac{1}{2}[+2\Omega(A13_{6s} + A13_{2s})] & -4\Omega \cdot \left(A13_o - \frac{1}{2}A13_{8c}\right) & -\frac{1}{2}(-4\Omega \cdot A13_{8s}) \end{bmatrix}$$

$$A13_{LTI} = \begin{bmatrix} A13_o & \frac{1}{2}A13_{2c} & \frac{1}{2}A13_{2s} & \frac{1}{2}A13_{4c} & \frac{1}{2}A13_{4s} \\ A13_{2c} & A13_o + \frac{1}{2}A13_{4c} & \frac{1}{2}A13_{4s} & \frac{1}{2}\left(A13_{6c} + A13_{2c}\right) & \frac{1}{2}\left(A13_{6s} + A13_{2s}\right) \\ A13_{2s} & \frac{1}{2}A13_{4s} & A13_o - \frac{1}{2}A13_{4c} & \frac{1}{2}\left(A13_{6s} - A13_{2s}\right) & \frac{1}{2}\left(A13_{2c} - A13_{6c}\right) \\ A13_{4c} & \frac{1}{2}\left(A13_{6c} + A13_{2c}\right) & \frac{1}{2}\left(A13_{6s} - A13_{2s}\right) & A13_o + \frac{1}{2}A13_{8c} & \frac{1}{2}A13_{8s} \\ A13_{4s} & \frac{1}{2}\left(A13_{6s} + A13_{2s}\right) & \frac{1}{2}\left(A13_{2c} - A13_{6c}\right) & \frac{1}{2}A13_{8s} & A13_o - \frac{1}{2}A13_{8c} \end{bmatrix}$$

$$A31_{LTI} = \begin{bmatrix} A31_o & \frac{1}{2}A31_{2c} & \frac{1}{2}A31_{2s} & \frac{1}{2}A31_{4c} & \frac{1}{2}A31_{4s} \\ A31_{2c} & A31_o + \frac{1}{2}\left(A31_{4c}\right) & \frac{1}{2}A31_{4s} & \frac{1}{2}\left[\left(A31_{6c} + A31_{2c}\right)\right] & \frac{1}{2}\left[\left(A31_{6s} + A31_{2s}\right)\right] \\ A31_{2s} & \frac{1}{2}A31_{4s} & A31_o - \frac{1}{2}\left(A31_{4c}\right) & \frac{1}{2}\left[\left(A31_{6s} - A31_{2s}\right)\right] & \frac{1}{2}\left[\left(A31_{2c} - A31_{6c}\right)\right] \\ A31_{4c} & \frac{1}{2}\left[\left(A31_{6c} + A31_{2c}\right)\right] & \frac{1}{2}\left[\left(A31_{6s} - A31_{2s}\right)\right] & A31_o + \frac{1}{2}\left(A31_{8c}\right) & \frac{1}{2}A31_{8s} \\ A31_{4s} & \frac{1}{2}\left[\left(A31_{6s} + A31_{2s}\right)\right] & \frac{1}{2}\left[\left(A31_{2c} - A31_{6c}\right)\right] & \frac{1}{2}A31_{8s} & A31_o - \frac{1}{2}\left(A31_{8c}\right) \end{bmatrix}$$

$$K_{LTI} = \begin{bmatrix} K_o & \frac{1}{2}K_{2c} & \frac{1}{2}K_{2s} & \frac{1}{2}K_{4c} & \frac{1}{2}K_{4s} \\ K_{2c} & K_o + \frac{1}{2}K_{4c} & \frac{1}{2}K_{4s} & \frac{1}{2}(K_{6c} + K_{2c}) & \frac{1}{2}(K_{6s} + K_{2s}) \\ K_{2s} & \frac{1}{2}K_{4s} & K_o - \frac{1}{2}K_{4c} & \frac{1}{2}(K_{6s} - K_{2s}) & \frac{1}{2}(K_{2c} - K_{6c}) \\ K_{4c} & \frac{1}{2}(K_{6c} + K_{2c}) & \frac{1}{2}(K_{6s} - K_{2s}) & K_o + \frac{1}{2}K_{8c} & \frac{1}{2}K_{8s} \\ K_{4s} & \frac{1}{2}(K_{6s} + K_{2s}) & \frac{1}{2}(K_{2c} - K_{6c}) & \frac{1}{2}K_{8s} & K_o - \frac{1}{2}K_{8c} \end{bmatrix}$$

$$+ \begin{bmatrix} 0 & 0 & 0 & 0 & 0 \\ 0 & (2\cdot\Omega)^2 I - \frac{1}{2}2\Omega\cdot C_{4s} & 2\cdot\Omega\left(C_o + \frac{1}{2}C_{4c}\right) & -\frac{1}{2}4\Omega(C_{6s} + C_{2s}) & \frac{1}{2}4\Omega(C_{6c} + C_{2c}) \\ 0 & -2\cdot\Omega\left(C_o - \frac{1}{2}C_{4c}\right) & (2\cdot\Omega)^2 I + \frac{1}{2}2\Omega\cdot C_{4s} & -\frac{1}{2}4\Omega(C_{2c} - C_{6c}) & \frac{1}{2}4\Omega(C_{6s} - C_{2s}) \\ 0 & -\frac{1}{2}2\Omega(C_{6s} - C_{2s}) & \frac{1}{2}2\Omega(C_{6c} + C_{2c}) & (4\cdot\Omega)^2 I - \frac{1}{2}4\Omega\cdot C_{8s} & 4\cdot\Omega\left(C_o + \frac{1}{2}C_{8c}\right) \\ 0 & -\frac{1}{2}2\Omega(C_{2c} - C_{6c}) & \frac{1}{2}2\Omega(C_{6s} + C_{2s}) & -4\cdot\Omega\left(C_o - \frac{1}{2}C_{8c}\right) & (4\cdot\Omega)^2 I + \frac{1}{2}4\Omega\cdot C_{8s} \end{bmatrix}$$

$$C_{LTI} = \begin{bmatrix} C_o & \frac{1}{2}C_{2c} & \frac{1}{2}C_{2s} & \frac{1}{2}C_{4c} & \frac{1}{2}C_{4s} \\ C_{2c} & C_o + \frac{1}{2}C_{4c} & \frac{1}{2}C_{4s} & \frac{1}{2}(C_{6c} + C_{2c}) & \frac{1}{2}(C_{6s} + C_{2s}) \\ C_{2s} & \frac{1}{2}C_{4s} & C_o - \frac{1}{2}C_{4c} & \frac{1}{2}(C_{6s} - C_{2s}) & \frac{1}{2}(C_{2c} - C_{6c}) \\ C_{4c} & \frac{1}{2}(C_{6c} + C_{2c}) & \frac{1}{2}(C_{6s} - C_{2s}) & C_o + \frac{1}{2}C_{8c} & \frac{1}{2}C_{8s} \\ C_{4s} & \frac{1}{2}(C_{6s} + C_{2s}) & \frac{1}{2}(C_{2c} - C_{6c}) & \frac{1}{2}C_{8s} & C_o - \frac{1}{2}C_{8c} \end{bmatrix}$$

$$+ \begin{bmatrix} 0 & 0 & 0 & 0 & 0 \\ 0 & 0 & -2\cdot 2\Omega\cdot I & 0 & 0 \\ 0 & 2\cdot 2\Omega\cdot I & 0 & 0 & 0 \\ 0 & 0 & 0 & 0 & -2\cdot 4\Omega\cdot I \\ 0 & 0 & 0 & 2\cdot 4\Omega\cdot I & 0 \end{bmatrix}$$

REFERENCES

[1] Shaw, J., Albion, N., Hanker, E.J., Teal, R.S, "Higher Harmonic Control: Wind Tunnel Demonstration of Fully Effective Vibratory Hub Force Suppression", AHS 41st Annual Meeting, Texas, May 15-17, 1985.

[2] Jacklin, S. A., Blaas, A., Teves, D., and Kube, R., "Reduction of Helicopter BVI Noise, Vibration, and Power Consumption through Individual Blade Control," Proceedings of the 51st Annual Forum of the American Helicopter Society, May 1995.

[3] Swanson, S. M., Jacklin, S. A., Blaas, A., Niesl, G., and Kube, R., "Acoustic Results from a Full- Scale Wind Tunnel Test Evaluating Individual Blade Control," Proceedings of the 51st Annual Forum of the American Helicopter Society, May 1995.

[4] Bae, E.S., Gandhi, F., Maughmer, M., “Optimally Scheduled Deployments of Miniature Trailing Edge Effectors for Rotorcraft Power Reduction”, 65th Annual National Forum of the American Helicopter Society, Grapevine, Texas, May 27-29, 2009.

[5] Jacklin, S.A., Lau, B.H., Nguyen, K.Q., Smith, R.L., McNulty, M.J.,"Full-Scale Wind Tunnel Test of the McDonnell Douglas Five-Bladed Advanced Bearingless Rotor: Performance, Stability, Loads, Control Power, Vibration and HHC Data",

American Helicopter Society Aeromechanics Specialists Conference, San Francisco, CA, January 19-21, 1994

[6] Norman et al., "Low-Speed Wind Tunnel Investigation of a Full-Scale UH-60 Rotor System", Proceedings of the 58th Annual Forum of the American Helicopter Society, Montreal Canada, June 11-13, 2002

[7] Dawson et. al., "Wind Tunnel Test of an Active Flap Rotor: BVI Noise and Vibration Reduction," Proceedings of the 51st Annual Forum of the American Helicopter Society, May 1995.

[8] Montanye, P. L., Smith, E.C., Rahn, C.D., Conlon, S.C., "Shipboard Helicopter Gust Response Alleviation Using Active Trailing Edge Flaps", 65th Annual National Forum of the American Helicopter Society, Grapevine, Texas, May 27-29, 2009.

[9] Skjoldan , P., "Modal Dynamics of Wind Turbines with Anisotropic Rotors", 47th AIAA Aerospace Sciences Meeting Including The New Horizons Forum and Aerospace Exposition, Orlando, FL, 5-8 January, 2009.

[10] Arnold, U.T.P., Furst, D., "Closed Loop IBC Results from CH-53G Flight Tests", Aerospace Science and Technology 9, pp. 421–435, 2005.

[11] Cheng, R.P., Tischler, M.B. and Celi, R., "A Higher-Order, Time-Invariant, Linearized Model for Application to HHC/AFCS Interaction Study," Proceedings

of the 59th Annual Forum of the American Helicopter Society, Phoenix, AZ, May 6-8, 2003.

[12] Floquet, G., "Sur les équations différentielles linéaires à coefficients périodiques", Ann. École Norm. Sup. 12: 47–88, 1883

[13] Peters, D.A., Hohenemser, K.H., "Application of the Floquet Transition Matrix to Problems of Lifting Rotor Stability", American Helicopter Society 26th Annual National Forum, Washington, D.C., June 16-18, 1970

[14] Loewvy, R.J., "Review of Rotary-Wing V/STOL Dynamic and Aeroelastic Problems", Journal of the American Helicopter Society, 14, (3), July 1969

[15] Sissingh, G.J., "Dynamics of Rotors Operating at High Advance Ratios", Journal of the American Helicopter Society, 13, (3), July 1968

[16] Lowis, 0.J., "The Stability of Rotor Blade Flapping Motion at High Tip Speed Ratios", Reports and Memoranda No. 3544, January 1968.

[17] Wilde, E., Bramwell, A, Summerscales, R., "The Flapping Behavior of a Helicopter Rotor at High Tip Speed Ratios", British Aeronautical Research Council, Report CP 877, 1966.

[18] Crimi, P., "A Method for Analyzing the Aeroelastic Stability of a Helicopter Rotor in Foreward Flight, NASA-CR-1332, August 1969.

[19] Piarulli, V.J. and White, R.P. Jr., "A Method for Determining the Characteristic Functions Associated with the Aeroelastic Instabilities of Helicopter Rotor Blades in Forward Flight", NASA CR-1577, Washington, D.C., June 1970.

[20] Hill, G.W., "On the part of the motion of the lunar perigee which is a function of the mean motions of the sun and moon", February 1886, Acta Mathematica Vol. 8, Number 1, 1-36.

[21] Peters, D.A., Lieb, S.M., “Significance of Floquet Eigenvalues and Eigenvectors for the Dynamics of Time-Varying Systems”, 65th Annual National Forum of the American Helicopter Society, Grapevine, Texas, May 27-29, 2009.

[22] Bittanti, S., Colaneri, P., “Invariant representation of discrete-time periodic systems”, Automatica 36, pp1777-1793, 2000

[23] Colaneri, P., Celi, R., Bittanti, S., “Constant-coefficient representations of periodic-coefficient discrete linear systems”, AHS 4th Decennial Specialist’s Conference on Aeromechanics, San Fransisco, CA, January 21-23, 2004

[24] Pandyan, R. and Sinha, S.C., “Time-Varying Controller Synthesis for Nonlinear Systems subjected to Periodic Parametric Loading,” Journal of Vibration and Control, Vol. 7, pp73-90, 2001.

[25] Ramirez, A., Semlyen, A., Iravani, R., "Harmonic Domain Characterization of the Resonant Interaction Between Generator and Transmission Line", IEEE Transactions on Power Delivery, Vol. 20, No. 2, pp.1753-1762, April 2005.

[26] Jugo, J., Lizarraga, I., Arredondo, I., “Nonlinear Modeling and Analysis of Active Magnetic Bearing Systems in the Harmonic Domain: A Case Study”, IET Control Theory Appl., Vol. 2, No. 1, pp.61-71, 2008.

[27] Cheng, R.P., Tischler, M.B. and Celi, R., “A High Order, Linear Time Invariant Model for Application to Higher Harmonic Control and Flight Control Systems,” NASA-TP-2006-213460, 2006.

[28] Stewart, W., "Second Harmonic Control on the Helicopter Rotor", Aeronautical Research Council Reports and Memoranda 2997, Great Britain, August 1952.

[29] Johnson, W, “Helicopter Theory”, Princeton University Press, 1980.

[30] Jacklin et al., "Full-Scale Wind Tunnel Test of an Individual Blade Control System for a UH-60 Helicopter", Proceedings of the 58th Annual Forum of the American Helicopter Society, Montreal Canada, June 11-13, 2002

[31] Friedmann, P., Millot, T., “Vibration Reduction in Rotorcraft Using Active Control: A Comparison of Various Approaches,” Journal of Guidance, Control, and Dynamics, Vol 18, No 4, 1995

[32] Molusis, J. A., Hammond, C. E., and Cline, J. H., "A Unified Approach to the Optimal Design of Adaptive and Gain Scheduled Controllers to Achieve Minimum Helicopter Vibration," Journal of the American Helicopter Society, Vol. 28, No. 2, 1983, pp. 9-18

[33] Hammond, C. E., "Wind Tunnel Results Showing Rotor Vibratory Loads Reduction Using Higher Harmonic Blade Pitch," Journal of the American Helicopter Society, Vol. 28, No. 1, 1983, pp. 10-15.

[34] Taylor, R. B., Farrar, F. A., and Miao, W., "An Active Control System for Helicopter Vibration Reduction by Higher Harmonic Pitch," Proceedings of the AIAA/ASME/ASCE/AHS 21st Structures, Structural Dynamics, and Materials Conference (Seattle, WA), AIAA, New York, 1980

[35] Kretz, M., "Research in Multicyclic and Active Control of Rotary-Wings," Vertica, Vol. 1, No. 1/2, 1976, pp. 95-105.

[36] Ham, N. D., "Helicopter Gust Alleviation, Attitude Stabilization and Vibration Alleviation Using Individual-Blade-Control Through a Conventional Swashplate," Proceedings of the Eleventh European Rotorcraft Forum (London), 1985, pp. 75.1-75.5.

[37] Ham, N. D., Behal, B. L., and McKillip, R. M., "Helicopter Rotor Lag Damping Augmentation Through Individual-Blade-Control," Vertica, Vol. 7, No. 4, 1983, pp. 361-371.

[38] Min, B.Y., Sankar, L.N., Rajmohan, N, Prasad, J. V. R., "Computational Investigation of Gurney Flap Effects on Rotors in Forward Flight", Journal of Aircraft Vol. 46, No. 6, November–December 2009.

[39] Hassan, A.A., Straub, F.K., Charles, B.D., "Effects of Surface Blowing/Suction on the Aerodynamic of Rotor Blade-Vortex Interactions--A Numerical Simulation", Journal of the American Helicopter Society, vol. 42, No. 2; Apr. 1997.

[40] Standish, K.J., Van Dam, C.P., “Computational Analysis of a Microtab-Based Aerodynamic Load Control System for Rotor Blades,” American Helicopter Society Aeromechanics Specialists' Conference, San Francisco, CA, January 2004.

[41] Lemnios, A. Z., and Smith, A. F, "An Analytical Evaluation of the Controllable Twist Rotor Performance and Dynamic Behavior," Kaman Report R-794, 1972.

[42] Robinson, L. H., and Friedmann, P. P., "A Study of Fundamental Issues in Higher Harmonic Control Using Aeroelastic Simulation," Journal of the American Helicopter Society, Vol. 36, No. 2, 1991, pp. 32-43.

[43] Robinson, L. H., "Aeroelastic Simulation of Higher Harmonic Control," Ph.D. Dissertation, Mechanical, Aerospace and Nuclear Engineering Dept., Univ. of California, Los Angeles, June 1989.

[44] Abraham, M.D, Olcer, F.E., Costello, M.F., Takahashi, M.D., Tischler, M.B., "Integrated Design of AFCS and HHC for Rotorcraft Vibration Reduction", AHS 67th Annual Forum, Virginia Beach, VA, May 3-5, 2011.

[45] Abraham, M., Olcer, E., Prasad, JVR, Tischler, M, Takahashi, M, Theodore, C., Validation of LTI Dynamic Helicopter Model for High-Harmonic Control Using Wind Tunnel Data, AHS Technical Note (accepted for publishing), 2010

[46] Van der Wall, B.G., Yin, J., "Simulation of Active Rotor Control by Comprehensive Rotor Code with Prescribed Wake using HART II Data", 65th Annual National Forum of the American Helicopter Society, Grapevine, Texas, May 27-29, 2009.

[47] Prasad, J.V.R., Olcer, F.E., Sankar, L,N. and He, C., "Linear Models for Integrated Flight and Rotor Control," 34th European Rotorcraft Forum, Birmingham, UK, September 16-18, 2008.

[48] Padfield, G.D., "Helicopter Flight Dynamics: The Theory and Application of Flying Qualities and Simulation Modeling", AIAA Education Series, 1995.

[49] Voskuijl, M., Manimala, B., Walker, D.J., Kureemun, R., "First Steps Towards the Design of an Active Pitch Link Loads Reduction System Using Novel Control Techniques", 31st European Rotorcraft Forum, Florence, Italy, September 2005.

[50] Voskuijl, M., Padfield, G.D., Walker, D.W., Manimala B., Gubbels, A.W., "Simulation of automatic helicopter deck landings using nature inspired flight control", The Aeronautical Journal of the RAeS, 114(1151), pp.25-34, 2010

[51] Bhagwat, M.J., Leishman, J.G. "Time-Accurate Free-Vortex Wake Model for Dynamic Rotor Response", Aeromechanics 2000, American Helicopter Society Specialist Meeting, Atlanta, GA, November 13-14, 2000

[52] He, C., Development and Application of a Generalized Dynamic Wake Theory for Lifting Rotors, Ph.D. thesis, School of Aerospace Engineering, Georgia Institute of Technology, Atlanta, Georgia, 1989.

[53] Pitt, D. M. and Peters, D. A., “Theoretical Prediction of Dynamic Inflow Derivatives,” Vertica, Vol. 5, No. 1, 1981.

[54] Prasad, J.V.R., Olcer, F.E., Sankar, L.N., He, C., "Development and Evaluation of Reduced Order Models of On-Blade Control for Integrated Flight and Rotor Control", 66th Annual Forum of the American Helicopter Society, Phoenix, AZ, May 11-13, 2010.

[55] Advanced Rotorcraft Technology, Inc., “FLIGHTLAB Theory Manual (Vol. I),” March 2004.

[56] Prasad, J.V.R., Olcer, F.E., Sankar, L.N., He, C., "Linear Time Invariant Models for Integrated Flight and Rotor Control", 35th European Rotorcraft Forum, Hamburg, Germany, September 22-25, 2009.

[57] Xu, J. & Gasch, R., “Modale behandlung linearer periodisch zeitvarianter Bewegungsgleichungen”, Archive of Applied Mechanics, Vol. 65, No. 3, pp. 178-193, 1995, (in German).

[58] Rene, H.C, Ilmar, F.S, "Modal Controllability and Observability of Bladed Disks and their Dependency on the Angular Velocity", Journal of Vibration and Control, June 2005, Vol. 11 No. 6 801-828.

[59] Love, G.N., Wood, A.R., "Harmonic State Space Model of Power Electronics", The 13th IEEE International Conference on Harmonics and Quality of Power, Wollongong Australia, September 28-October 1, 2008.

[60] Anderson et. al, "LAPACK Users’ Guide, 3rd Ed. Society for Industrial and Applied Mathematics", 1999, Philadelphia, PA.

[61] Biggers, J.C., "Some Approximations to the Flapping Stability of Helicopter Rotors", Rotorcraft Dynamics Conference, NASA-SP-352. pp 45-54, February 13-15, Moffet Field, CA, 1974.

[62] Zhou, J., Hagiwara, T., Araki, M., “Stability Analysis of Continuous-Time Periodic Systems Via the Harmonic Analysis”, IEEE Transactions on Automatic Control, Vol. 47, No. 2, pp.292-298, February 2002.

[63] Nagabhushanam, J., Gaonkar, G.H., "Automatic Identification of Modal Damping from Floquet Analysis", Journal of the American Helicopter Society, Vol 40, No. 2, pp. 39-42, April, 1995.

[64] Tischler, M.B. and Remple, R.K.: Aircraft and Rotorcraft system Identification: Engineering Methods with Flight Test Examples, AIAA Publications, Virginia, USA, 2006.

[65] Bain, J., Samuel, R., Sankar, L. N., and Prasad, JVR, “Neural Network Models for the On-Board and Individual Blade Control of Helicopter Rotors”, AIAA Paper 2009-3521, 27th AIAA Applied Aerodynamics Conference, San Antonio, Texas, June 22-25, 2009.

[66] He, C., Zhao, J., Bain, J., Sankar, L., Prasad, J.V.R., “Development of a Reduced Order Modeling Framework for Flight Mechanics Oriented Modeling of On-Blade Control Concepts”, 35th European Rotorcraft Forum, Hamburg, Germany, September22-25, 2009.

[67] Bain, J., Sankar, L.N., Prasad, J.V.R., Bauchau, O., Peters, D.A., and He, C., “Computational Modeling of Variable-Droop Leading Edge in Forward Flight,” Journal of Aircraft, Vol. 46, Issue, 2, April, 2009

[68] Tischler, M.B., Cauffman, M. G., "Frequency- Response Method for Rotorcraft System Identification: Flight Applications to BO-105 Coupled Rotor/Fuselage Dynamics," Journal of the American Helicopter Society, Vol 37, No. 3, pp. 3-17, July, 1992.

[69] Hockney, R.W., "The Science of Computer Benchmarking (Software, Environments, Tools)", John Wiley & Sons, Inc., 1996

[70] Gulcat, U., "Fundamentals of Modern Unsteady Aerodynamics", Springer, 2011

[71] Leishman, G., "Principles of Helicopter Aerodynamics", Cambridge University Press, 2006.

VITA

Mr. Fahri Ersel Olcer was born in Istanbul, Turkey on March 24, 1980. He had Bachelor of Science in Aeronautical Engineering and Master of Science in Aerospace Engineering at Istanbul Technical University in 2004 and 2007, respectively. He was accepted to the School of Aerospace Engineering at Georgia Institute of Technology in 2007. He is a student member of American Helicopter Society.